Exponentially-Varying, Unsteady Standing Waves in Parallel-Flow Boundary Layers

Harold L. Rogler
United Research Corporation
428 Hill Street, Suite 21
Santa Monica, California 90405

May 1983

Final Report for Period March 1979 - January 1982

ARNOLD ENGINEERING DEVELOPMENT CENTER
ARNOLD AIR FORCE STATION, TENNESSEE
AIR FORCE SYSTEMS COMMAND
UNITED STATES AIR FORCE

This report has been reviewed by the Office of Public Affairs (PA) and is releasable to the National Technical Information Service (NTIS). At NTIS, it will be available to the general public, including foreign nations.

APPROVAL STATEMENT

This report has been reviewed and approved.

KEITH L. KUSHMAN
Directorate of Technology
Deputy for Operations

Approved for publication:

FOR THE COMMANDER

MARION L. LASTER
Director of Technology
Deputy for Operations

REPORT DOCUMENTATION PAGE		READ INSTRUCTIONS BEFORE COMPLETING FORM
1. REPORT NUMBER AEDC-TR-83-4	2. GOVT ACCESSION NO.	3. RECIPIENT'S CATALOG NUMBER
4. TITLE *(and Subtitle)* EXPONENTIALLY-VARYING, UNSTEADY STANDING WAVES IN PARALLEL-FLOW BOUNDARY LAYERS		5 TYPE OF REPORT & PERIOD COVERED Final Report March 1979 – January 1982
		6 PERFORMING ORG. REPORT NUMBER
7. AUTHOR(s) Harold L. Rogler		8. CONTRACT OR GRANT NUMBER(s) F40600-79-C-0002
9. PERFORMING ORGANIZATION NAME AND ADDRESS United Research Corporation 428 Hill Street, Suite 21 Santa Monica, CA 90405		10 PROGRAM ELEMENT, PROJECT, TASK AREA & WORK UNIT NUMBERS 65807F
11. CONTROLLING OFFICE NAME AND ADDRESS Arnold Engineering Development Center/DOS Air Force Systems Command Arnold Air Force Station, TN 37389		12. REPORT DATE May 1983
		13 NUMBER OF PAGES 107
14. MONITORING AGENCY NAME & ADDRESS*(if different from Controlling Office)*		15 SECURITY CLASS. *(of this report)* Unclassified
		15a DECLASSIFICATION/DOWNGRADING SCHEDULE N/A

16. DISTRIBUTION STATEMENT *(of this Report)*

Approved for public release; distribution unlimited.

17. DISTRIBUTION STATEMENT *(of the abstract entered in Block 20, if different from Report)*

18. SUPPLEMENTARY NOTES

Available in Defense Technical Information Center (DTIC).

19. KEY WORDS *(Continue on reverse side if necessary and identify by block number)*

free-stream disturbances	boundary layer	potential oscillations
roughness	stability	unsteady aerodynamics
unsteady boundary layers	transition	unsteady flows
Orr-Sommerfeld equation	leading edge	numerical solutions
sublayer	irrotational fluctuations	standing waves

20. ABSTRACT *(Continue on reverse side if necessary and identify by block number)*

Fluctuations which oscillate in time and grow or decay exponentially in the streamwise direction are found as solutions of the Orr-Sommerfeld equation. The x-wavenumber is purely imaginary; the frequency is real. Since these disturbances do not propagate in the streamwise direction, they are called "standing waves". In the direction normal to the wall, they behave as two travelling waves of unequal strength. Inside the boundary layer and near the edge, the flow field has fluctuating vorticity. The disturbance in the distant free stream is irrotational. Inside the boundary layer, the vorticity

20. (continued)

originates primarily from the production term, through viscous diffusion
to/from the wall, and by convection. Near the wall, an unsteady viscous
sublayer forms. Analytical solutions for fluctuations in a uniform mean
flow near a wall are presented, along with numerical solutions obtained
for Falkner-Skan boundary layers. The mean boundary layer can be influ-
enced by the mean pressure gradient and surface roughness.

The feature which distinguishes these solutions from the instability waves,
and also distinguishes these solutions from those with free-stream vorticity
fluctuations, is the characteristic irrotational fluctuations in the
"free stream". The standing waves are other means for upstream and down-
stream influence in the boundary layer.

PREFACE

This report is one in a series of AEDC Technical Reports prepared by United Research Corporation which document the solutions of the Orr-Sommerfeld equation and how these oscillations are initiated in a boundary layer. The reports in this series are:

AEDC-TR-83-3
Rotational and Irrotational Freestream Disturbances
Interacting Inviscidly with a Semi-Infinite Plate

AEDC-TR-83-4
Exponentially-Varying, Standing Waves
in Parallel-Flow Boundary Layers (this report)

AEDC-TR-83-7
Waves Which Travel Upstream in Boundary Layers

AEDC-TR-83-8
Spatially-Decaying Arrays of Rectangular Vortices
Interacting with Falkner-Skan Boundary Layers

AEDC-TR-83-9
The Boundary-Value Problem
for Two-Dimensional Flunctuations in Boundary Layers

AEDC-TR-83-10
Nonperiodic Flunctuations Induced by Surface Waviness
Near the Leading Edge of a Model

The last report presents the spectrum of standing waves excited by surface waviness. This spectrum, with appropriate nondimensionalizations, also applies to the case of freestream disturbances encountering a semi-infinite plate.

All reproducibles used in the reproduction of this report were supplied by the author.

1

CONTENTS

APPENDIXES

1.0 INTRODUCTION AND LITERATURE SURVEY

1.1 INTRODUCTORY COMMENTS

The simulation of boundary layer transition in test facilities would be a useful capability to have in the development of higher performance and more efficient vehicles. An obstacle to our developing the capability to simulate transition has been the freestream disturbances in the test facilities which are not completely similar to the disturbances in the atmosphere. Another obstacle has been that the surface roughness and other fine geometric details of the subscale models are not completely similar to those details on the full-scale flight vehicle. A related problem is our inability to systematically develop boundary layer trips to fix transition in a specified region. However, (dimensional) duplication or (nondimensional) complete similarity of the disturbances and roughness are excessively severe and impractical requirements. The practical need exists to identify the significant properties of the freestream disturbances and roughness which influence stability and transition.

An obstacle to identifying those properties has been the inability of theory to link freestream disturbances to the instability waves and other oscillations in an initial-value problem. Another obstacle has been the inability to show how roughness, either isolated elements or distributed roughness, affects the initial amplitudes of the various oscillations. When analyzing such a problem, the theoretician must know all of the possible solutions so that the energy from the freestream disturbances is channeled to the proper waves.

When the author and Dr. Shunichi Tsuge studied an initial-value problem in space, their objective was to describe the evolution of disturbances in the downstream direction in terms of a superposition of solutions of the Orr-Sommerfeld equation. The set of stability waves and two solutions representing vortical freestream disturbances appear in the analysis. However, two additional mathematical poles appear in the analysis. These poles indicate that two additional solutions exist of the Orr-Sommerfeld equation. These standing wave solutions are generalizations to oscillations previously analyzed by Rogler and Reshotko (Refs. 1,2). This report documents the structure of these standing waves. The initial-value problem, which provides the framework to link the initial conditions with the amplitudes and phases of the various waves, will be summarized in later writings.

Waves which do not travel or propagate are called standing waves. They may be steady or unsteady. Standing waves of a simpler form than considered herein have been studied using the unsteady boundary layer equations with the oscillating freestream

$$U_\infty(t) = \overline{U}_\infty + f_\infty e^{-i\omega t} \tag{1.1}$$

This freestream oscillation does not depend on position. Analytical solutions, and related numerical calculations and experiments have been

extensively reported in the literature, as surveyed by Rogler and Reshotko (Ref. 3) and Telionis (Ref. 4). Loehrke, Morkovin, and Fejer (Ref. 5) reviewed the stability and transition literature in oscillating boundary layers. The author believes that this simple standing wave is a limiting case of a more general standing wave with far broader applicability.

Before we examine the more general case, however, we wish to illustrate how an oscillating freestream (1.1) interacts with a parallel-flow boundary layer. Since the x-derivatives vanish, the momentum equations for small-amplitude fluctuations reduce to

$$p_y = 0, \quad u_t = -\frac{p_x}{\rho} + \nu u_{yy} \quad \text{where } -p_x/\rho = -i\omega f_\infty e^{-i\omega t} \tag{1.2}$$

The reduced form is merely the one-dimensional, unsteady diffusion equation with a known forcing term, p_x/ρ. The longitudinal velocity fluctuation, u, is uncoupled from both the mean flow and the fluctuation velocity normal to the plate. It is merely the flow driven by the exterior pressure gradient (which oscillates in time) and altered by the diffusion of vorticity to and from the wall so that the no-slip condition is satisfied.

However, another form of standing waves is possible in the form of waves which grow or decay exponentially in space, as well as oscillating sinusoidally in time. Generally these waves have both u and v velocity fluctuations and are coupled with the mean boundary layer profile. To our knowledge, these waves have not be studied in any shearing layers before, although they have appeared in several studies with uniform mean flows which are summarized in the following sections. These oscillations are believed to arise in many practical situations, and have a role in the initial-value problem in space for disturbances described by the Orr-Sommerfeld equation. These waves also have a role when specifying boundary conditions for numerical solutions of the Navier-Stokes equations on a rectangular domain.

Our objectives are to formulate and solve the mathematical system for 2-D, unsteady, standing wave disturbances with amplitudes which vary exponentially in the streamwise direction. The mean flow will be represented by a parallel-flow boundary layer. The first evidence which we saw of the existence of these waves was in an analytical solution of spatially-decaying vortices in the freestream. We will summarize those results in the next section. In later sections, we will extend these analytical solutions to include the presence of a nearby wall, and later to numerical solutions with Falkner-Skan boundary layers. While our attention here is focused on either oscillations in the freestream or with a wall (and boundary layer) present, these disturbances should arise in a wide variety of shear layers, jets, wakes, etc.

1.2 STANDING WAVES AND VORTICES IN A UNIFORM MEAN FLOW

The Navier-Stokes equations can be separated into mean and disturbance quantities, the (time or ensemble) average taken, those mean equations subtracted from those equations with separated quantities, and simplified for a parallel-flow boundary layer with small-amplitude disturbances. With appropriate derivatives in the x and y directions taken, a fluctuating vorticity equation can be found and nondimensionalized. For a uniform mean flow, this vorticity equation is

$$\xi_t + \xi_x - \epsilon(\xi_{xx} + \xi_{yy}) = 0 \tag{1.3}$$

where $\xi = v_x - u_y$. In Refs. 1,2, Rogler and Reshotko sought the spatially decaying solution of this equation subject to the initial condition on vorticity

$$\xi(0, y, t) = 2\pi \sin(\pi y + y_i) \sin \pi t \tag{1.4}$$

and the far-downstream condition that the vorticity vanishes

$$\xi \to 0 \quad as \quad x \to \infty \tag{1.5}$$

Conditions on the velocity field are imposed later. By generalized Fourier transforms, a solution was extracted as

$$\xi = -i\pi \sin(\pi y + y_i) \left[e^{m_3 x + i\pi t} - e^{m_4 x - i\pi t} \right] \tag{1.6}$$

where

$$m_{3,4} = \left[1 - (1 + 4\pi^2 \epsilon^2 \pm 4i\pi\epsilon)^{1/2} \right] / 2\epsilon \tag{1.7}$$

or equivalently

$$\xi = -2\pi \sin(\pi y + y_i) e^{-f_1 \pi x} \sin \pi f_2 (x - ct) \tag{1.8}$$

This result is a slowly decaying wave in the downstream direction propagating at speed $c \geq 1$.

The solution of interest here follows from Poisson's equation which links the vorticity field and the streamfunction

$$\nabla^2 \psi = \xi \tag{1.9}$$

where we imposed an initial condition on the streamfunction

$$\psi(0,y,t) = -\frac{1}{\pi} \sin(\pi y + y_1) \sin \pi t \qquad (1.10)$$

Again, far downstream, the streamfunction vanishes

$$\psi \rightarrow 0 \quad as \quad x \rightarrow \infty \qquad (1.11)$$

If a solution of form

$$\psi = \sin(\pi y + y_1) \, \theta(x; t, \epsilon) \qquad (1.12)$$

is sought of Poisson's equation, then it reduces to

$$\theta_{xx} - \pi^2 \theta = 2\pi \, e^{-f_1 \pi x} \sin \pi \left(f_2 x - t\right) \qquad (1.13)$$

subject to the conditions

$$\theta(0; t, \epsilon) = -\frac{\sin \pi t}{\pi} \quad and \quad \theta \rightarrow 0 \ as \ x \rightarrow \infty \qquad (1.14)$$

The complementary solution is

$$\theta_c(x; t, \epsilon) = c_1(t) \, e^{\pi x} + c_2(t) \, e^{-\pi x} \qquad (1.15)$$

and it is this solution which serves as the initial seed for this research. We shall return to this solution after we have written the particular integral, obtained by the method of variation of parameters. Combining the complementary and particular solutions and applying the boundary conditions, then the disturbance streamfunction is

$$\psi = \frac{1}{\pi} \sin(\pi y + y_1) \Big[\underset{Term\,(1)}{\pi c_2(t, \epsilon) \, e^{-\pi x}} + \underset{Term\,(2)}{X(x, t, \epsilon) \, e^{-f_1 \pi x}} \Big] \qquad (1.16)$$

where the following are defined

$$\pi c_2(t, \epsilon) = [-f_2 \cos \pi t + (1 + f_1) \sin \pi t][(1 + f_1)^2 + f_2^2]^{-1}$$

$$+ [f_2 \cos \pi t + (1 - f_1) \sin \pi t][(1 - f_1)^2 + f_2^2]^{-1} - \sin \pi t$$

$$X(x; t, \epsilon) = [(1 + f_1) \sin \pi(f_2 x - t) + f_2 \cos \pi(f_2 x - t)][(1 + f_1)^2 + f_2^2]^{-1}$$

$$+ [(1 - f_1) \sin \pi(f_2 x - t) - f_2 \cos \pi(f_2 x - t)][(1 - f_1)^2 + f_2^2]^{-1} \qquad (1.17a,b)$$

Term (1) represents a near-grid effect which is an irrotational, standing wave which decays exponentially downstream. The second term is a traveling wave and represents the flowfield of the convecting and diffusing vorticity field. The streamlines for these two flowfields

are plotted in Fig. 1.1

The standing wave was "initiated" by the initial condition imposed on the streamfunction. It would have been possible to describe initial conditions in which that standing wave vanished, and indeed for the case studied, this wave vanished in the inviscid limit. With other initial conditions, that wave would remain in the inviscid limit.

1.3 STANDING WAVE ARISING IN A QUARTER-PLANE PROBLEM

In Ref. 6, a more complex standing wave showed up in an inviscid, quarter-plane problem of an array of vortices input along the y-axis with a plate positioned along the x-axis as shown in Figure 1.2. The mathematical system solved was

$$\xi_t + \xi_x = 0 \quad \Rightarrow \quad \xi = -2\pi \sin\pi(x-t) \sin(\pi y + y_1) \tag{1.18}$$

$$\nabla^2 \psi = \xi \tag{1.19}$$

$$\psi = \psi^{(a)} - \psi^{(i)} \tag{1.20}$$

$$\psi^{(a)} = \frac{1}{\pi} \sin(\pi y + y_1) \sin\pi(x-t) \tag{1.21}$$

$$\nabla^2 \psi^{(i)} = 0 \tag{1.22}$$

$$\psi^{(i)} = \frac{1}{\pi} \sin y_1 \sin\pi(x-t) - C \quad \text{for } y = 0, x > 0$$

$$\psi^{(i)} = 0 \quad \text{for } x = 0, y > 0$$

$$\psi^{(i)} \rightarrow 0 \text{ as } y \rightarrow \infty ; \ \psi^{(i)} \text{ is bounded as } x \rightarrow \infty \tag{1.23a-d}$$

and the solution was extracted by a half-range Fourier transform in the y-direction. The solution for the streamfunction $\psi = \psi^{(a)} - \psi^{(i)}$ was

$$\psi = \frac{1}{\pi} \left[\underbrace{\sin(\pi y + y_1)}_{Term(A_1)} - \underbrace{\sin y_1 e^{-\pi y}}_{Term(A_2)} \right] \sin\pi(x-t)$$

$$+ \underbrace{F(z) \sin y_1 \sin\pi t}_{Term(B)}$$

9
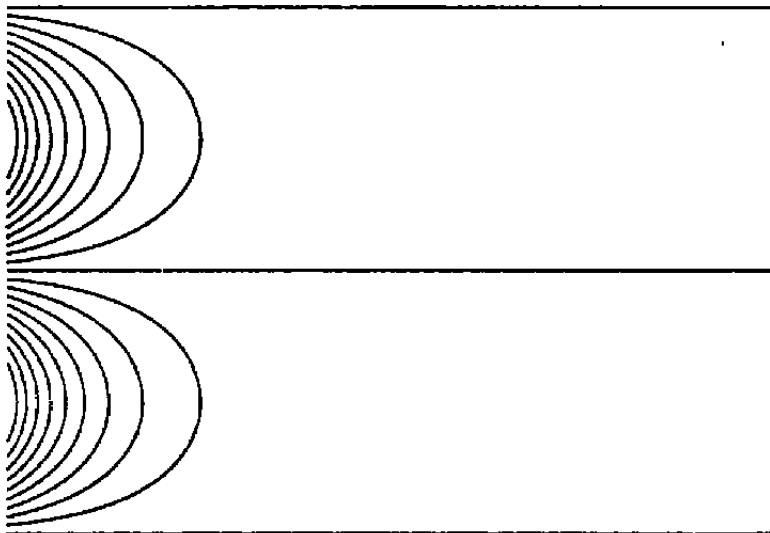
(1.1a) Irrotational standing wave which decays exponentially.
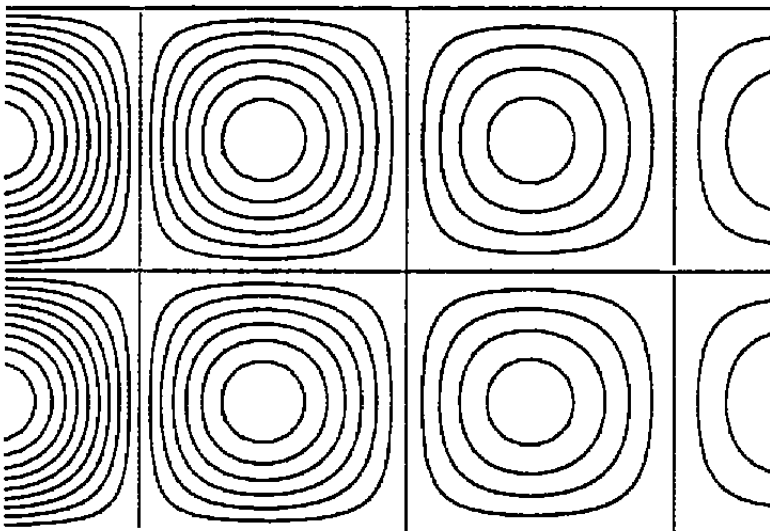
(1.1b) Rotational vortices which propagate downstream.

Figure 1.1 The standing and traveling waves downstream of a grid.
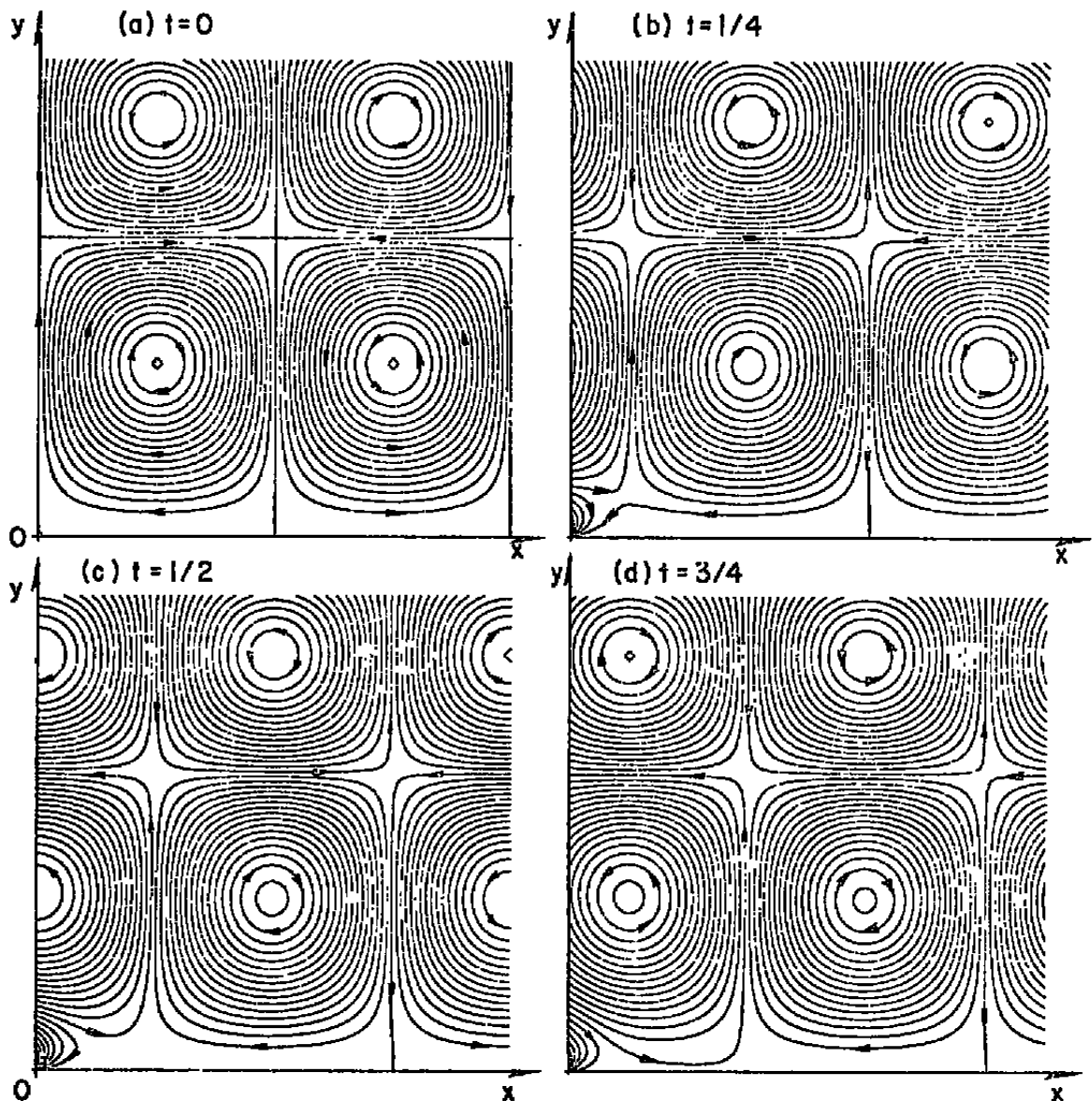
Figure 1.2 Disturbance streamlines at different times as vortices
are introduced along the upstream boundary and propagate
downstream. This flowfield consists of both irrotational
and rotational parts. The irrotational part is composed
of both standing and traveling waves.

$$\bar{z} = x + i y$$

$$F(\bar{z}) = -\frac{2}{\pi^2} \, Imag \left\{ ci(\pi \bar{z}) \cos \pi \bar{z} + si(\pi \bar{z}) \sin \pi \bar{z} \right\} \quad (1.25a,b)$$

and $ci(\pi z)$ and $si(\pi z)$ are the cosine and sine integrals. Term (A1) denotes the flow induced by the vorticity in an unbounded flow, with term (A2) representing an irrotational, traveling wave superimposed and associated with the impermeability condition. The term of importance here is term (B) which is a standing wave, and oscillates only in time. Far downstream of the grid, it vanishes.

1.4 DECAYING WAVES WITH SEMI-INFINITE PLATES

Decaying, oscillating waves have been found in several problems where freestream disturbances interact with the leading edge of a semi-infinite plate. The author has investigated these waves for many forms of freestream disturbances, including

(1) Arrays of square vortices (Refs. 1,7,and 8) arrays of rectangular vortices (Refs. 9 and 10), and oblique plane waves of vorticity (Refs. 9 and 10).

(2) Vortex sheets (Refs. 9 and 10) convecting downstream at speed $c = 1$. This is interesting case which clearly illustrates the blockage caused by the plate and differences between the flows above and below the plate.

(3) Vortex streets (Refs. 9 and 10) composed of potential vortices in a stable (Karman) configuration. These vortices propagate at a speed dictated by the strength, sense, and spacing of the vortices. This speed can be less than or greater than unity (depending on the direction of rotation), and reduces to $c = 1$ in the limit of vanishing circulation or infinite spacing.

(4) Fluctuations wholly irrotational (Refs. 9 and 10) which propagate at arbitrary speeds. Many examples are possible, depending on the relative strengths and phases of the irrotational waves. While this model blows up exponentially in the direction normal to the plate, the model is useful in analyses (and perhaps computations) for some studies with freestream fluctuations.

Despite the different characters and speeds of these freestream disturbances, the streamfunctions for the case of freestream disturbances with a semi-infinite plate can all be written in the unified form

$$\Psi(x,y,t) = \Psi^{(a)}(x,y,t) - \Psi^{(i)}(x,y,t) \qquad (1.26)$$

where $\Psi^{(a)}$ is the streamfunction for the freestream disturbance (if the plate were not present) and $\Psi^{(i)}$ is the streamfunction of an irrotational flow which causes the impermeability condition to be satisfied. We illustrate this second streamfunction in Figure 1.3. Interestingly, this streamfunction is also the linearized solution of a semi-infinite, 2-D (i.e., ribbon-shaped) snake swimming through the water.

As suggested in Figure 1.3 and supported by the theory of Refs. 9 and 10, the streamfunction has a simple asymptotic limit far-downstream of the leading edge

$$\Psi^{(i)} \longrightarrow e^{-\alpha|y|} e^{i\alpha(x-ct)} \equiv \Psi^{(i)}_{asymp}. \qquad (1.27)$$

which is a traveling, irrotational wave which decays away from the plate. If (for simplicity) we consider the quarter-plane on the top of the plate beginning at the leading edge and extending downstream, then one could subtract out the asymptotic solution $\Psi^{(i)}_{asymp}$ from $\Psi^{(i)}$. The result is an irrotational flow decaying downstream of the leading edge,

$$\Psi^{(i)} - \Psi^{(i)}_{asymp} \longrightarrow 0 \quad as \ x \longrightarrow \infty \qquad (1.28)$$

If this flow ($\Psi^{(i)} - \Psi^{(i)}_{asymp}$.) were Fourier-analyzed in the y-direction, then one would obtain the spectrum of waves which oscillate neutrally in the y-direction and decay exponentially downstream. These spectral components are related to the spectral waves investigated in this report. Thus we believe that such waves arise for a wide class of practical freestream disturbances which intersect with the leading edges of plates.

1.5 DECAYING AND GROWING WAVES WITH FINITE-LENGTH PLATES

If the plate has finite length, with both leading and trailing edges, then the resultant flow has some features similar to those summarized in the previous section, although made more complicated by the trailing edge. The flow also has some new features associated with the oscillating circulation about the plate and the vortex sheet emitted from the trailing edge and convecting downstream.

For the purpose of identifying physically-realizable situations where standing waves grow or decay in the streamwise direction, we offer the following observations based on the analyses of Ref. 7:

(1) The irrotational flow associated with the bound circulation oscillates in time and has streamlines as plotted in Fig. 1.4. This flow is irrotational, oscillates sinusoidally in time, decays from the leading edge to the midspan, and grows from the midspan to the trailing edge.
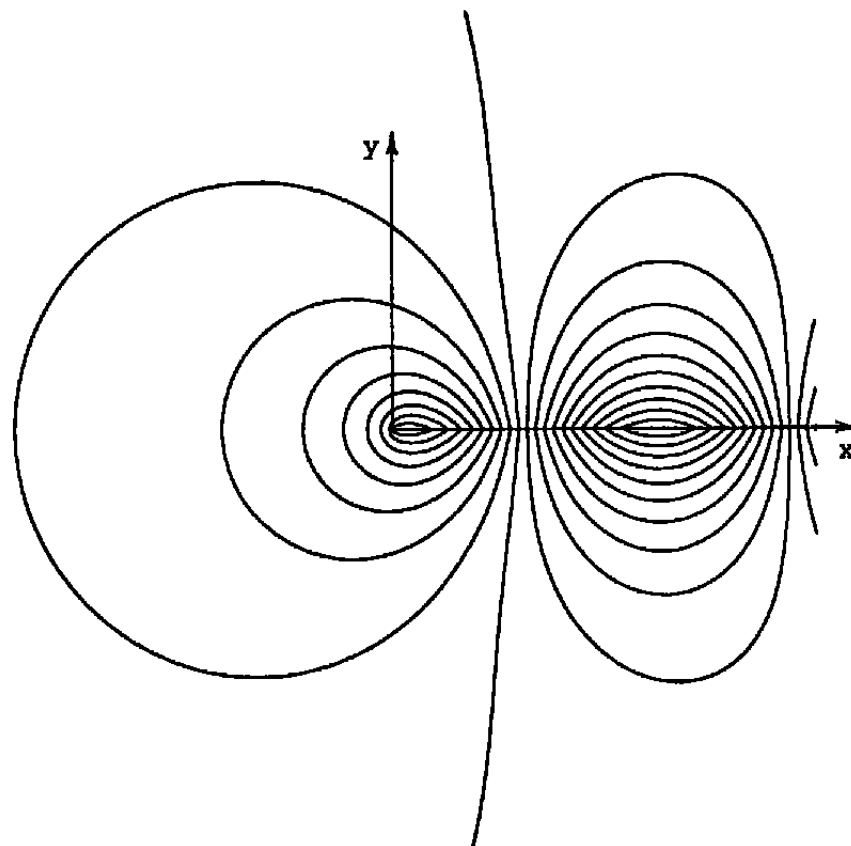
Figure 1.3   The streamlines for an irrotational flow which arises when a semi-infinite plate encounters a traveling-wave freestream disturbance. The leading edge is at the origin. Downstream of the leading edge, this flowfield consists of a superposition of standing waves and a traveling wave.
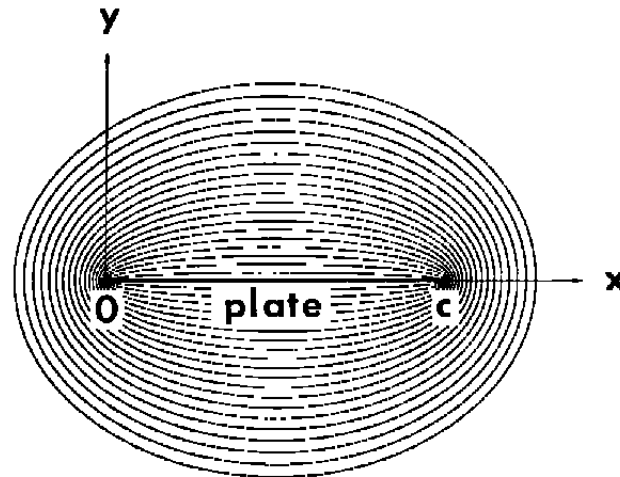
Figure 1.4   Streamlines for the oscillating, bound circulation   about
             a finite-length flat plate (Ref.7). This flow decelerates
             from the leading edge to the mid-span, and accelerates
             from the mid-span to the trailing edge. This flowfield is
             irrotational and oscillates sinusoidally in time. It
             is one of the fluctuations arising when an airfoil
             encounters a traveling-wave freestream disturbance.

(2) The trailing vortex sheet induces an oscillating, irrotational flow about the plate as shown in Fig. 1.5.

(3) To satisfy impermeability, another irrotational wave is produced which is related to the wave discussed in the previous section. If the plate is very long, then this wave has the character of standing waves near the leading and trailing edges. A traveling wave is also present everywhere along the plate. The streamline pattern associated with this flow has not been drawn; the explicit solution is presented in Ref. 7.

In summary for freestream disturbances interacting with finite-length plates, growing and decaying standing waves are present simultaneously. Several mechanisms exist to produce standing waves. While a unified theory is available, no attempt has been made to compare the relative strengths of these various waves.

1.6 RELATED STUDIES OF FOURIER-LAPLACE AND POTENTIAL FLUCTUATIONS

This study is concerned with the solutions of the incompressible parallel-flow equations for a boundary layer on an impermeable plate. To help provide some perspective for the various Fourier-Laplace solutions, the following references are cited. Of course, many other investigators have made significant contributions to analyze, calculate, and measure these oscillations, and to extend and apply them to many other problems.

Tollmien (Ref. 11) first obtained neutral eigenvalues and a critical Reynolds number for the fundamental stability wave. Jordinson (Ref. 36), Mack (Ref. 12), Antar and Benek (Ref. 37), Corner, Houston, and Ross (Ref. 13) obtained the (temporal and/or spatial) eigenvalues for the higher discrete modes with a Blasius layer. Rogler and Reshotko (Refs. 1,2,3), the present author (Refs. 15 and 39), Murdock (Ref. 40), Salwen and Grosch (Refs. 41,14), and Ellinwood (Ref. 42) obtained solutions with downstream propagating vortical fluctuations in the freestream. The forced response of a boundary layer to a Karman vortex sheet was obtained by Rogler (Ref. 38). Rogler and Reshotko (Ref. 2), Rogler and Tsuge (Refs. 17), and the present author (Ref. 27) obtained solutions for waves travelling in the upstream direction. Those authors (Ref.16) also obtained solutions for the standing waves, with details summarized in the present report. In Ref. 17, spatial solutions for longitudinal vortices in a boundary layer were summarized. Related temporal solutions were obtained by Rogler and Reshotko (Ref. 18) and Hultgren and Gustavsson (Ref. 19). The boundary-value and initial-value problems will be reviewed in a later report.

For temporal solutions of the Orr-Sommerfeld equation in a channel, Mack (Ref. 12) presented numerical evidence of how the discrete solutions for a channel carry over to the solutions for a semi-infinite domain $(0 \leq y < \infty)$. There should be a link between the standing waves of the present report (as $\beta \to 0$) and oscillations in a

U$_\infty$ →

finite-length plate

leading
edge

trailing
edge

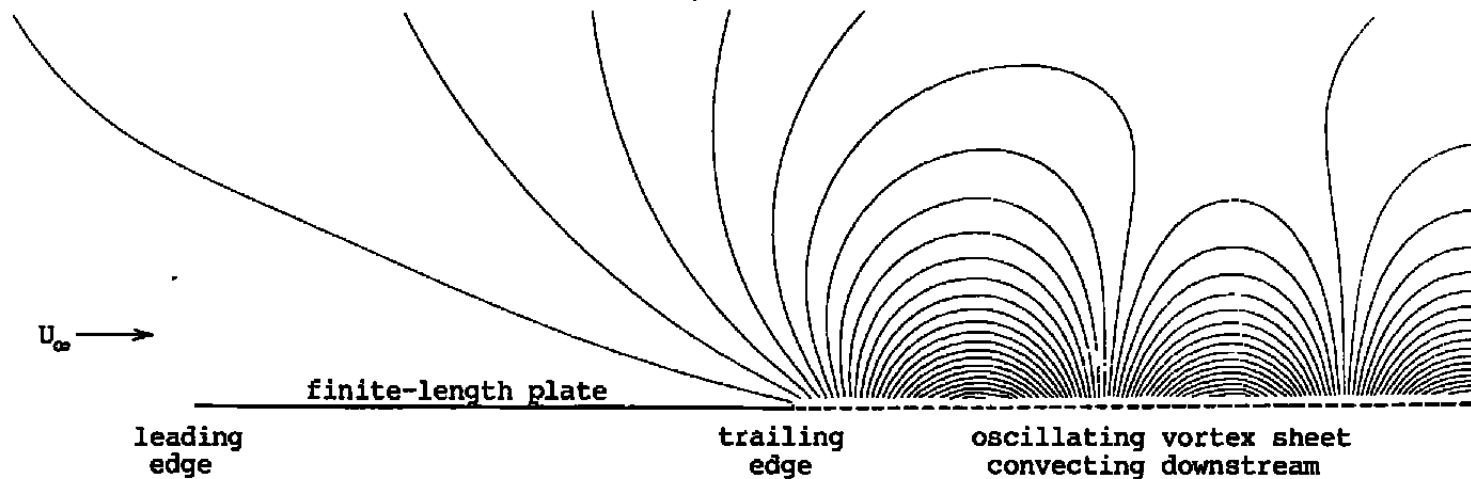oscillating vortex sheet
convecting downstream

Figure 1.5   Streamlines of the flow induced by the vortex sheet
emitted from the trailing edge of a finite-length plate
(Ref. 7). Only the top half has been drawn. Except at tne
vortex sheet itself, the flow is irrotational, oscillates
sinusoidally in time, and has characteristics of both
traveling and standing waves.

channel (as the channel width $\rightarrow \infty$ and the x-wavenumber $\rightarrow 0$). The neutral oscillation $v=0$, $u=f(y)\exp(-i\omega t)$ should be a limiting solution for both cases.

The importance of these Fourier-Laplace solutions are that (1) they can be superimposed to represent more general disturbances, (2) the separate solutions contain many of the features arising through instabilities, walls, viscosity, details of the mean shearing layer, roughness, freestream disturbances, etc., and (3) the Fourier-Laplace tools lead to a powerful and flexible framework for the study of transition and mixing. This framework is important because progress is often based upon generations of work by many investigators, a diversity of (analytical, numerical, and experimental) tools, and engineering and scientific problems of many types. The usefulness of stability theory has been firmly established. Now, the potential exists for a broader theory, which includes the normal modes, but also incorporates some features of freestream disturbances, surface waviness and roughness, surface vibration, and forcing.

The reader is reminded, however, that not all monochromatic Fourier-Laplace disturbances in the freestream yield a monochromatic response in a parallel-flow boundary layer, nor even in a uniform mean flow near a wall. In the temporal initial-value problems which have been worked, the wavenumber of the freestream disturbance is preserved, but the frequency is transformed into a spectrum. In the spatial boundary-value problems carried out by the author for an inviscid flow, the frequency of the freestream disturbance is preserved, but an integral spectrum and/or a series of wavenumbers result.

The work by Bechert and Michel (Ref. 20) is an example of a potential fluctuation in the form of an oscillating source/sink used to excite a step-function free-shear layer in an inviscid analysis. The experimental investigation of Dovgal, Kozlov, and Levchenko (Ref. 21) is believed to include, amongst the various fluctuations, the standing wave. In other experiments, the author cannot distinguish whether compressibility is an essential feature of the input disturbance, or if the input disturbance is partly composed of incompressible standing waves. Other incompressible feedback problems with free-shear layers emitted from trailing edges, and the incompressible coupling between the trailing edge and a leading edge positioned further downstream also have some elements of the standing waves which are investigated here. Additionally, some of the incompressible, potential fluctuations in unsteady airfoil theory also have certain characteristics of the standing waves, as discussed in Section 1.5.

Hence the present work might be viewed as a contribution toward bringing these additional features into an Orr-Sommerfeld description of unsteadiness in a shearing layer. As discussed by Reshotko (Ref. 22), a mathematical and physical understanding of the processes at the beginning of transition "would be most welcome."

In the next chapter, the mathematical system describing the standing waves in viscous, parallel-flow boundary layers is formulated.

2.0 FORMULATION OF THE MATHEMATICAL SYSTEM

2.1 THE ORR-SOMMERFELD EQUATION AND BOUNDARY CONDITIONS

The linearized, parallel-flow, viscous momentum equations can be combined into the following fourth-order partial differential equation in terms of the fluctuating velocity, $v(x,y,t)$, in the y-direction (and normal to a plate)

$$\left\{ \frac{\partial}{\partial t} + \overline{U}(y)\frac{\partial}{\partial x} - \epsilon \nabla^2 \right\} \nabla^2 v - \overline{U}_{yy}(y) \frac{\partial v}{\partial x} = 0 \tag{2.1}$$

The inverse Reynolds number based upon the freestream velocity and characteristic thickness of the boundary layer is $\epsilon = \nu/U_\infty \delta$. For Falkner-Skan boundary layers, the characteristic thickness is taken as

$$\delta \equiv \left(\frac{2}{m_{FS}+1} \; \frac{\nu x}{U_\infty(x)} \right)^{1/2}$$

where $m_{FS} = \beta_{FS} / (2 - \beta_{FS})$ \hfill (2.2a,b)

$\pi\beta_{FS}$ is the vertex angle of the wedge along which the boundary layer develops. The lengths in eqn. 2.1 have been nondimensionalized against δ and the time has been nondimensionalized against δ/U_∞. We now seek solutions of form

$$v(x,y,t) = \psi(y) e^{i\alpha x - i\omega t} \tag{2.3}$$

where the x-wavenumber (times i) for the cases of interest here are

$$i\alpha = \pm\beta = r\beta \quad or \quad \alpha = -ir\beta \tag{2.4}$$

where β is pure real, and where the coefficient r has values +1 and -1 corresponding to the cases

$\quad\quad\quad\quad$ r = +1 for a wave growing as $\exp(+\beta x)$
$\quad\quad\quad\quad$ r = -1 for a wave decaying as $\exp(-\beta x)$ \hfill (2.5a,b)

The x-wavenumber is pure imaginary. Substituting eqn. 2.3 into 2.1, then after some rearrangement, the Orr-Sommerfeld equation results

$$\left\{ \left(\overline{U} - \frac{\omega}{\alpha} \right)(D^2 - \alpha^2) - \overline{U}_{yy} - \frac{1}{i\alpha R_\delta}(D^2 - \alpha^2)^2 \right\} \varphi = 0 \tag{2.6a}$$

or equivalently

$$\left\{ \left(\overline{U} - \frac{ir\omega}{\beta} \right)(D^2 + \beta^2) - \overline{U}_{yy} - \frac{1}{r\beta R_\delta}(D^2 + \beta^2)^2 \right\} \varphi = 0 \tag{2.6b}$$

The phase speed is pure imaginary for the standing wave solutions

$$c \equiv \omega/\alpha = ir\omega/\beta \qquad (2.7)$$

Either equation is subject to impermeability and no-slip at the wall

$$\varphi = D\varphi = 0 \quad at \ y = 0 \qquad (2.8)$$

When $\bar{U} = 1$ outside the boundary layer, then the system reduces to

$$\left\{ \left(1 - \frac{ir\omega}{\beta}\right) - \frac{1}{r\beta R_s}\left(D^2 + \beta^2\right) \right\}\left(D^2 + \beta^2\right)\varphi = 0 \qquad (2.9)$$

with solutions $e^{\pm i\beta y}$ or $\cos\beta y$ and $\sin\beta y$ (which oscillate neutrally) and $e^{\pm my}$ (which oscillate and grow or decay). (2.10a,b)

where m is the root of the quadratic equation with positive real part

$$\left(1 - \frac{ir\omega}{\beta}\right) - \frac{1}{r\beta R_s}\left(m^2 + \beta^2\right) = 0 \qquad (2.11)$$

or $m = \left(r\beta R_s - \beta^2 - iR_s\omega\right)^{1/2}$ with r = ±1 for exp(±βx) waves (2.12)

The exterior solution is

$$\varphi^{(e)}(y) = A e^{-my} + B e^{my} + C\cos\beta y + D\sin\beta y \qquad (2.13)$$

where B = 0 in the present problem and we normalize by setting C = 1. This normalization is not always appropriate; see Appendix A.1 for an exception. We require that the exterior solution and the first three derivatives agree with the interior solution and the corresponding derivatives at the "edge" of the boundary layer, $y=y_e$

$$D^n\varphi(y_e^-) = D^n\varphi(y_e^+) \quad for \ n = 0, 1, 2, 3 \qquad (2.14)$$

Our objective now is to solve the mathematical system composed of the Orr-Sommerfeld equation (eqn. 2.6a,b), the two wall conditions (eqn. 2.8), and the four conditions at the boundary layer edge (eqns. 2.13 and 2.14). The exponents m and the other parameters for the cases of decaying and growing waves are given in Table 1 as a typical example. Note that the exponent m for the decaying case is nearly i times m for the growing case. The slight difference arises from the term $-\beta^2$ in the square root.

2.2 COMPLEX AMPLITUDES FOR LONGITUDINAL VELOCITY, VORTICITY, STREAMFUNCTION, AND PRESSURE

Let the velocity fluctuations in the x and y directions be represented as

$$u, v = \{f(y), \varphi(y)\} e^{i\alpha x - i\omega t} \tag{2.15}$$

Substituting into the continuity equation, $u_x + v_y = 0$, then $i\alpha f + \varphi_y = 0$ and the amplitude of the longitudinal velocity fluctuation is related to the amplitude of the normal velocity fluctuation by

$$f(y) = i\varphi_y(y)/\alpha \tag{2.16}$$

The fluctuating vorticity is $\zeta = v_x - u_y$. Letting $\zeta = Z(y) e^{i\alpha x - i\omega t}$, then the vorticity amplitude is related to the two velocity amplitudes by

$$Z(y) = i\alpha \varphi - f_y = -\frac{i}{\alpha}\left(\varphi_{yy} - \alpha^2 \varphi\right) \tag{2.17}$$

Letting $\psi = \Psi(y) e^{i\alpha x - i\omega t}$, since the normal velocity and streamfunction are related by $v = \psi_x$, then the amplitude of the streamfunction is

$$\Psi(y) = \varphi(y)/i\alpha \tag{2.18}$$

The pressure disturbance can be found from the linearized, parallel-flow, x-momentum equation

$$u_t + \bar{U} u_x + \bar{U}_y v = -P_x/\rho + \nu(u_{xx} + u_{yy}) \tag{2.19}$$

Introducing the dimensionless variables $u \rightarrow qu$, $v \rightarrow qv$, $t \rightarrow \delta t/U$, $\bar{U} \rightarrow U_\infty \bar{U}$, $p \rightarrow \rho q U p$, $x \rightarrow \delta x$, and $y \rightarrow \delta y$, where q is the characteristic disturbance velocity, then

$$P_x = -u_t - \bar{U} u_x - \bar{U}_y v + \frac{1}{R_\delta}(u_{xx} + u_{yy}) \tag{2.20}$$

Letting
$$P = \pi(y) e^{i\alpha x - i\omega t} \tag{2.21}$$

then
$$\pi(y) = \left(\frac{\omega}{\alpha} - \bar{U}\right) f + \frac{i \bar{U}_y \varphi}{\alpha} - \frac{i}{\alpha R_\delta}\left(f_{yy} - \alpha^2 f\right) \tag{2.22}$$

Thus knowing the amplitudes of the velocity fluctuations and the mean velocity profile, then the pressure fluctuation can be found. In a manner analogous to the streamlines, the pressure isobars can be calculated and plotted.

2.3 ROOT-MEAN-SQUARE QUANTITIES AND OTHER CORRELATIONS

Let a disturbance quantity $\theta^{(1)}$ be represented as

$$\theta^{(1)}(x,y,t) = R\left\{\left(\theta_r^{(1)} + i\theta_i^{(1)}\right)\left(\cos(\alpha x - \omega t) + i\sin(\alpha x - \omega t)\right)\right\}$$

$$= \theta_r^{(1)}(y)\cos(\alpha x - \omega t) - \theta_i^{(1)}(y)\sin(\alpha x - \omega t) \qquad (2.23)$$

Similarly, a second disturbance quantity $\theta^{(2)}$ can be represented as

$$\theta^{(2)}(x,y,t) = \theta_r^{(2)}(y)\cos(\alpha x - \omega t) - \theta_i^{(2)}(y)\sin(\alpha x - \omega t) \qquad (2.24)$$

The product of these two (real) quantities is

$$\theta^{(1)}\theta^{(2)} = \theta_r^{(1)}\theta_r^{(2)}\cos^2(\alpha x - \omega t) + \theta_i^{(1)}\theta_i^{(2)}\sin^2(\alpha x - \omega t)$$

$$- \left(\theta_r^{(1)}\theta_i^{(2)} + \theta_i^{(1)}\theta_r^{(2)}\right)\cos(\alpha x - \omega t)\sin(\alpha x - \omega t) \qquad (2.25)$$

By the mean of a variable in a spatial analysis, we refer to the time average over one time period $T = 2\pi/\omega$ of that variable

$$\overline{\theta^{(1)}\theta^{(2)}} \equiv \frac{1}{T}\int_{t=0}^{T}\theta^{(1)}\theta^{(2)}dt \qquad (2.26)$$

Carrying out the integrals for $\theta^{(1)}\theta^{(2)}_i$ the contributions arise only from the squared quantities, and the result is

$$\overline{\theta^{(1)}\theta^{(2)}} = \frac{1}{2}\left(\theta_r^{(1)}\theta_r^{(2)} + \theta_i^{(1)}\theta_i^{(2)}\right) \qquad (2.27)$$

The autocorrelations are thus

$$\left(\overline{u^2}\right)^{1/2} = \left[\left(f_r^2 + f_i^2\right)/2\right]^{1/2}$$

$$\left(\overline{v^2}\right)^{1/2} = \left[\left(\phi_r^2 + \phi_i^2\right)/2\right]^{1/2}$$

$$\left(\overline{p^2}\right)^{1/2} = \left[\left(\pi_r^2 + \pi_i^2\right)/2\right]^{1/2} \qquad (2.28)$$

The Reynolds stress is $-\overline{uv} = -\left(f_r\phi_r + f_i\phi_i\right)/2 \qquad (2.29)$

The energy production is $-\overline{uv}\,d\bar{U}/dy \qquad (2.30)$

The (instantaneous) kinetic energy per unit mass is

$$\frac{1}{2}\left(\mathcal{U}^2 + V^2\right) = \frac{1}{2}\left(\bar{U}^2 + 2\bar{U}u + u^2 + \cancel{\bar{V}^2}^0 + \cancel{2\bar{V}v}^0 + v^2\right) \qquad (2.31)$$

The mean of this quantity is

$$\frac{1}{2}\left(\bar{U}^2 + \overline{u^2} + \overline{v^2}\right) \qquad (2.32)$$

which has a contribution from the mean flow and another contribution from the unsteady flow. The quantity $(u^2+v^2)/2$ is plotted in the following chapter, along with the other variables introduced above.

Table 1
Example Numerical Value of the Exponent m

	β	ω	R_δ	α	m
exp(−βx) mode	0.5	0.5	1000	0.5i	10.1743201 −i24.5716664
exp(+βx) mode	0.5	0.5	1000	−0.5i	24.5629806 −i10.1779179 ·

3.0 NUMERICAL SOLUTIONS FOR STANDING WAVES

3.1 SUMMARY OF THE NUMERICAL TECHNIQUE

To obtain the coefficients $\bar{U}(y)$ and $\bar{U}_{yy}(y)$ of the mean flow, numerical solutions of the Falkner-Skan equation are obtained by the method of Nachtsheim and Swigert (Ref. 23) as modified and summarized in Ref. 3. The equation is solved by shooting from the wall outward, using 4th-order Runge-Kutta integration in double-precision arithmetic. The exterior boundary condition, $F_p \rightarrow 1$ as $\eta \rightarrow \infty$, is not specified at the boundary layer edge, $y = y_e$, but rather the _error is minimized_ in a least squares sense.

The Orr-Sommerfeld system of equations (2.6b, 2.8, 2.13, 2.14) is solved by an expansion in Chebyshev polynomials

$$\varphi(\hat{\eta}) = \sum_{m=0}^{N-1} a_m \, T_m(\hat{\eta})$$

(3.1)

with polynomials defined as

$$T_m(\hat{\eta}) = \cos[m(\text{arc}\cos\hat{\eta})]$$

(3.2)

and where the variable $\hat{\eta}$ is related to the dimensionless y by the linear transformation

$$\hat{\eta} = \frac{2y}{y_e} - 1$$

(3.3)

A set of linear, algebraic equations results from the Orr-Sommerfeld equation, the two wall boundary conditions, and the four matching conditions at the boundary layer edge. The matrix of coefficients related to this system is reduced by Gauss-Jordan elimination with maximum pivoting by column and rows. With the coefficients known, the expansion 3.1 can be carried out for $\varphi(y)$, and identities used to obtain the y-derivatives of $\varphi(y)$. With φ and its derivatives known, the longitudinal velocity, vorticity, and vorticity production are calculated. From the x-momentum equation, the pressure fluctuations are found, and then the correlations are calculated for rms quantities, including Reynolds stress, kinetic energy, etc. The streamlines, iso-vorticity contours, pressure isobars, and equi-value contours of the vorticity production term are drawn.

The _numerical checks_ included numerical experiments to determine the effects of number of terms in the expansion, precision of arithmetic for the matrix reduction, and influence of the y-value where the edge boundary conditions were imposed. Comparisons were made between analytical and numerical solutions for the cases of (1) a uniform mean flow, and (2) the viscous sublayer. The same computer

program used to obtain solutions for the standing waves, except with different patching conditions at the boundary layer edge, was also used to recover the Tollmien-Schlicting waves.

To assist the reader in comparing the figures with different values of the parameters, different wall boundary conditions, and the two cases of growing or decaying waves, Table 2 has been prepared.

3.2 NUMERICAL RESULTS FOR DECAYING WAVES IN FALKNER-SKAN BOUNDARY LAYERS

3.2.1 Blasius Case with Decaying Waves

The velocity profile and derivatives for the Blasius boundary layer are plotted in Figure 3.1 with the same y-scale as the following figures for amplitudes, streamlines, etc., except for the sublayer plots where the y-scale is stretched.

To aid in the interpretation of these calculations, since

$$v = (\phi_r + i\phi_i)\, e^{-\beta x - i\omega t} = [\phi_r(y)\cos\omega t + \phi_i(y)\sin\omega t]\, e^{-\beta x} \tag{3.4}$$

then for
$$\omega t = 0, \quad v(x,y,0) = \phi_r(y)\, e^{-\beta x}$$
$$\omega t = \pi/2, \quad v(x,y,t) = \phi_i(y)\, e^{-\beta x}$$
$$\omega t = \pi, \quad v(x,y,t) = -\phi_r(y)\, e^{-\beta x}$$
$$\omega t = 3\pi/2, \quad v(x,y,t) = -\phi_i(y)\, e^{-\beta x} \tag{3.5a-d}$$

Hence the real and imaginary parts of the complex amplitude are the velocity profiles at the times $\omega t=0$ and $\pi/2$ respectively. With a reversal of sign, they are the velocity profiles at the times $\omega t = \pi$ and $3\pi/2$. At $\omega t=2\pi$, the flowfield at time t=0 is repeated in this sinusoidal oscillation. Analogous interpretations also apply for the other complex amplitudes.

Figures 3.2 through 3.19 are plots for a decaying wave with y-wavenumber and frequency, $\beta = \omega = 0.5$, and Reynolds number $R_\delta = 1000$. In Figure 3.2 for the normal velocity, note that the impermeability condition is satisfied at the wall and note the oscillatory behavior of the solution. Far from the boundary

$$\phi(y) \rightarrow \sin\beta y + D\cos\beta y \quad as \; y \rightarrow \infty \tag{3.6}$$

Also note, based on the above interpretation of the real and imaginary parts, that the flow structure shifts up as the time increases from 0 to $\pi/2\omega$. The structure nearest to the wall expands outward. To see

Table 2. Tabular-List of Figures for Chapter 3

$e^{-\beta x}$ or $e^{+\beta x}$ wave	$e^{-\beta x}$	$e^{-\beta x}$	$e^{-\beta x}$	$e^{+\beta x}$	$e^{-\beta x}$
Wall BC	no-slip		⟶		no-shear
y-wavenumber, β	0.5	0.5	0.5	0.5	0.5
x-wavenumber, α	0.5i	0.5i	0.5i	−0.5i	0.5i
frequency, ω	0.5	0.5	0.5	0.5	0.5
complex phase speed, $c=\omega/\alpha$	−1.0i	−1.0i	−1.0i	1.0i	−1.0i
Reynolds number, R_δ	1000	1000	1000	1000	1000
Falkner–Skan parameter, m_{FS}	0.0	0.5	−0.05	0.0	0.0
$\bar{U},\bar{U}_y,\bar{U}_{yy}$	Figure 3.1	3.20	3.27	3.1	3.1
$\varphi(y)$	3.2	3.21	3.28	3.42	3.48
$f(y)$	3.3	3.22	3.29	3.43	3.49
$f(y)$ sublayer	3.4				
streamlines	3.5				
$Z(y)$	3.6,3.7	3.23	3.30	3.44	3.50
iso-vorticity contours	3.8				
$-\varphi\bar{U}_{yy}$	3.9				
equi-value contours of $v\bar{\varphi}_y$	3.10				
$\pi(y)$	3.11	3.24	3.31	3.45	3.51
pressure isobars	3.12				
rms v	3.13				
rms u	3.14				
rms $\tilde{\varphi}$	3.15				
rms p	3.16				
$-\overline{uv}$	3.17	3.25	3.32	3.46	
$-\overline{uv}\bar{U}_y$	3.18	3.26	3.33	3.47	
$(\overline{u^2}+\overline{v^2})/2$	3.19				

Figures illustrating the effects of frequency, Reynolds number, and y-wavenumber

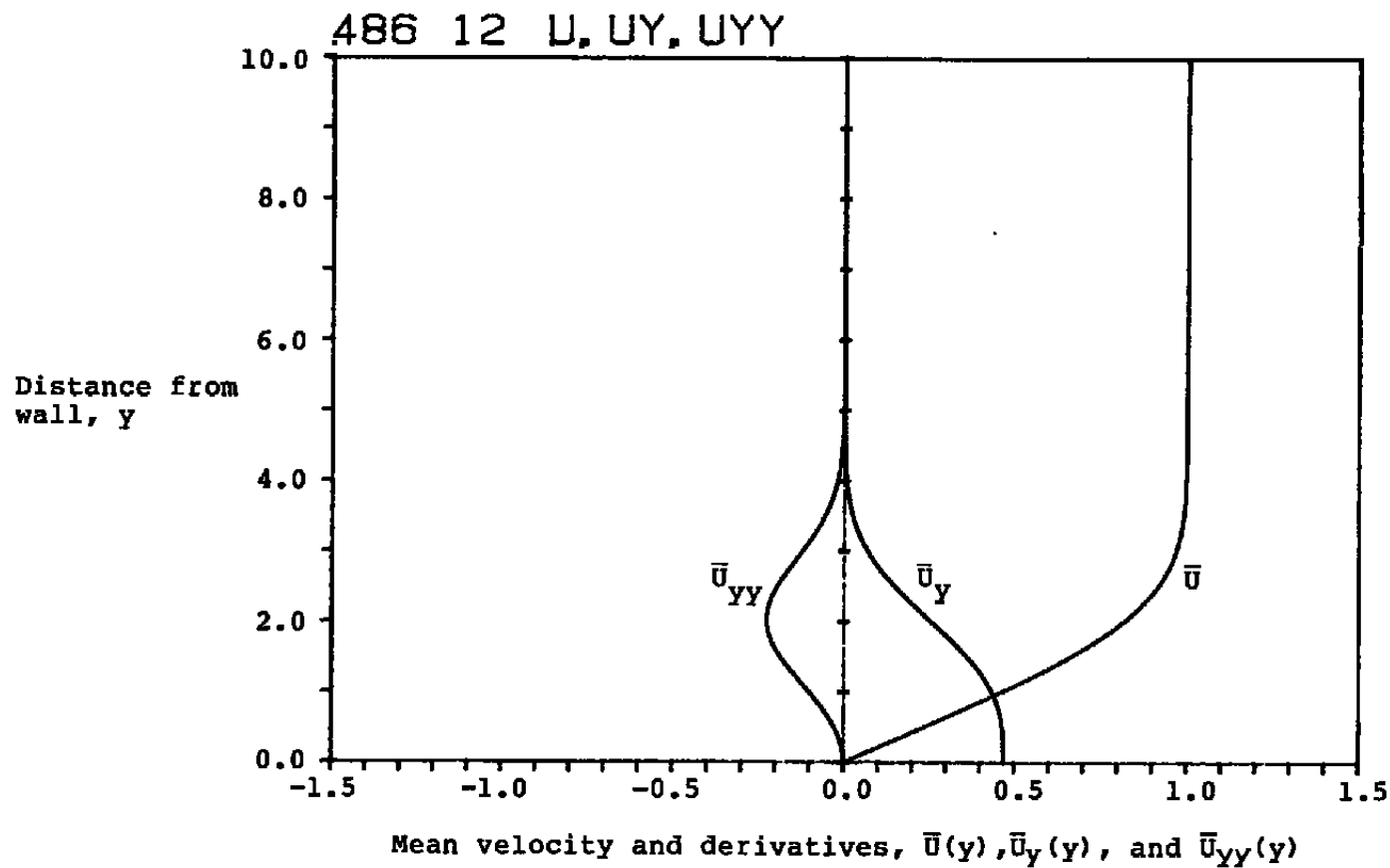|	
Effects of frequency on rms v	3.34
Effects of frequency on rms u	3.35
Effects of frequency on rms u in sublayer	3.36
Effects of Reynolds number on rms v	3.37
Effects of Reynolds number on rms u	3.38
Effects of Reynolds number on rms u in sublayer	3.39
Effects of R_δ and ω, holding ωR_δ constant	3.40
Effects of y-wavenumber or decay rate	3.41

486 12 U. UY. UYY

Figure 3.1   The mean velocity profile and first two derivatives for a
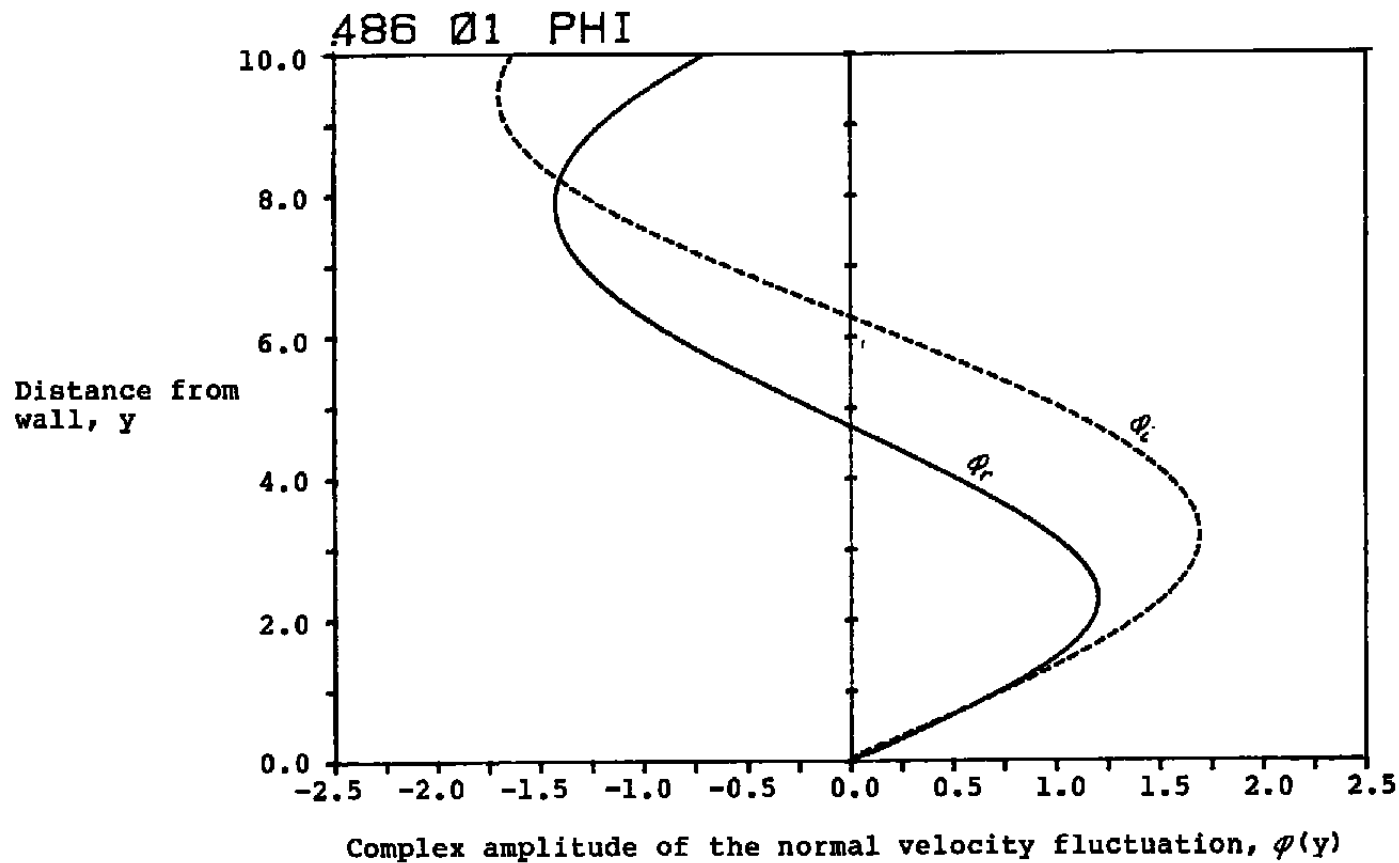Blasius boundary layer.

486 01 PHI

Figure 3.2 The variation of the normal velocity fluctuation with distance from the wall for a decaying wave, $\exp(-\beta x)$, for $\beta = \omega = 0.5$ and $R_\delta = 1000$ with a Blasius boundary layer.

this, observe that the node where $\phi_r = 0$ shifts upward to the node where $\phi_i = 0$.

In Figure 3.3 for the longitudinal velocity, note that the no-slip condition is satisfied and again note the general oscillatory behavior further away. The fluctuating velocity inside tne boundary layer is much larger than the velocity in the boundary layer witn decaying, vortical structures in the freestream.

In Figure 3.3, also note the thin viscous sublayer near the wall, with a velocity overshoot at the sublayer edge. In Figure 3.4, the ordinate is stretched and the longitudinal velocity is plotted for the sublayer region. The analytical solution for the sublayer, as presented in Appendix B, is also plotted in Figure 3.4. This solution is

$$f(y) = f_\infty \left(1 - e^{-my} \right)$$

(3.7)

where $\quad m = \left(i \omega R_\delta \right)^{1/2}$

and f_∞ = complex constant representing the value of f at the sublayer "edge".

The streamlines for the fluctuating flow at time zero are plotted in Figure 3.5. Note the oscillatory pattern in the y-direction and tne effects of the exponential decay in the streamwise direction, $\exp(-\beta x)$. A 16mm movie of the standing wave has been prepared using a sequence of 64 streamline patterns representing the flowfield at 64 times during a half-cycle.

The fluctuating vorticity, $\zeta = v_x - u_y$, is plotted in Figure 3.6, which shows a large spike of vorticity near the wall associated with the viscous sublayer. This vorticity mainly arises from the derivative $-u_y$ while the derivative v_x is zero or small. The large magnitude of the derivative u_y in the sublayer can be seen in Figures 3.3 and 3.4.

The abscissa in Figure 3.6 was stretched in Figure 3.7 to better display the layer of vorticity appearing about midway in the boundary layer; the much larger spike of vorticity in the sublayer is not completely plotted in Figure 3.7. Note in either Figure 3.6 or 3.7 that far above the boundary layer into the freestream, the flow is irrotational. The iso-vorticity contours are plotted in Figure 3.8 which shows the highly skewed nature of the vorticity waves in the sublayer. The single contour toward the center of the bounaary layer represents the bulge in vorticity near y = 2 in Figure 3.7.

The fluctuating vorticity positioned approximately midway in the boundary layer has interesting properties which we will describe by posing two mathematical systems for inviscid flows:
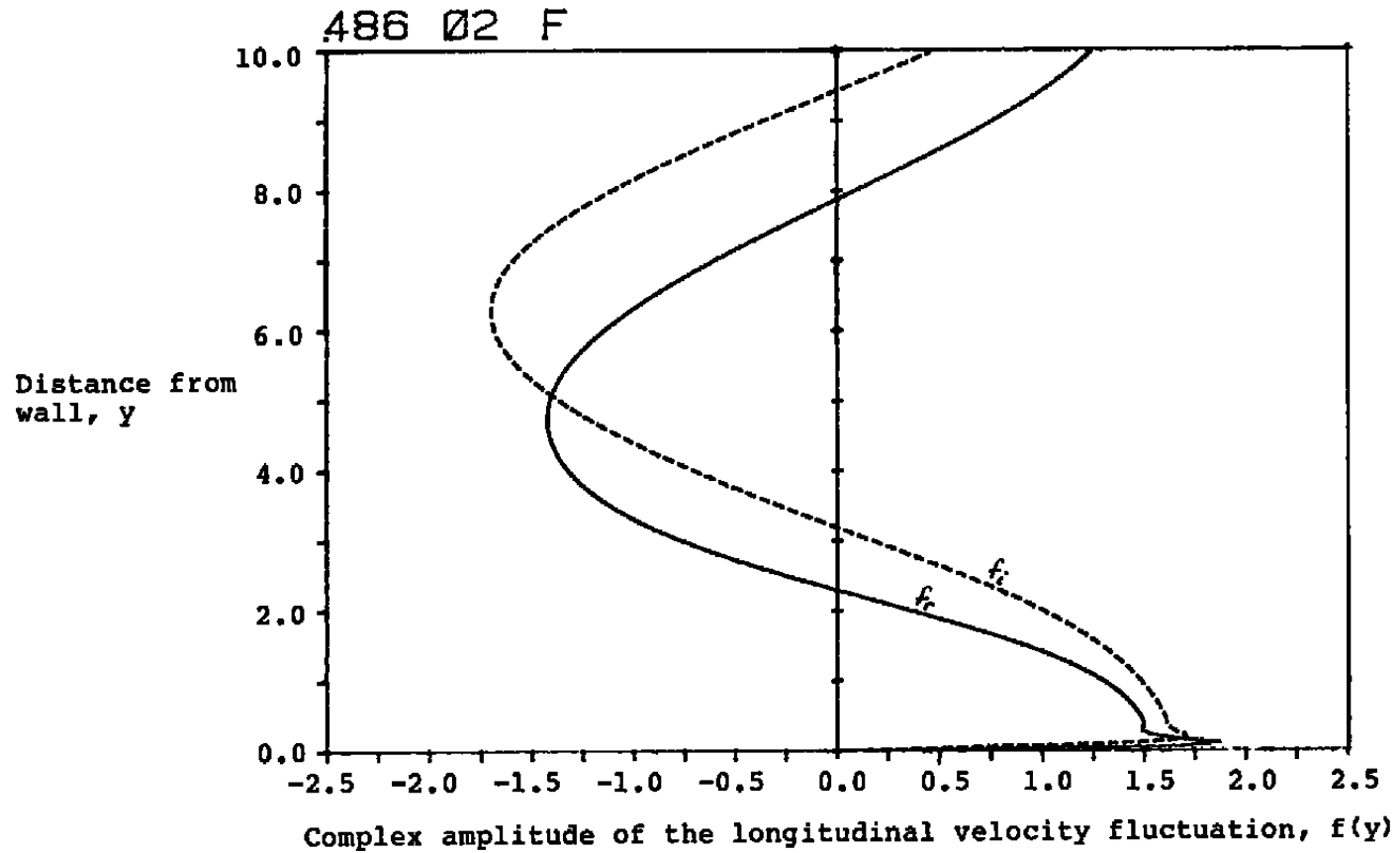
29

Figure 3.3 The variation of the longitudinal velocity fluctuation with distance from the wall for a decaying wave, $\exp(-\beta x)$, for $\beta = \omega = 0.5$ and $R_\delta = 1000$ with a Blasius boundary layer.

487 02 F

Figure 3.4   The longitudinal velocity fluctuation in the sublayer for a decaying wave, exp(-βx), for $\beta = \omega = 0.5$ and $R_\delta = 1000$ with a Blasius boundary layer.

486 Ø1 STREAMLINES

Figure 3.5   The streamlines of the unsteady flowfield for a decaying
wave, exp($-\beta$x), for $\beta = \omega = 0.5$ and R_δ=1000 with a Blasius
boundary layer.

486 03 Z

Figure 3.6 The variation of the vorticity fluctuation with distance
from the wall for a decaying wave, exp(-βx), for
β=ω= 0.5 and R_δ=1000 with a Blasius boundary layer. This
figure shows the vorticity in the sublayer. Figure 3.7
shows the vorticity in the middle of the boundary layer.

486 03 Z
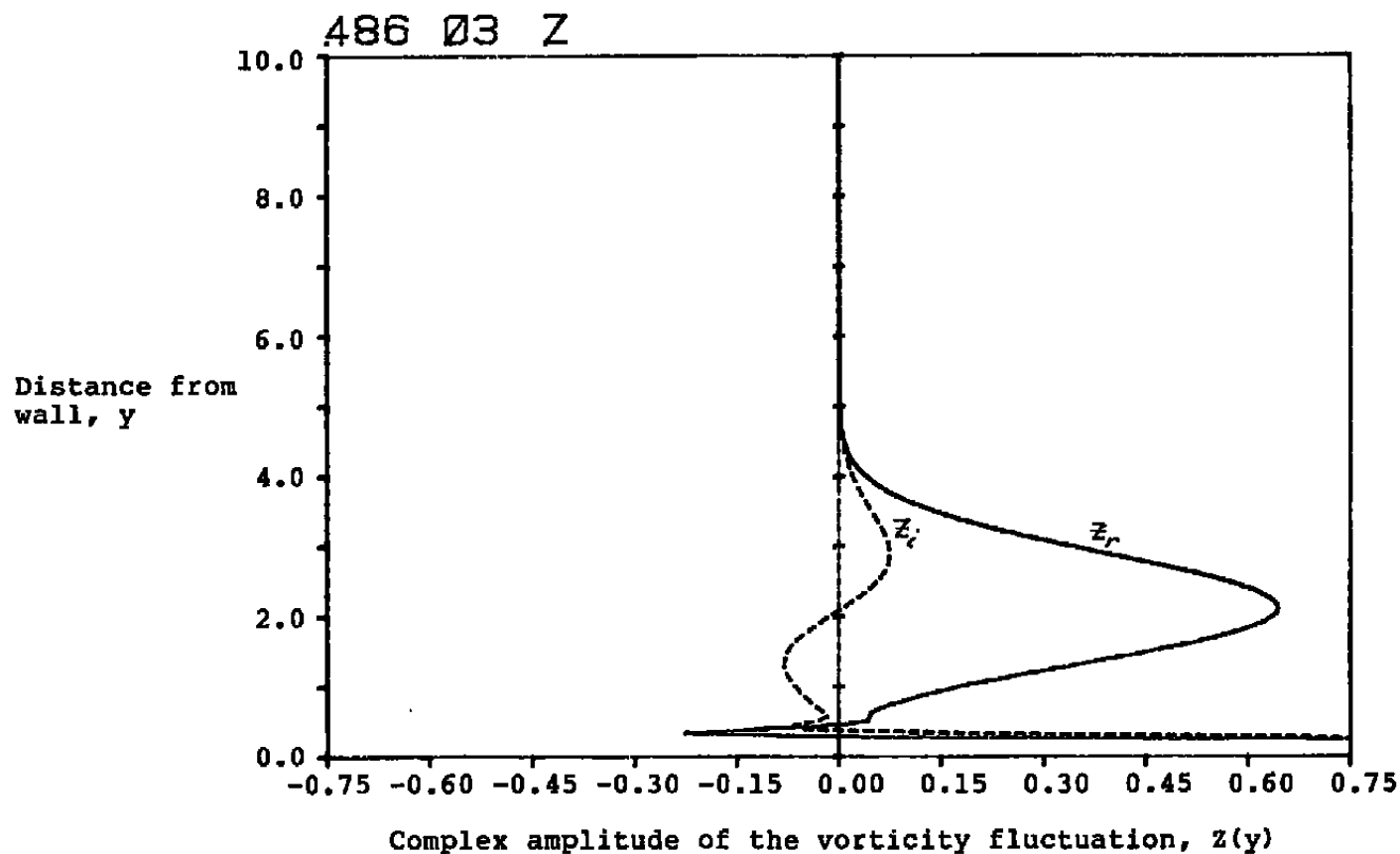
Figure 3.7 The variation of the vorticity fluctuation with distance from the wall for a decaying wave, exp($-\beta x$), for $\beta = \omega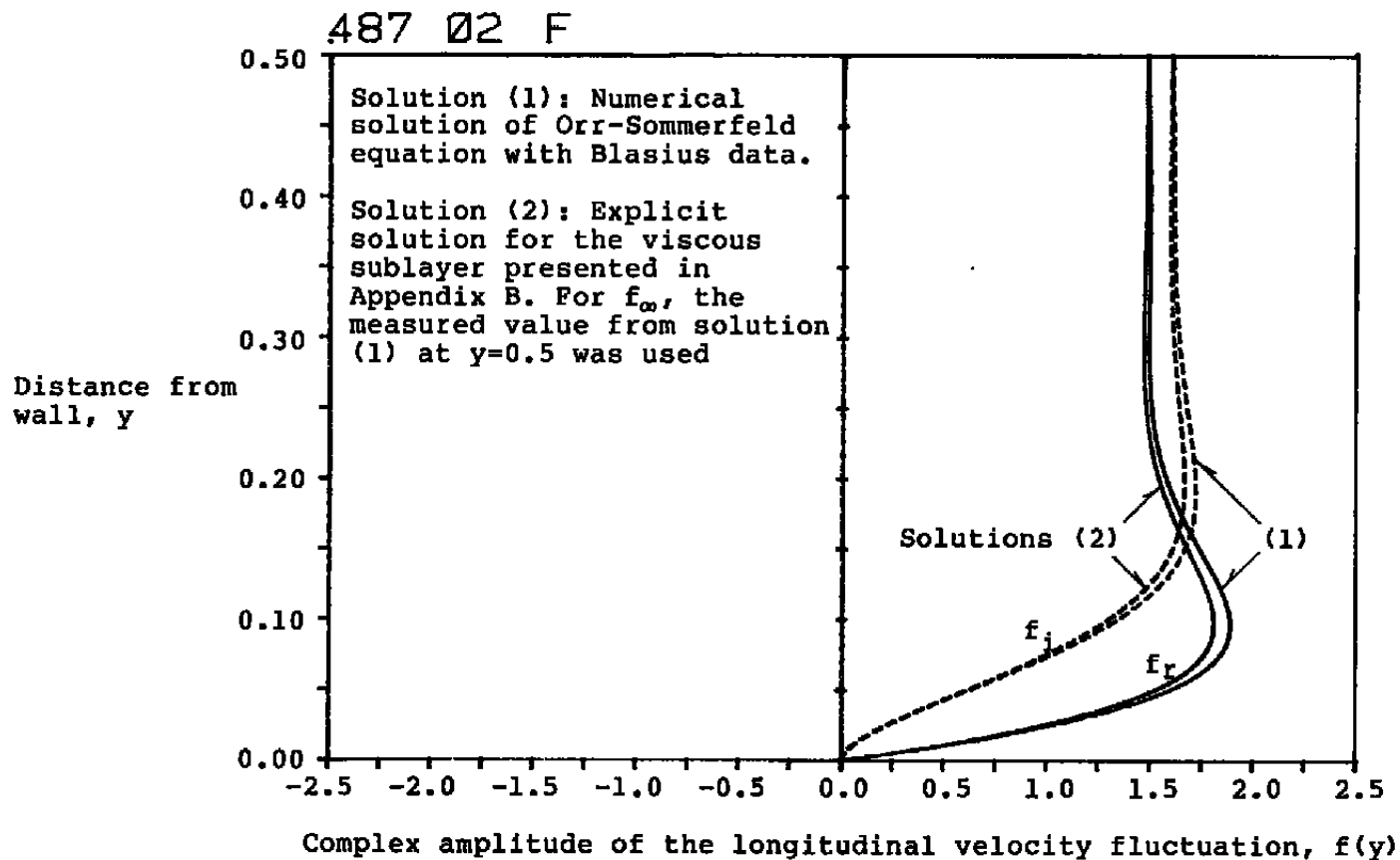 = 0.5$ and $R_\delta = 1000$ with a Blasius boundary layer. The abscissa has been stretched to show the details of the vorticity in the center of the boundary layer.

486 02 EQUI-VORTICITY CONTOURS

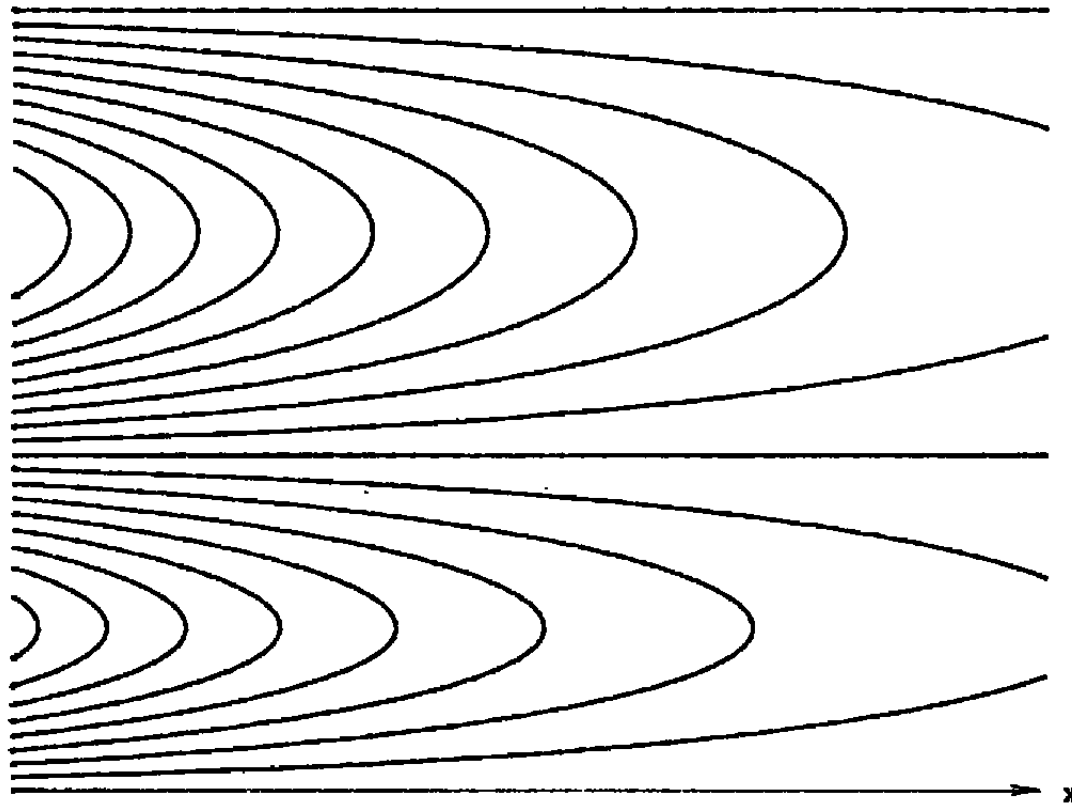Figure 3.8 The iso-vorticity contours of the unsteady flowfield for a decaying wave, $\exp(-\beta x)$, for $\beta = \omega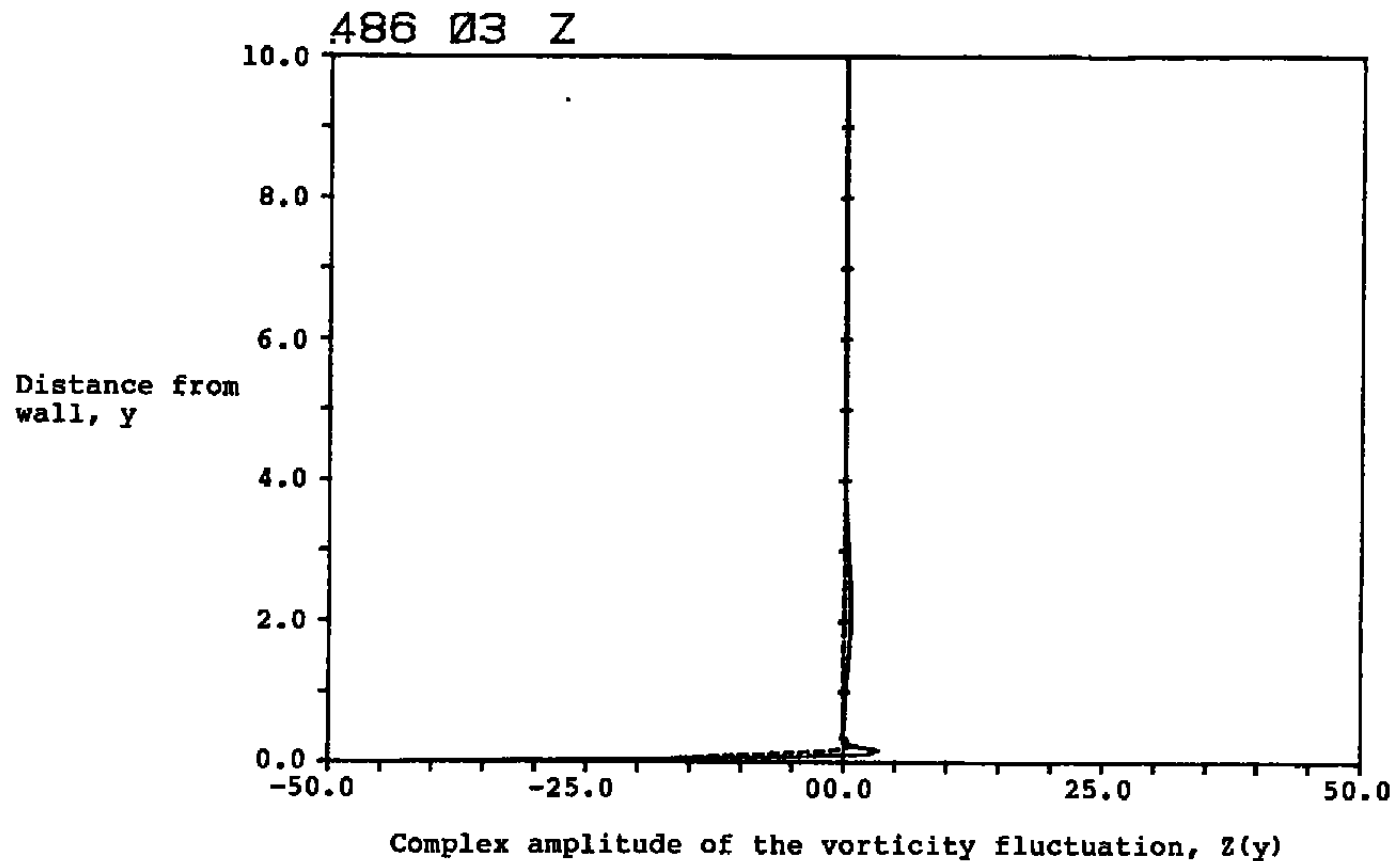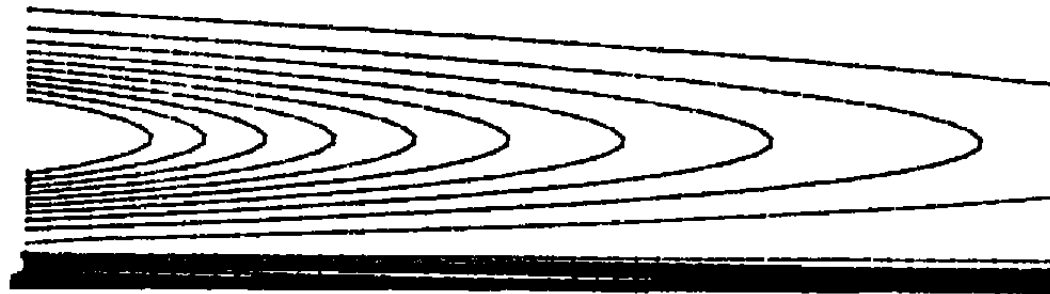 = 0.5$ and $R_\delta = 1000$ with a Blasius boundary layer. Fifty-seven contours were plotted with unequal increments of vorticity.

(1) If there were no vorticity production term, the relevant vorticity equation would be

$$\zeta_t + \bar{U}(y)\,\zeta_x = 0 \tag{3.8}$$

i.e., the vorticity at any station x,y at time t is the vorticity at x=0 at the earlier time t-x/U(y). The vorticity would merely convect downstream with the local mean velocity, $\bar{U}(y)$. Since the vorticity at x=0 oscillates in time

$$\zeta(0, y, t) = Z(y)\,e^{-i\omega t} \tag{3.9}$$

the solution further downstream would be

$$\zeta(x, y, t) = Z(y)\,e^{-i\omega(t - x/\bar{U})} = Z(y)\,e^{i\frac{\omega}{\bar{U}}(x - \bar{U}t)} \tag{3.10}$$

which is a <u>travelling wave, in disagreement with the assumed standing wave solution</u> of form

$$\zeta = Z(y)\,e^{-\beta x - i\omega t} \tag{3.11}$$

One may wonder then, for a standing wave, what causes the vorticity to decay exponentially in the streamwise direction (at one instant of time)? To an observor travelling with the mean flow, $\bar{U}(y)$, how can the vorticity oscillate?

(2) We believe that one mechanism which influences the vorticity to behave as a standing wave is the vorticity production term, $-v\bar{U}_{yy}$, which is a linearized version of the convection term $V\zeta_y$ in the vorticity equation. The linearized, inviscid equation for fluctuating vorticity is

$$\underset{\substack{\text{rate of change of vorticity}\\\text{as seen by an observor moving}\\\text{with the local mean flow}}}{\zeta_t + \bar{U}\zeta_x} + \underset{\substack{\text{rate of}\\\text{production}}}{v\,\bar{\zeta}_y} = 0 \tag{3.12}$$

For high Reynolds number, small y-wavenumber conditions, we suspect that fluctuating vorticity is created in the central region of the boundary layer, as described by the production term, in such a manner that a standing wave is possible. The magnitude of the vorticity which is produced depends on the time available, and hence the frequency. While this process occurs in the central region of the boundary layer, diffusion is possible in the sublayer. The relative roles of tne production term and the two diffusion terms (in the viscous

equation) could be determined by plotting the terms separately.

The complex amplitude of the vorticity production is plotted in Figure 3.9. The production vanishes at the wall and in the freestream. The contours of equi-value of the production, $-v(x,y,t)\bar{U}_{yy}(y)$ at time zero are plotted in Figure 3.10.

The diffusion term in the streamwise direction

$$\epsilon \, \zeta_{xx} = \epsilon \beta^2 Z(y) e^{-\beta x - i\omega t}$$

is merely $\epsilon \beta^2$ times the vorticity itself. The other diffusion term, $\epsilon \, \zeta_{yy}$, has not been plotted.

The smoothly oscillating amplitudes $\pi(y) = \pi_r + i\pi_i$ of the fluctuating pressure are plotted in Figure 3.11. Note the relative constancy of the pressure across the sublayer, but clearly the pressure varies across the mean boundary layer itself. The corresponding pressure isobars are plotted in Figure 3.12.

The rms quantities for the velocities, vorticity, and pressure are plotted in Figures 3.13-3.16. The oscillatory behavior in the direction normal to the wall is apparent in these figures. The viscous sublayer is shown clearly by the longitudinal velocity in Figure 3.14, and by the spike of vorticity near the wall in Figure 3.15.

The Reynolds stress, $-\overline{uv}$, and the kinetic energy production, $-\overline{uv}d\bar{U}/dy$, are plotted in Figures 3.17 and 3.18. The Reynolds stress oscillates into the freestream. The energy production is confined to the boundary layer, of course, where it is mainly negative although having a small positive region. It vanishes at the wall where $v=0$ and in the freestream where $\bar{U}_y=0$.

The averaged kinetic energy $(\overline{u^2}+\overline{v^2})/2$ of the fluctuation flow is plotted in Figure 3.19 which clearly shows the sublayer and overshoot at the sublayer edge. In the freestream, the kinetic energy is uniform in the y-direction; it decays as $\exp(-2\beta x)$ in the streamwise direction.

3.2.2 Favorable and Adverse Pressure Gradient Cases with Decaying Waves

Figures 3.20-3.26 are results for the decaying wave with a favorable pressure gradient boundary layer. Figures 3.27-3.33 are results with an adverse pressure gradient boundary layer. The corresponding figure numbers for these two cases and the Blasius case are tabulated below for reference.

486 13 VORTICITY PRODUCTION

Distance from
wall, y

Complex amplitude of the vorticity production, $-\varphi\bar{U}_{yy}$

Figure 3.9   The variation of the vorticity production with distance
from   the   wall   for   a   decaying   wave, $\exp(-\beta x)$,   for
$\beta = \omega = 0.5$ and $R_\delta = 1000$, and a Blasius boundary layer.

Figure 3.10   The equi-value contours of the production of fluctuating
               vorticity for a decaying wave, $\exp(-\beta x)$, for $\beta = \omega = 0.5$,
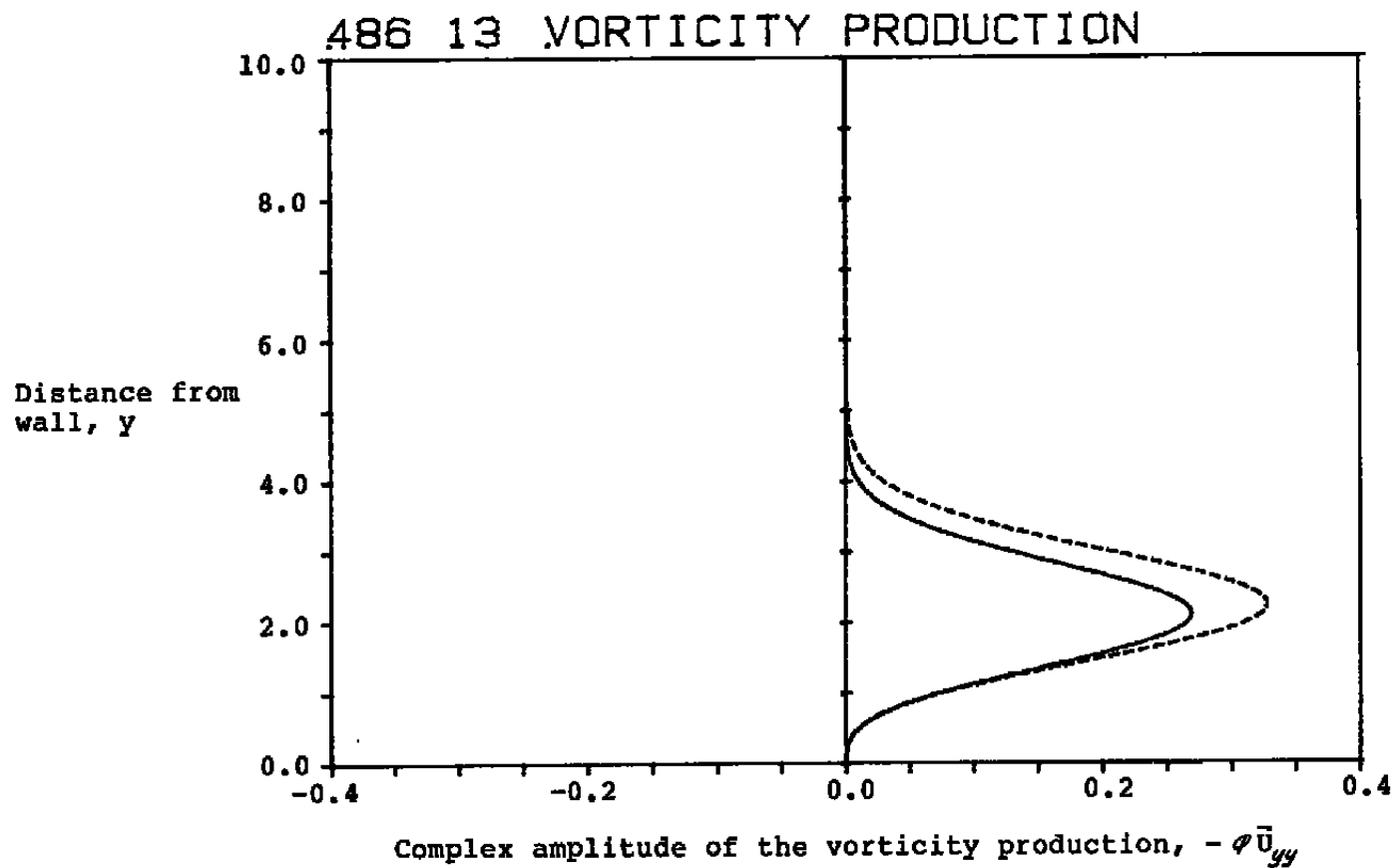 $R_\delta = 1000$ at time $t = 0$ with a Blasius boundary layer.

Figure 3.11 The variation of the pressure fluctuation with distance from the wall for a decaying wave, exp(−βx), for $\beta = \omega$ = 0.5 and R_δ=1000 with a Blasius boundary layer.

486 03 PRESSURE ISOBARS

Figure 3.12   The pressure isobars for a decaying wave,   exp($-\beta$x),   for
$\beta = \omega$ = 0.5, R_δ =1000, time   t = 0 with a Blasius boundary
layer.

Figure 3.13   The variation of the rms normal velocity fluctuation with
distance from the wall for a decaying wave, $\exp(-\beta x)$, for
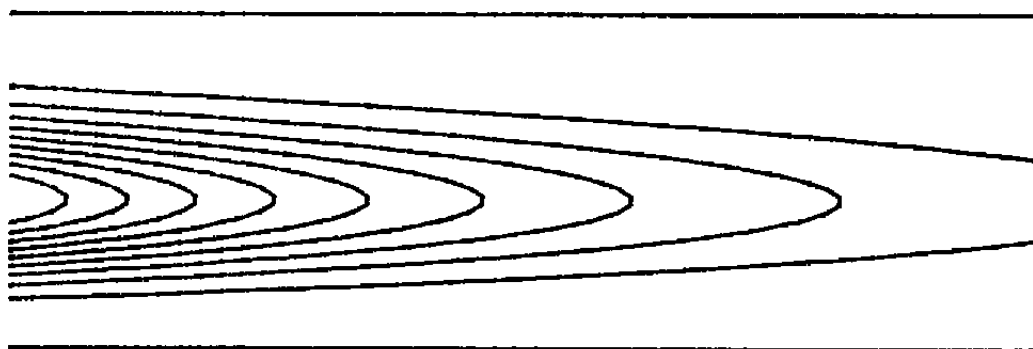$\beta = \omega = 0.5$ and $R_\delta = 1000$, and a Blasius boundary layer.

540 05 URMS
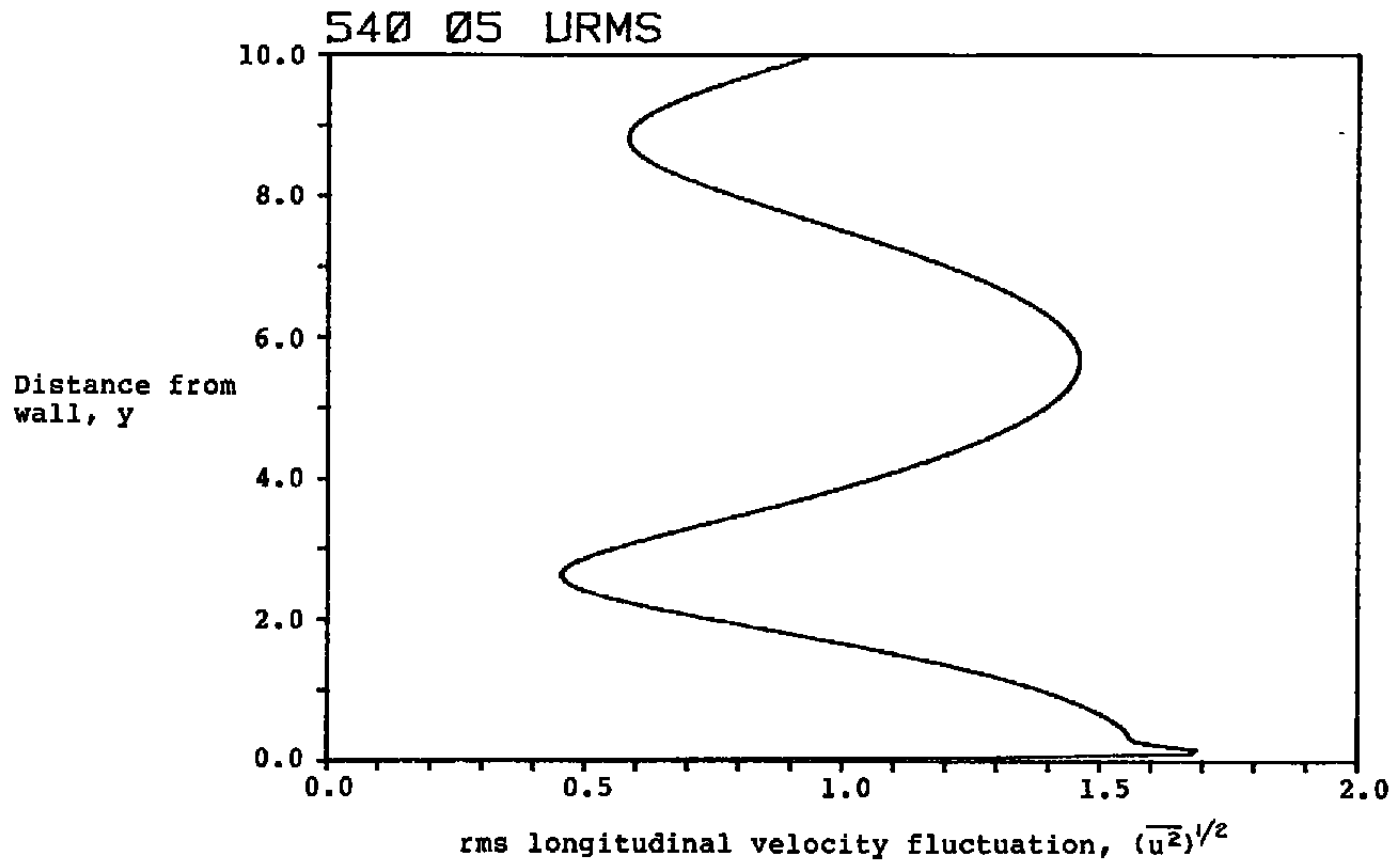
Figure 3.14 The variation of the rms longitudinal velocity fluctuation with distance from the wall for a decaying wave, exp(-βx), for $\beta = \omega = 0.5$ and $R_\delta = 1000$ with a Blasius boundary layer.
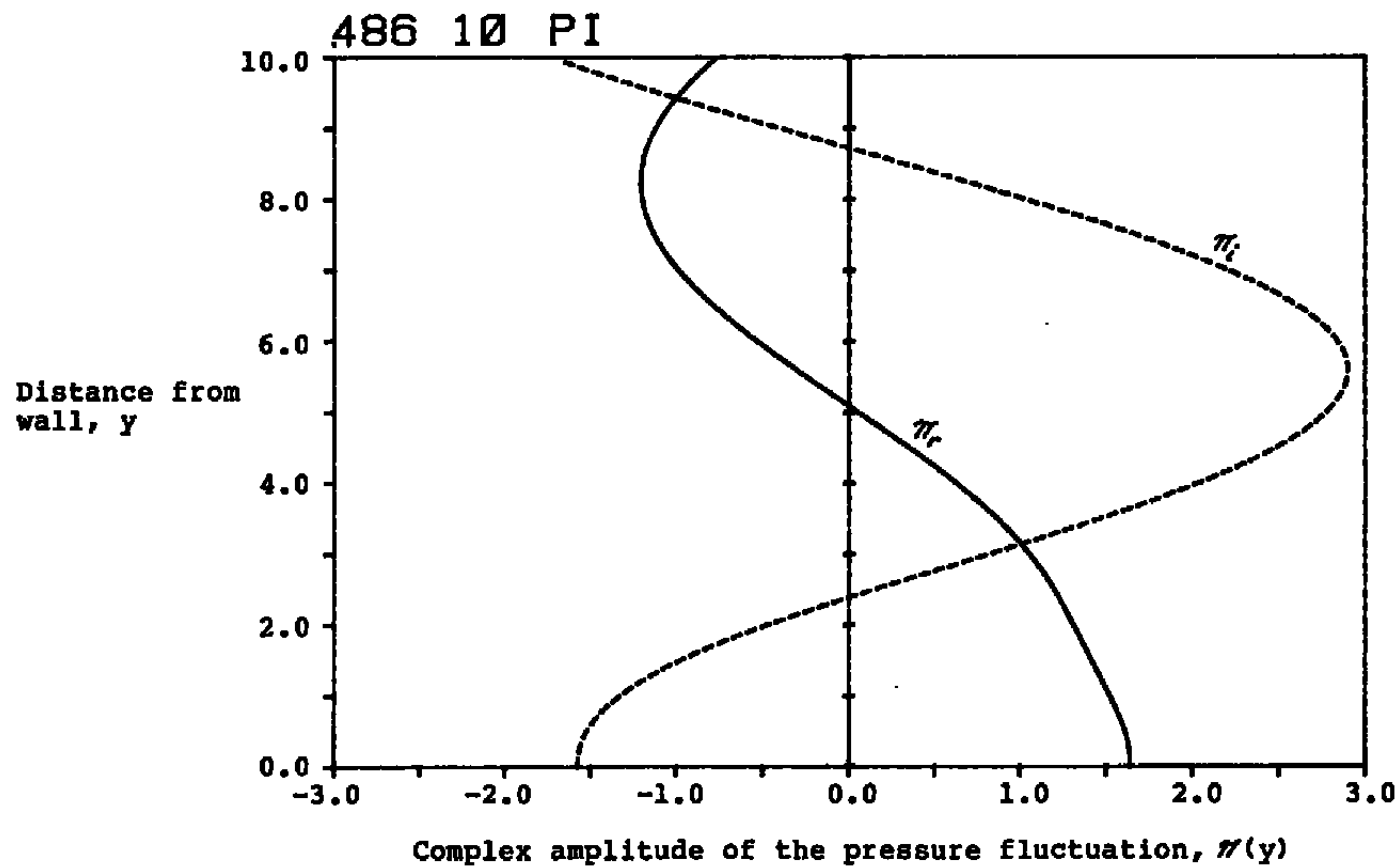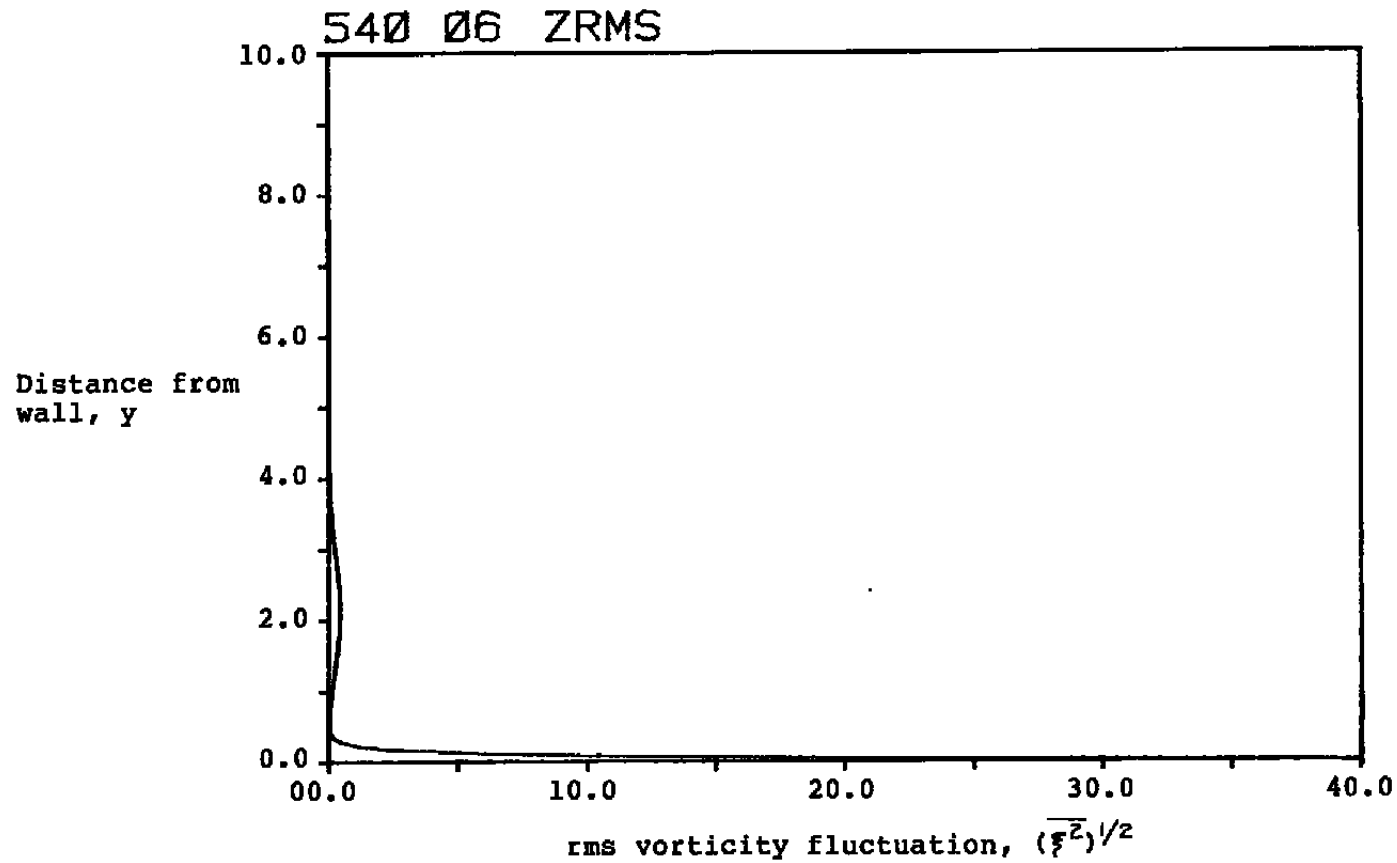
Figure 3.15   The variation of the rms vorticity fluctuation with distance from the wall for a decaying wave, $\exp(-\beta x)$, for $\beta = \omega = 0.5$ and $R_\delta = 1000$ with a Blasius boundary layer.

540 11 PRMS

Distance from
wall, y

rms pressure fluctuation, $(\overline{p^2})^{1/2}$
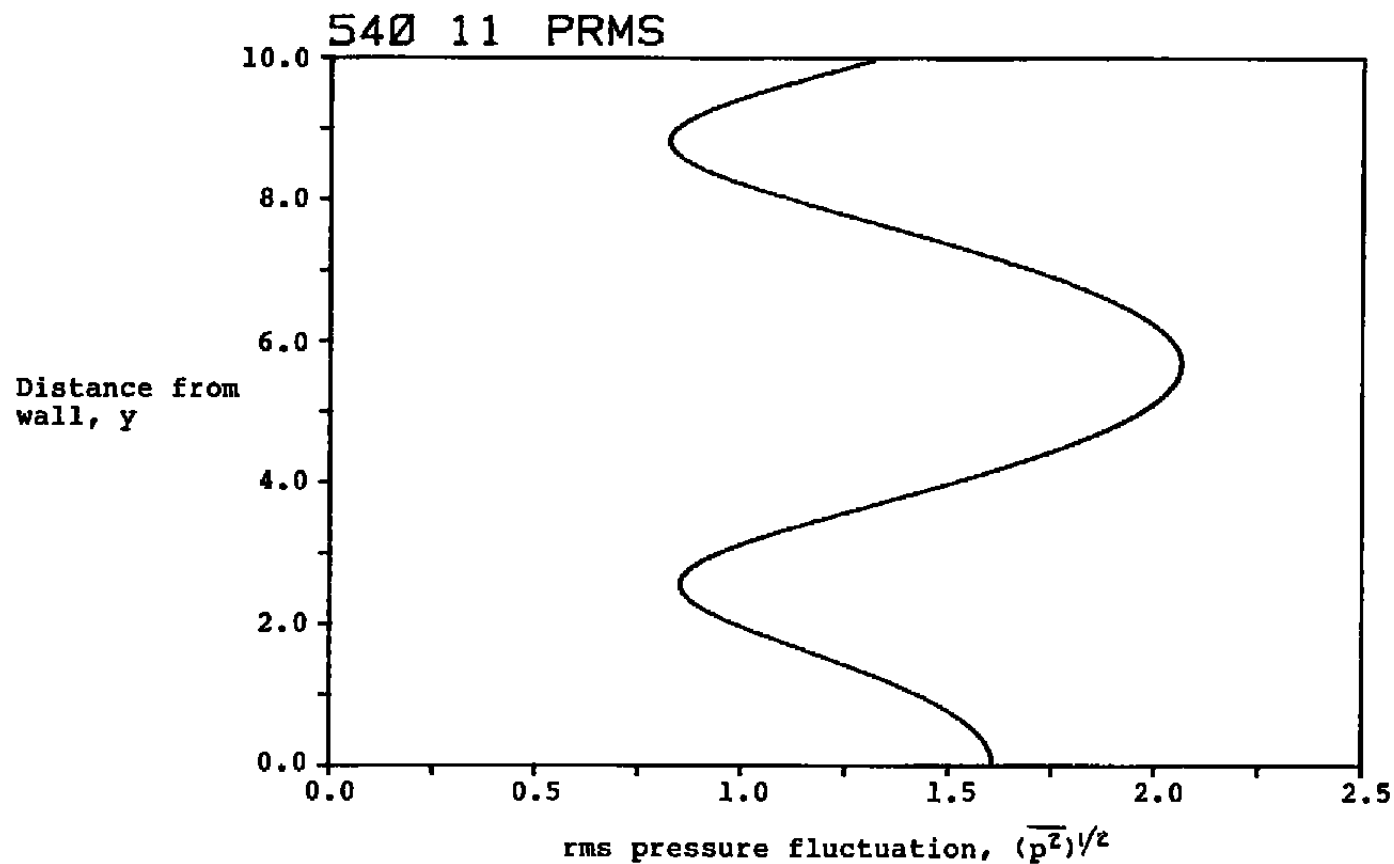
Figure 3.16   The   variation   of   the   rms   pressure   fluctuation   with
distance from the wall for a decaying wave, exp$(-\beta x)$, for
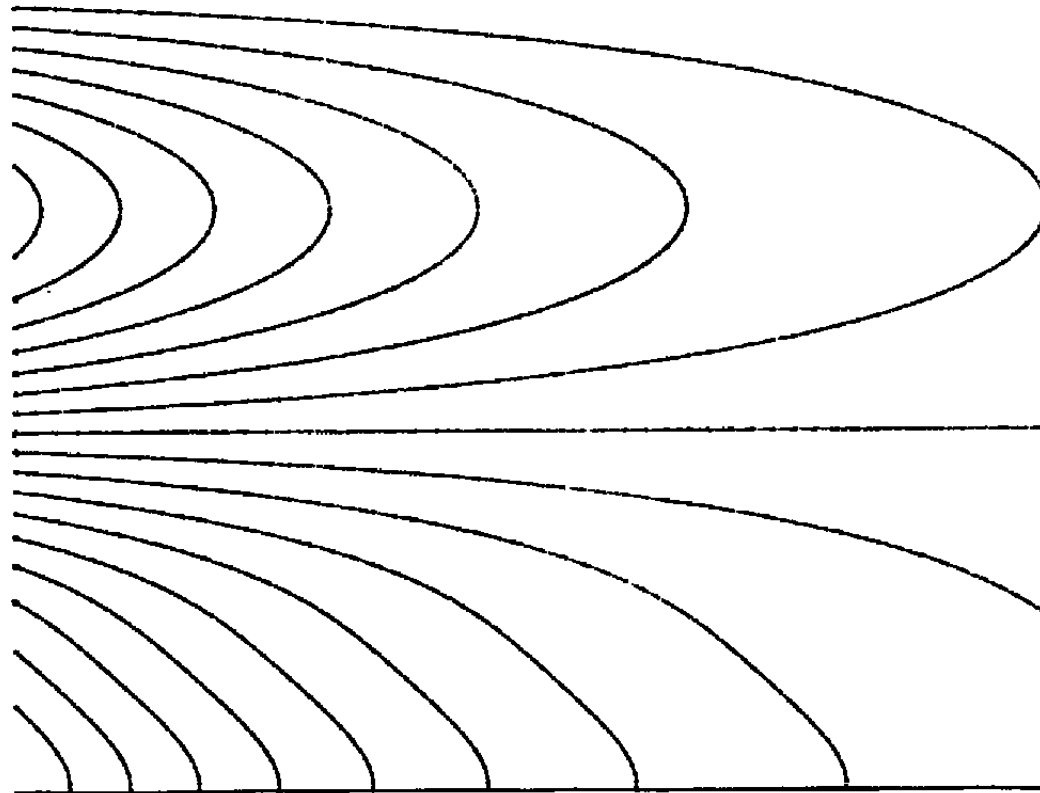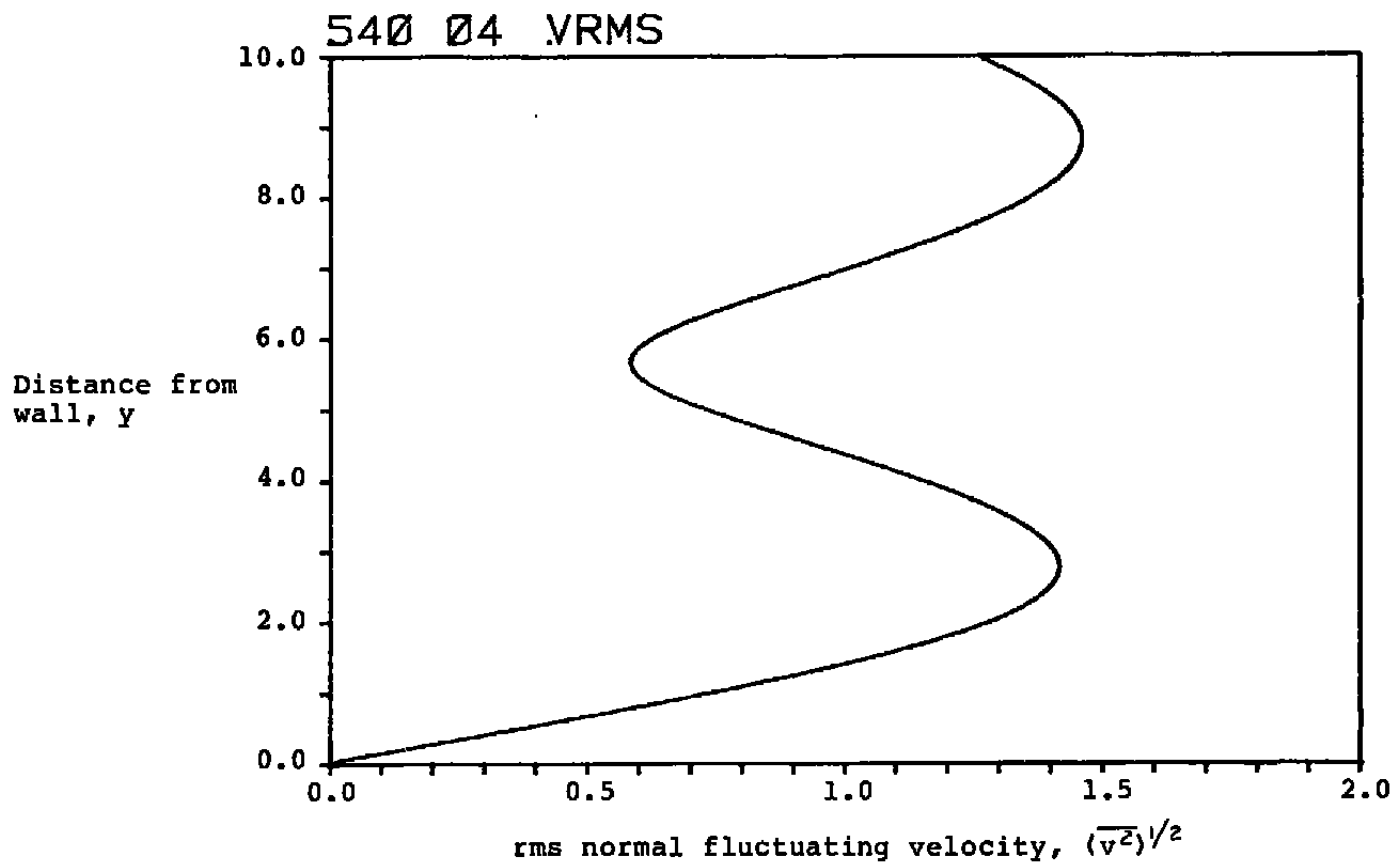$\beta = \omega = 0.5$ and $R_\delta = 1000$ with a Blasius boundary layer.
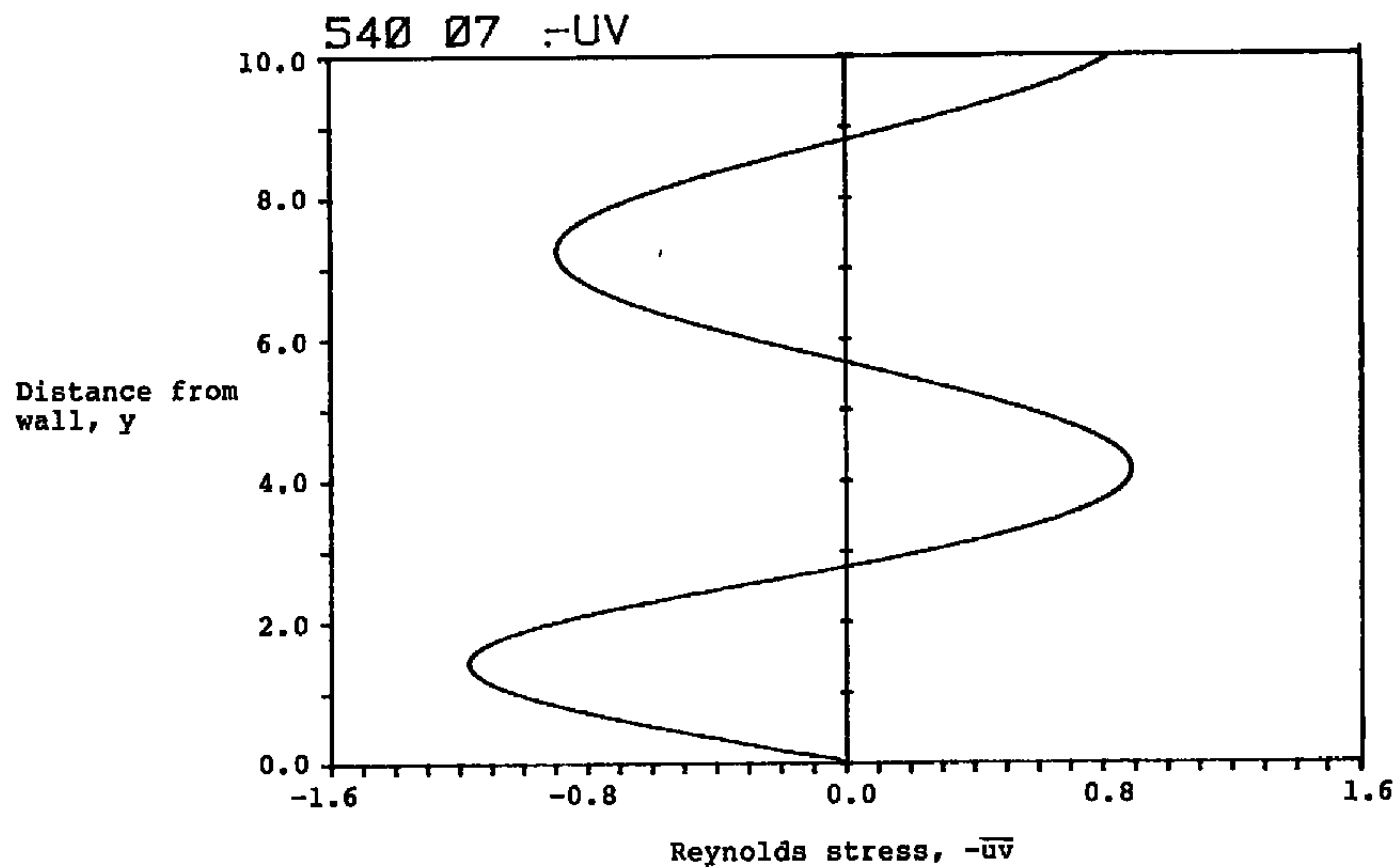
Figure 3.17   The variation of the Reynolds stress with distance from
the wall for a decaying wave for $\beta = \omega = 0.5$ and $R_\delta = 1000$
with a Blasius boundary layer.

549 09 -UVDU/DY

Figure 3.18   The variation of the energy production with distance from
the   wall   for   a decaying wave, exp(-βx), for $\beta = \omega$= 0.5
and R$_\delta$=1000 with a Blasius boundary layer.

Figure 3.19 The variation of the kinetic energy with distance from the wall for a decaying wave, exp(-βx), for $\beta = \omega = 0.5$ and R_δ=1000 with a Blasius boundary layer.

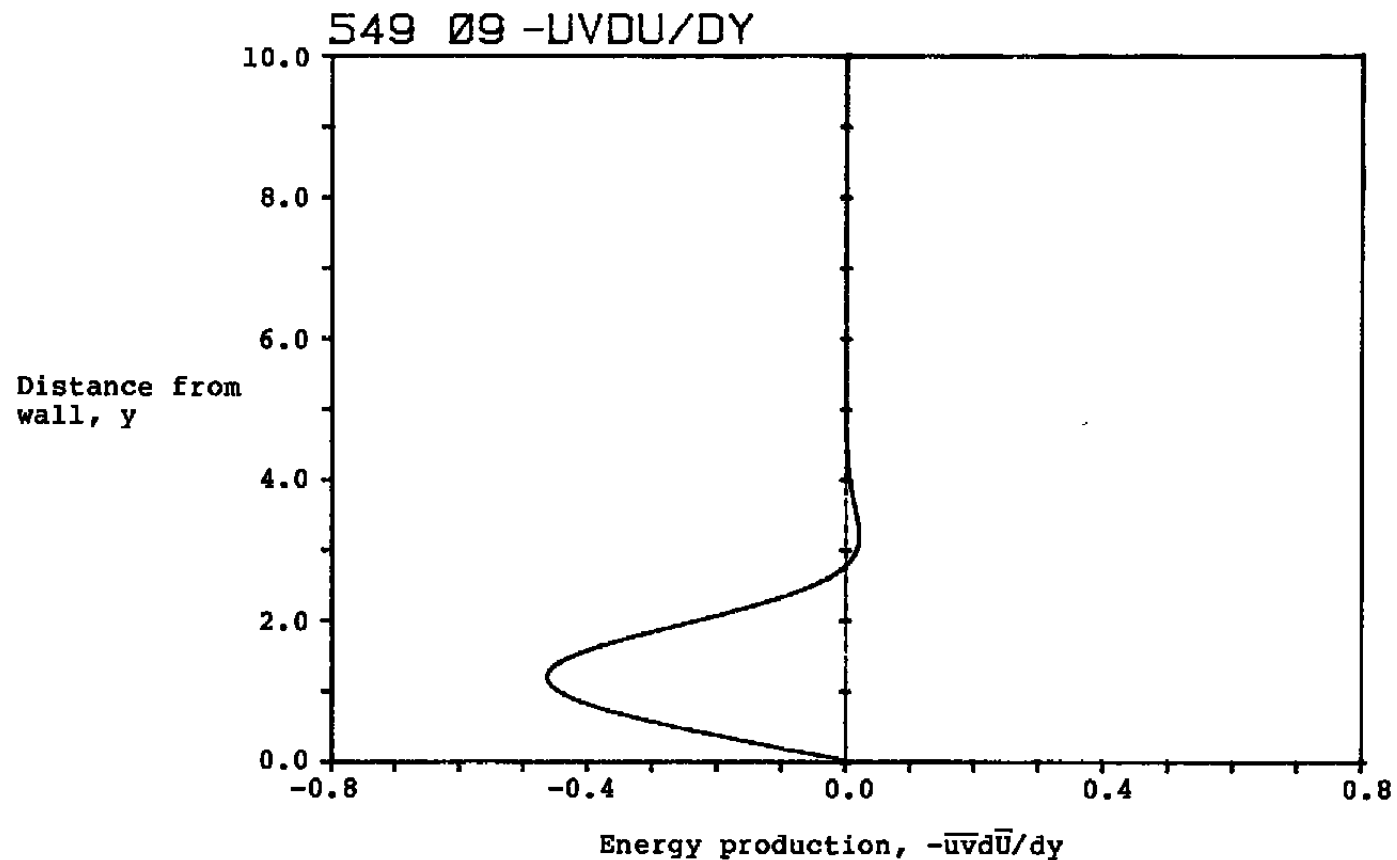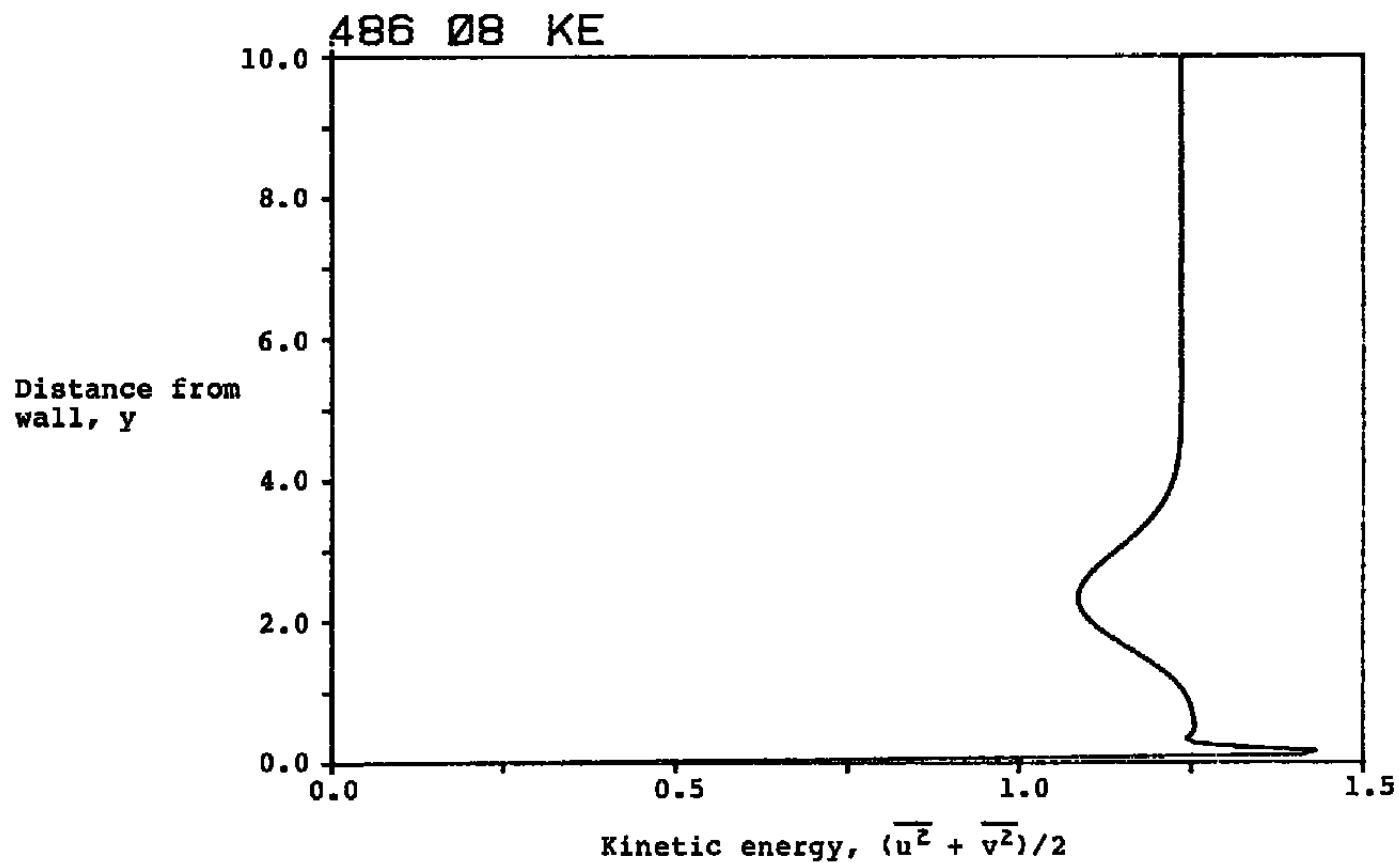|	favorable	Blasius	adverse
Falkner-Skan parameter, m_{FS}	0.5	0.0	−0.05
$\bar{U}$, $\bar{U}_y$, and $\bar{U}_{yy}$ Figure	3.20	3.1	3.27
	3.21	3.2	3.28
f	3.22	3.3	3.29
z	3.23	3.6	3.30
π	3.24	3.11	3.31
$-\overline{uv}$	3.25	3.17	3.32
$-\overline{uv}d\bar{U}/dy$	3.26	3.18	3.33

A plot-by-plot comparison of the three cases shows that the solutions for the standing wave depend on the Falkner-Skan parameter. The maximum values and the y-positions for those maximum values depend on the mean profile.

The general trend is that the curves are shifted upward as the Falkner-Skan parameter decreases. The energy production acquires a positive region near the boundary layer edge as the Falkner-Skan parameter takes on negative values.

Based upon the idea that one effect of surface roughness is to alter the mean velocity profile, then our calculations with different Falkner-Skan parameters indicates that the surface roughness would influence the standing waves.

3.2.3 Effects of Frequency

As shown in Figures 3.34 and 3.35, the frequency significantly influences the rms normal and longitudinal velocities. Both figures indicate that the amplitude increases as the frequency increases. In these figures, the frequency is increased by a factor of 16 from $\omega = 1/8$ to $\omega = 2$. The points of minimum amplitude also shift upward as the frequency increases. It may be useful to normalize in other ways to reduce this dependence of the amplitude in the freestream on frequency.

A possible explanation for the larger amplitudes as frequency increases is based on the analytical solution (A.9) of Appendix A for the viscous, uniform flow case. The amplitude is

$$\varphi(y) = -e^{-my} + \cos\beta y - \frac{m}{\beta}\sin\beta y \qquad (A.9)$$

where $m = (-\beta R_s - \beta^2 - i\omega R_s)^{1/2} \approx \omega^{1/2}R_s^{1/2}(-\frac{\beta}{\omega} - i)^{1/2}$ for $R_s \ggg \beta$ $\qquad (A.8)$

Hence, the coefficient of $\sin\beta y$ is proportional to the square root of frequency when $\beta/\omega \lll 1$. For other cases, eqn.(A.8) above also suggests that the coefficient m/β would increase as ω increases. We offer this explanation as tentative, however, because the above

49

5Ø9 12 U. UY. UYY

Figure 3.20 The mean velocity profile and first two derivatives for a favorable pressure gradient boundary layer with a Falkner-Skan parameter 0.5

509 01 PHI

Distance from wall, y

Complex amplitude of the normal velocity fluctuation, $\varphi(y)$

Figure 3.21   The variation of the normal velocity fluctuation with distance from the wall for a decaying wave, exp($-\beta$x), for $\beta = \omega = 0.5$ and $R_\delta = 1000$ for a favorable pressure gradient boundary layer with a Falkner-Skan parameter 0.5

Figure 3.22   The variation of the longitudinal velocity fluctuation with distance from the wall for a decaying wave, $\exp(-\beta x)$, for $\beta = \omega = 0.5$ and $R_\delta = 1000$ for a favorable pressure gradient boundary layer with a Falkner-Skan parameter 0.5

Figure 3.23 The variation of the vorticity fluctuation with distance
from the wall for a decaying wave, $\exp(-\beta x)$, for
$\beta = \omega = 0.5$ and $R_\delta = 1000$ for a favorable pressure gradient
boundary layer with a Falkner-Skan parameter 0.5

Figure 3.24 The variation of the pressure fluctuation with distance
from the wall for a decaying wave, exp(-βx), for
β = ω = 0.5 and R_δ=1000 for a favorable pressure gradient
boundary layer with a Falkner-Skan parameter 0.5

Figure 3.25 The variation of the Reynolds stress with distance from the wall for a decaying wave, exp($-\beta$x), for $\beta = \omega = 0.5$ and R_δ=1000 for a favorable pressure gradient boundary layer with a Falkner-Skan parameter 0.5

Figure 3.26 The variation of the energy production with distance from the wall for a decaying wave, $\exp(-\beta x)$, for $\beta = \omega = 0.5$ and $R_\delta = 1000$ for a favorable pressure gradient boundary layer with a Falkner-Skan parameter 0.5
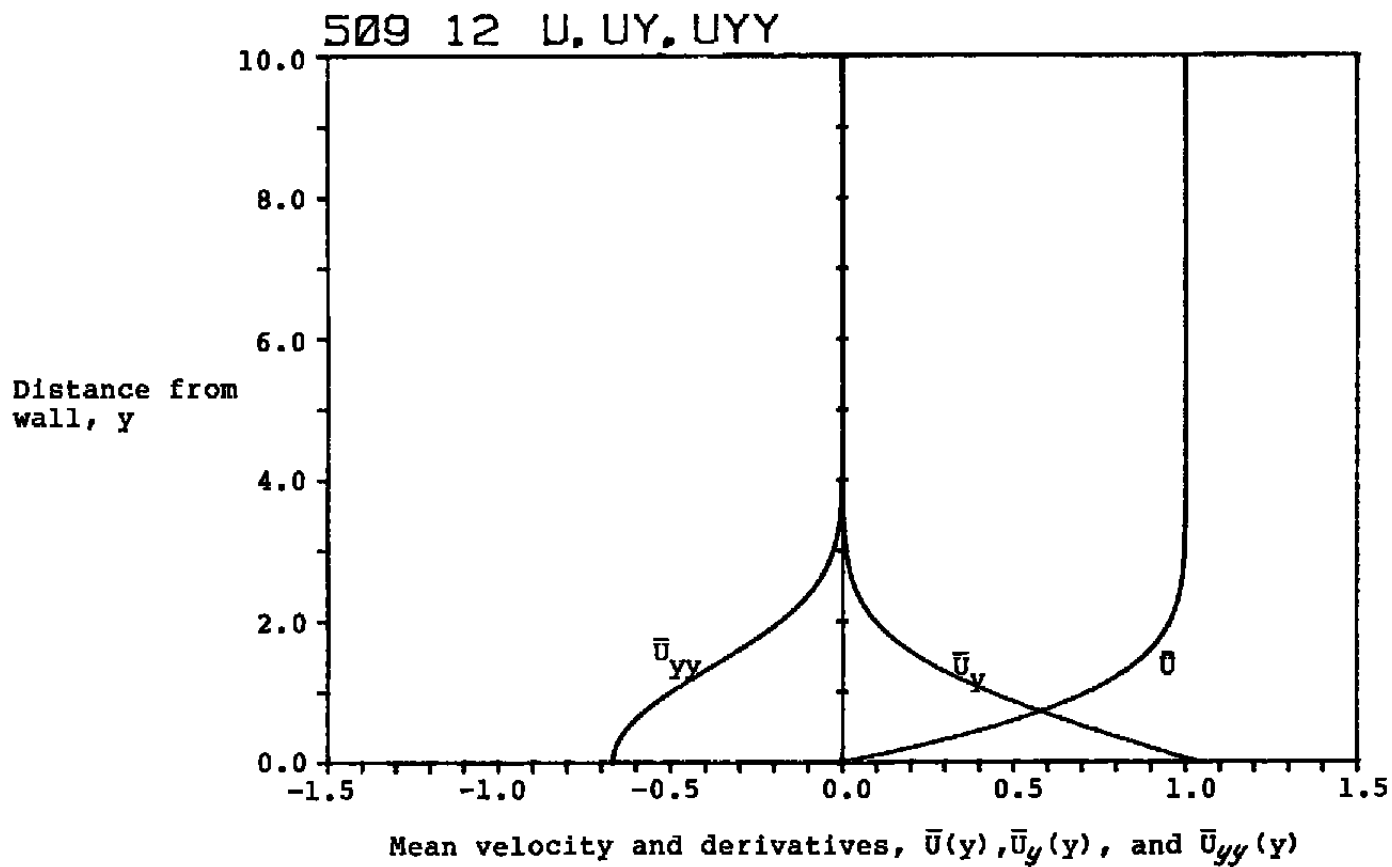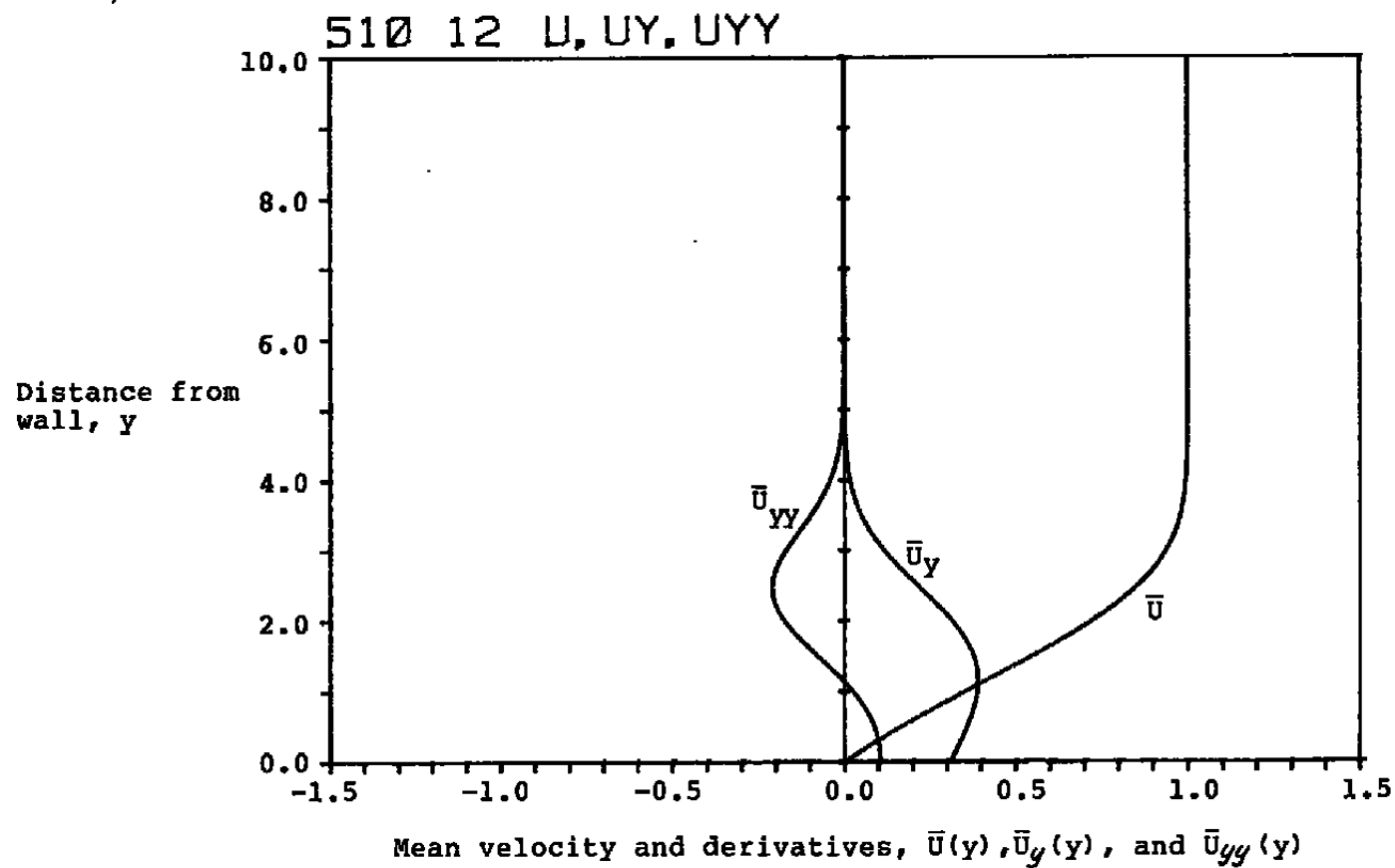
Figure 3.27 The mean velocity profile and first two derivatives for an unfavorable pressure gradient boundary layer with a Falkner-Skan parameter -0.05
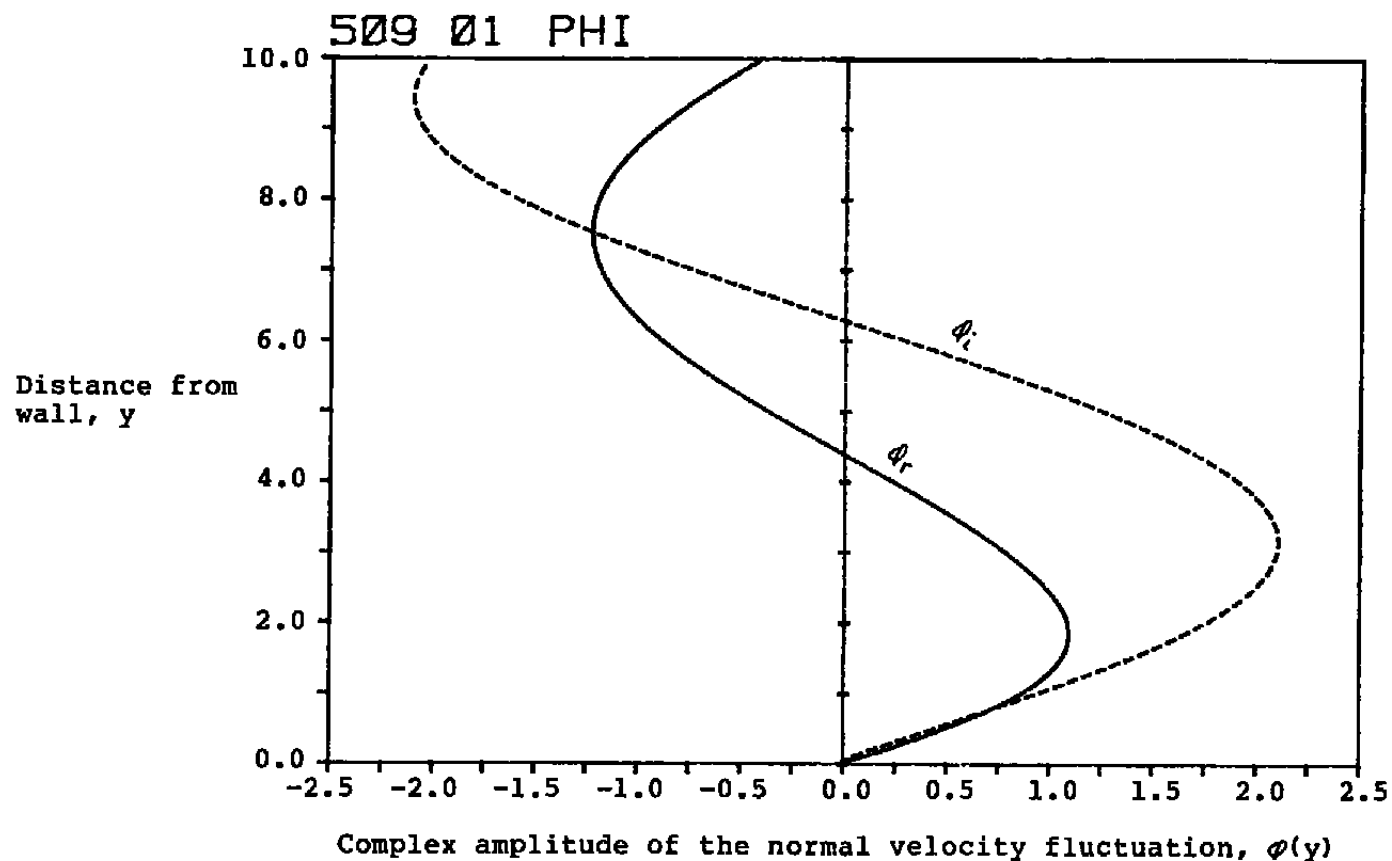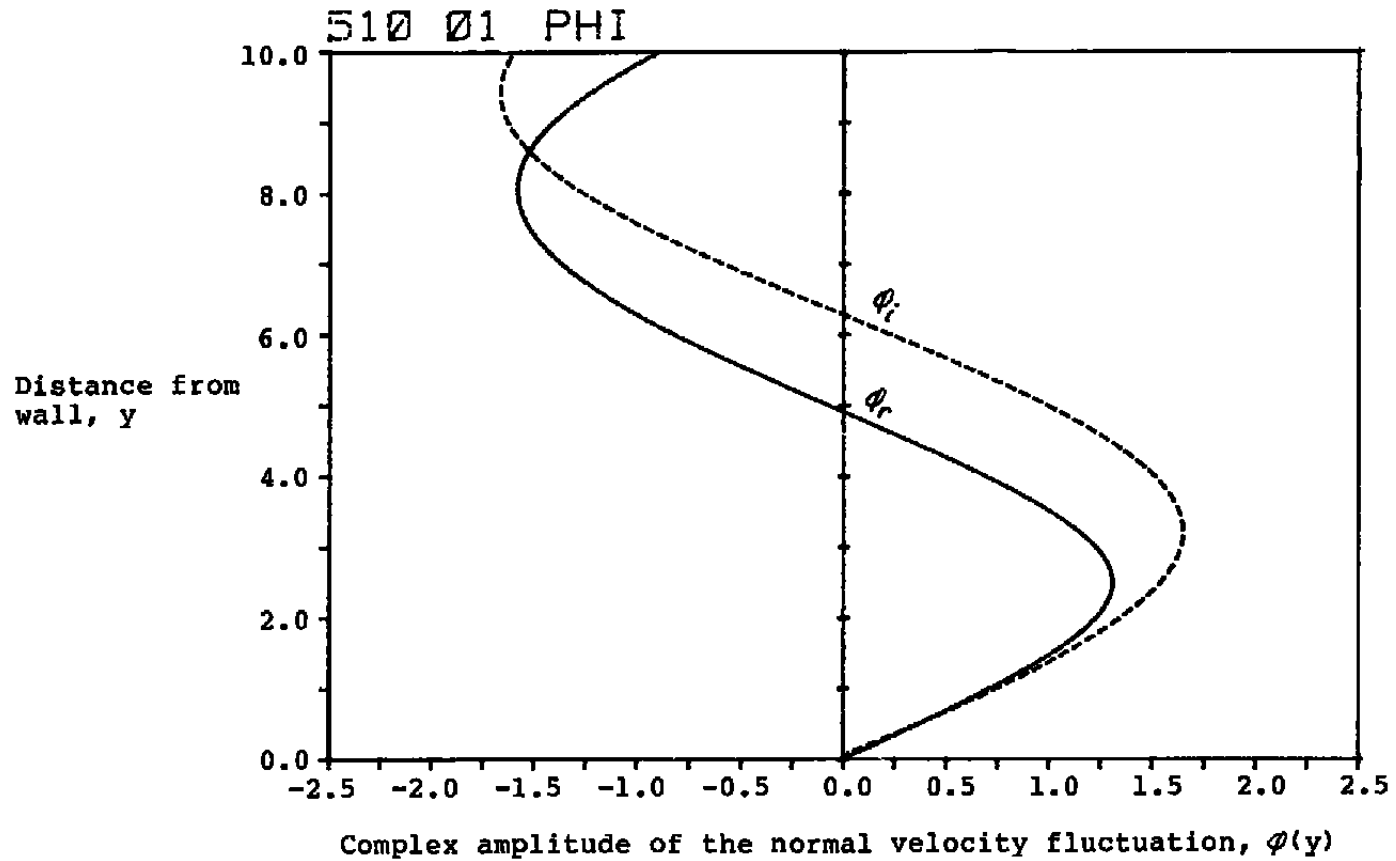
Figure 3.28   The variation of the normal velocity fluctuation with distance from the wall for a decaying wave, exp($-\beta$x), for $\beta = \omega = 0.5$ and $R_\delta = 1000$ for an unfavorable pressure gradient boundary layer with a Falkner-Skan parameter -0.05
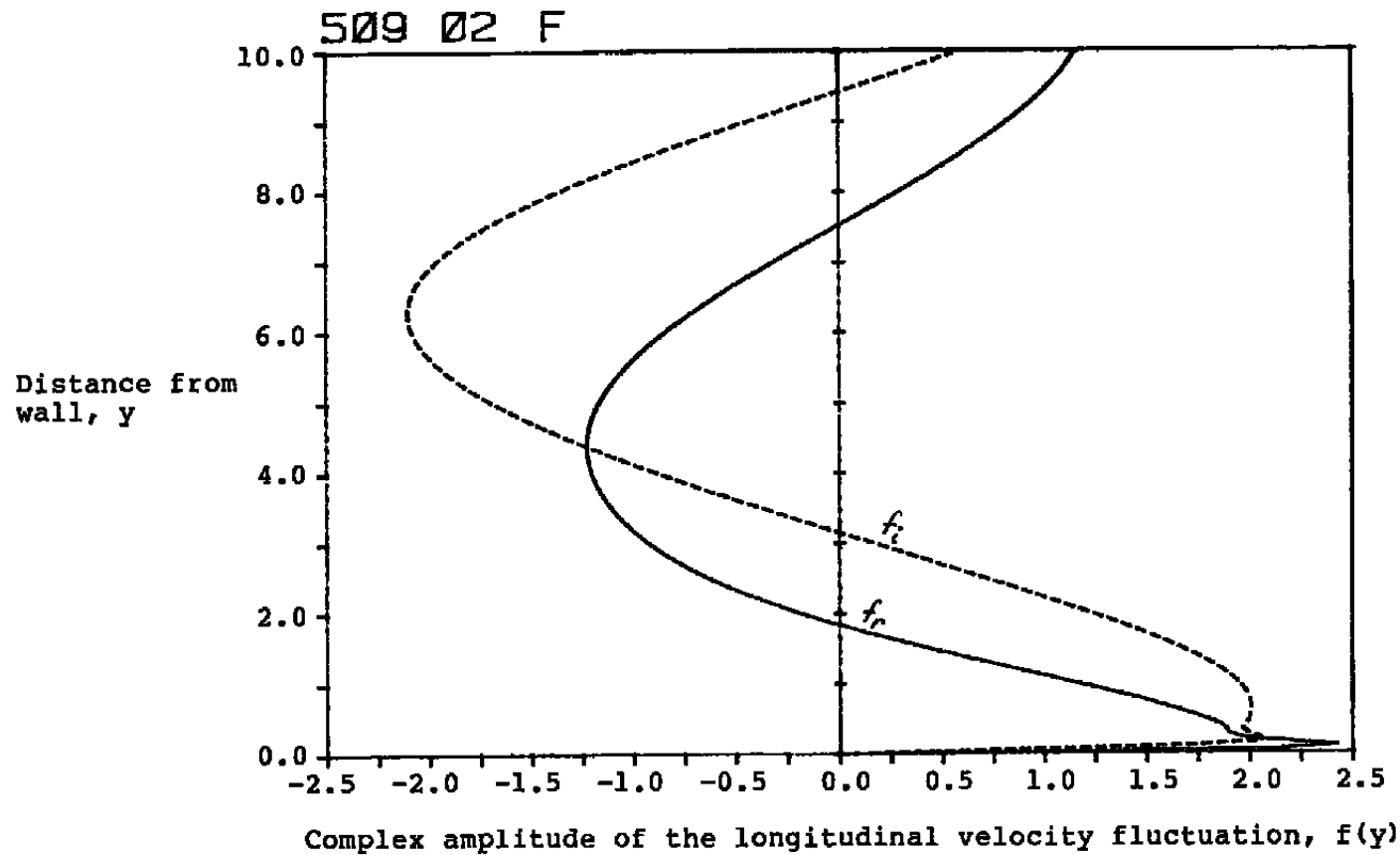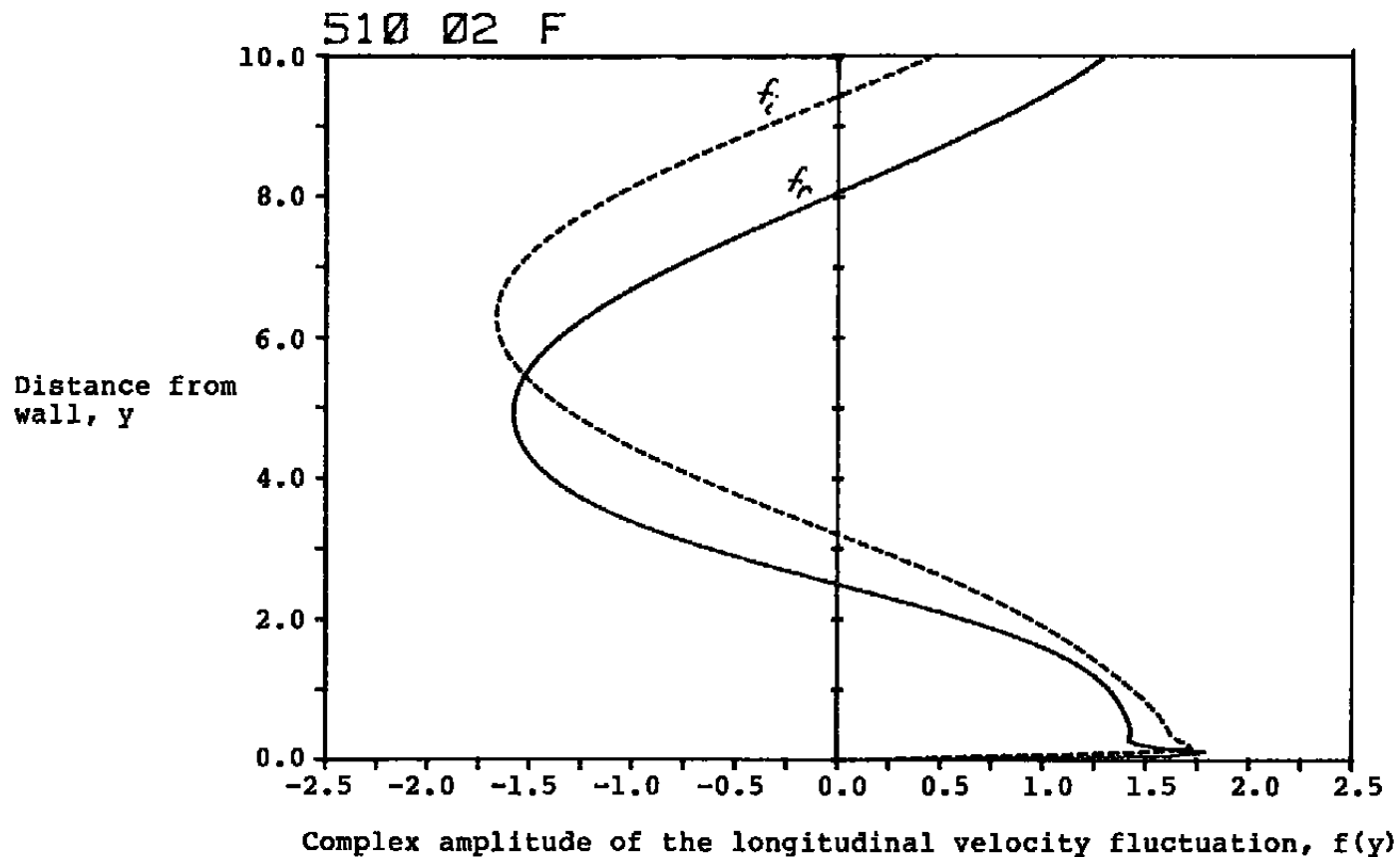
Figure 3.29 The variation of the longitudinal velocity fluctuation with distance from the wall for a decaying wave, $\exp(-\beta x)$, for $\beta = \omega = 0.5$ and $R_\delta = 1000$ for an unfavorable pressure gradient boundary layer with a Falkner-Skan parameter -0.05
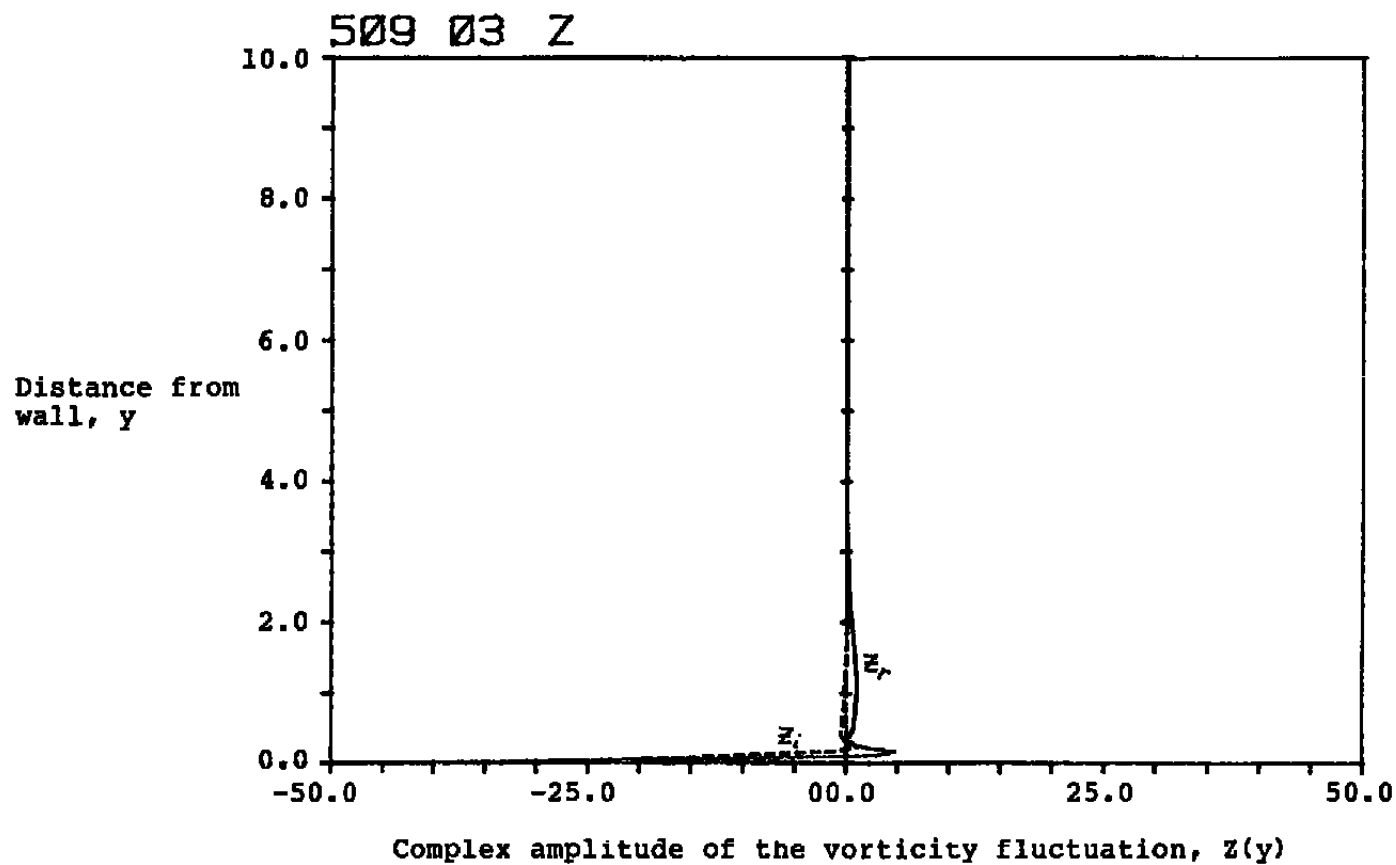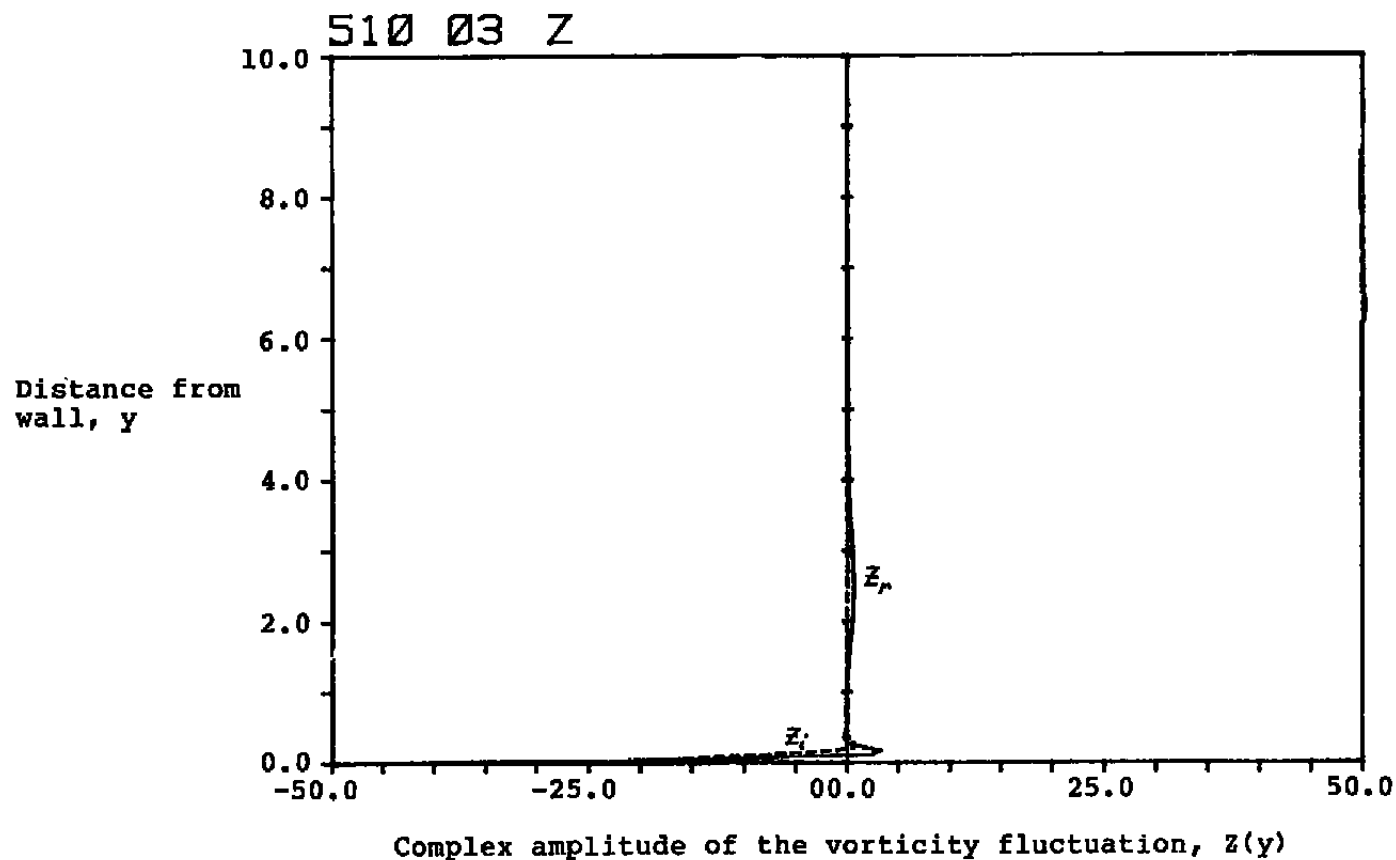
Figure 3.30   The variation of the vorticity fluctuation with distance
              from   the   wall   for   a   decaying   wave, $\exp(-\beta x)$,   for
              $\beta = \omega = 0.5$ and $R_\delta = 1000$ for   an   unfavorable   pressure
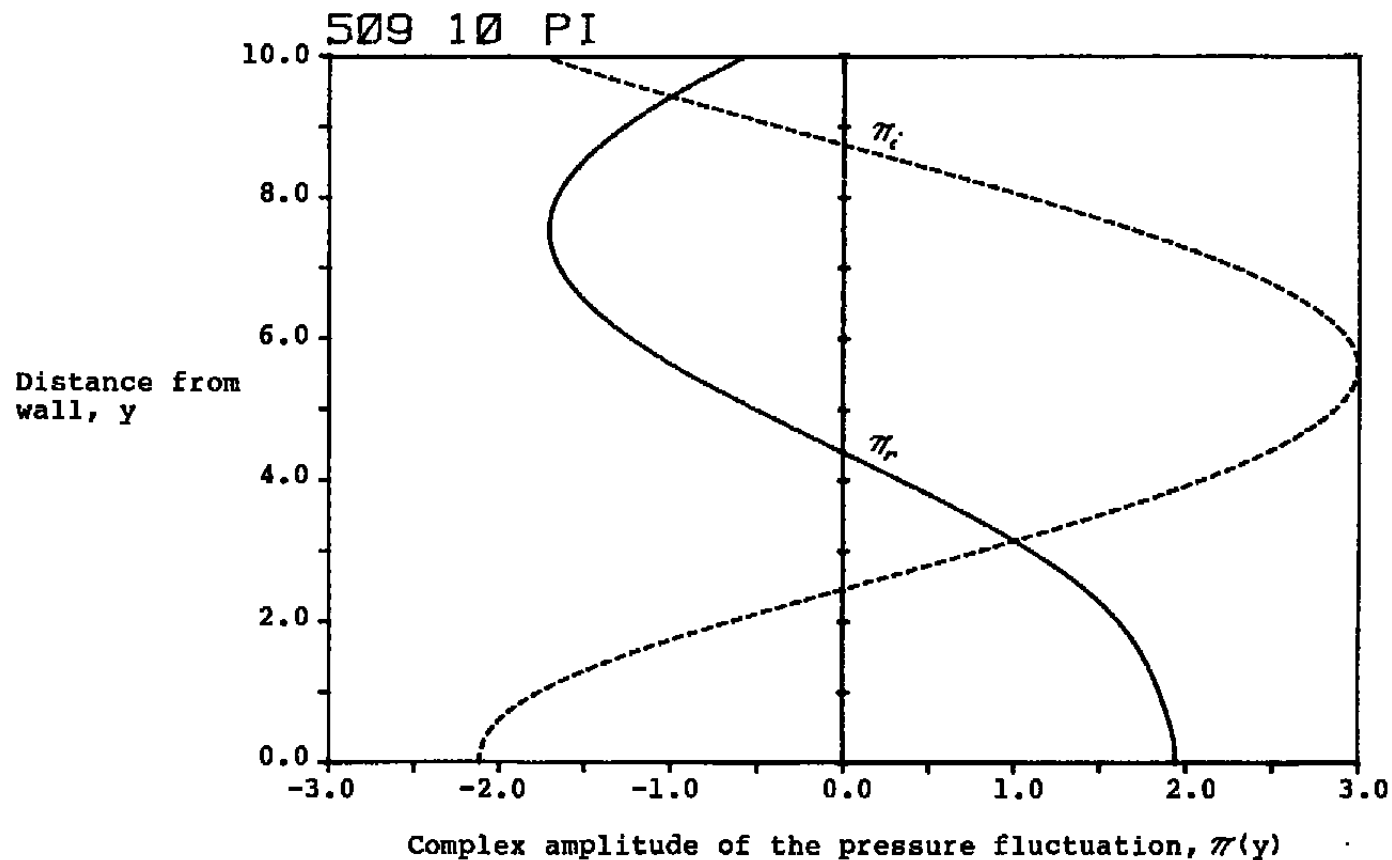   gradient boundary layer with a Falkner-Skan parameter
              -0.05

510 10 PI

Distance from wall, y

Complex amplitude of the pressure fluctuation, $\pi(y)$
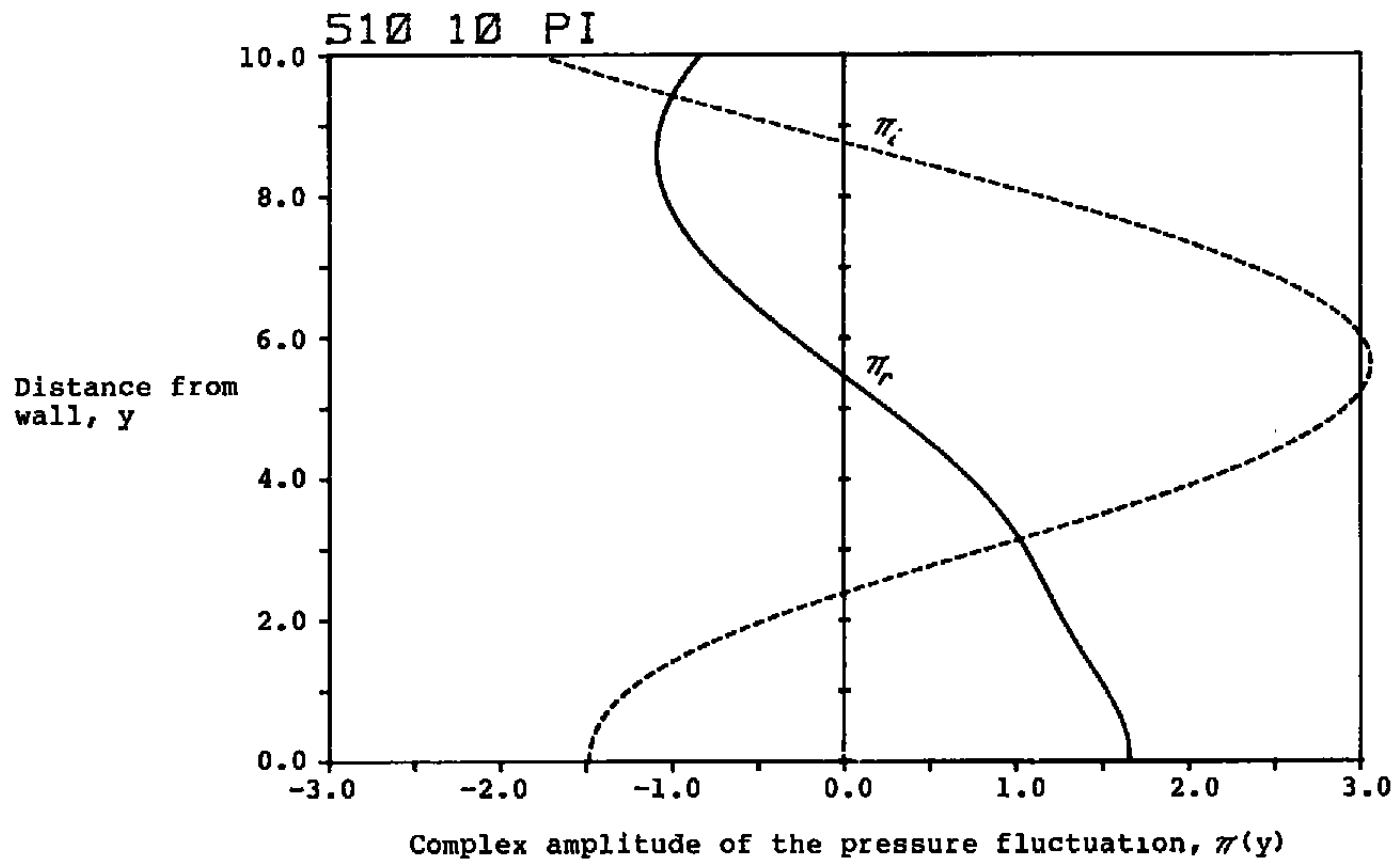
Figure 3.31 The variation of the pressure fluctuation with distance from the wall for a decaying wave, $\exp(-\beta x)$, for $\beta = \omega = 0.5$ and $R_\delta \approx 1000$ for an unfavorable pressure gradient boundary layer with a Falkner-Skan parameter -0.05
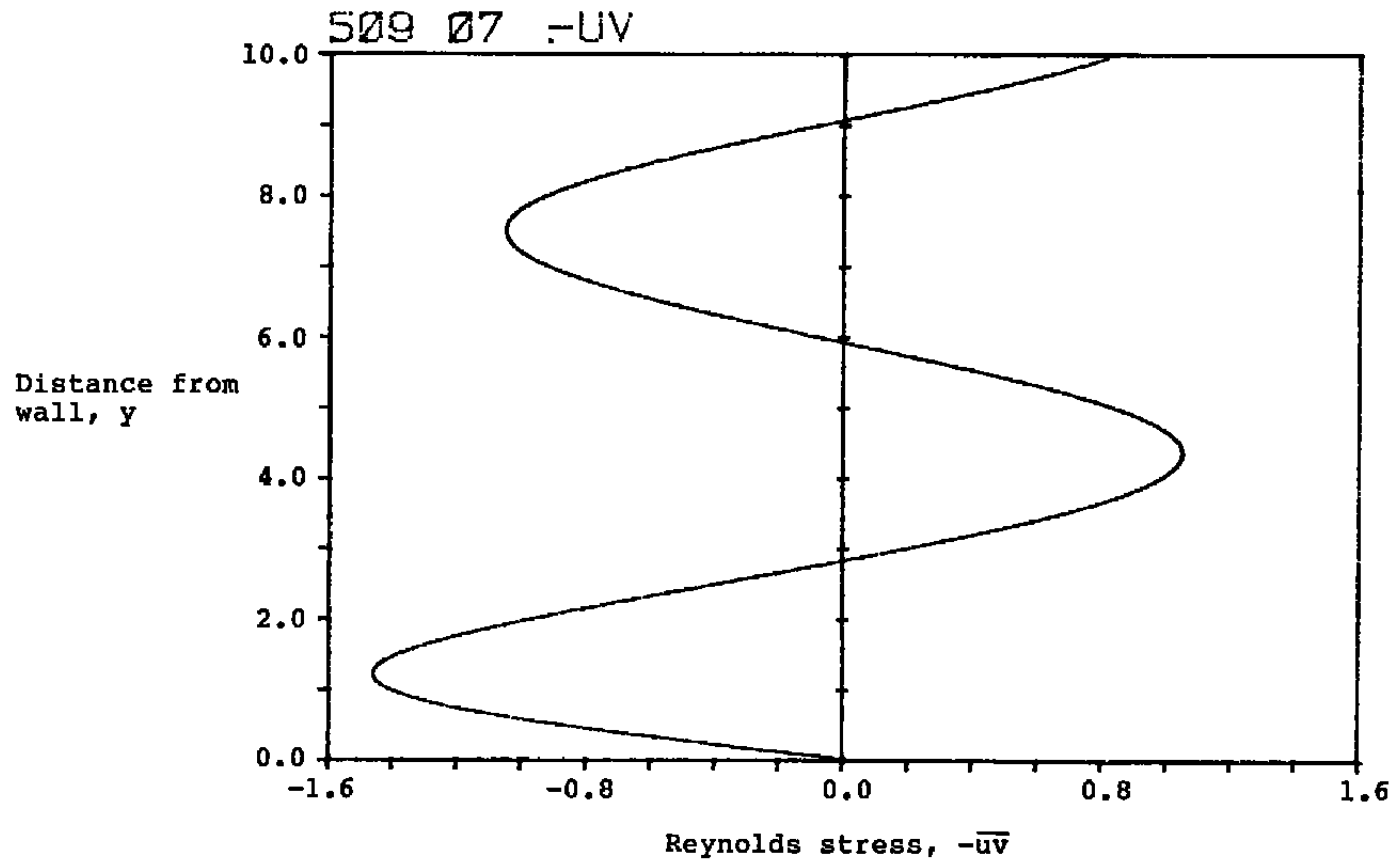
510 07 -UV
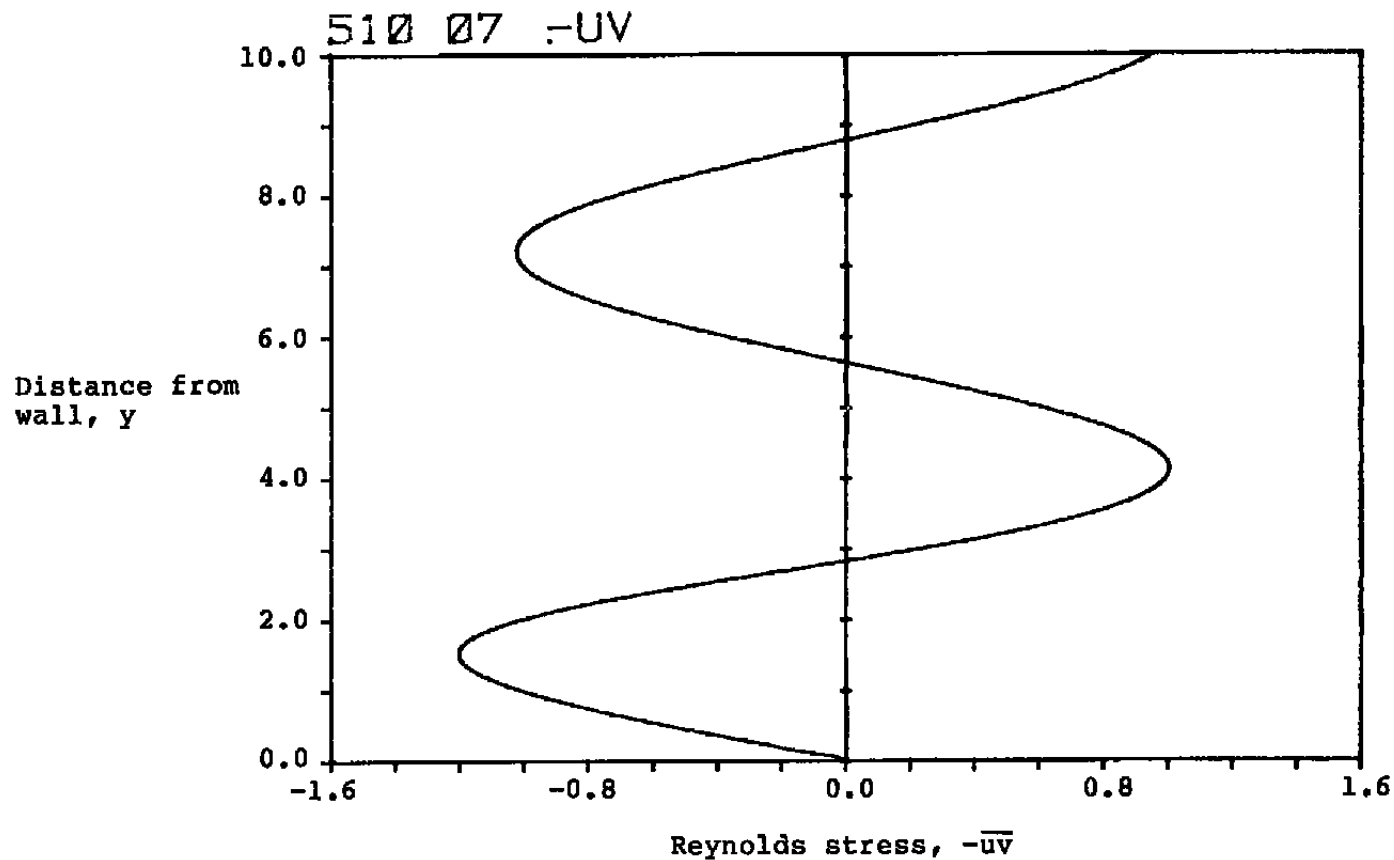
Figure 3.32 The variation of the Reynolds stress with distance from the wall for a decaying wave, exp(−βx), for $\beta = \omega = 0.5$ and $R_\delta = 1000$ for an unfavorable pressure gradient boundary layer with a Falkner–Skan parameter −0.05

510 09 -UVDU/DY
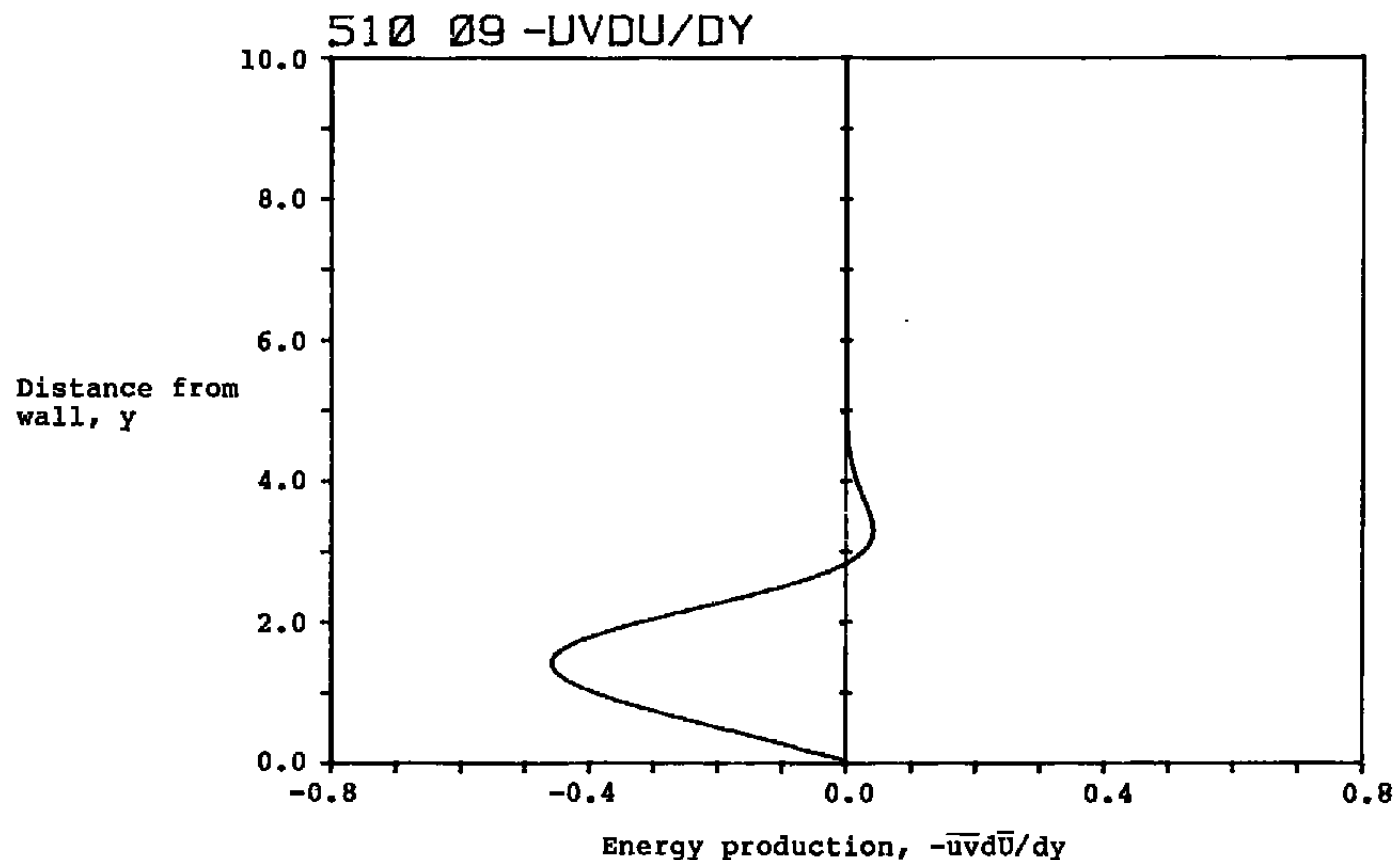
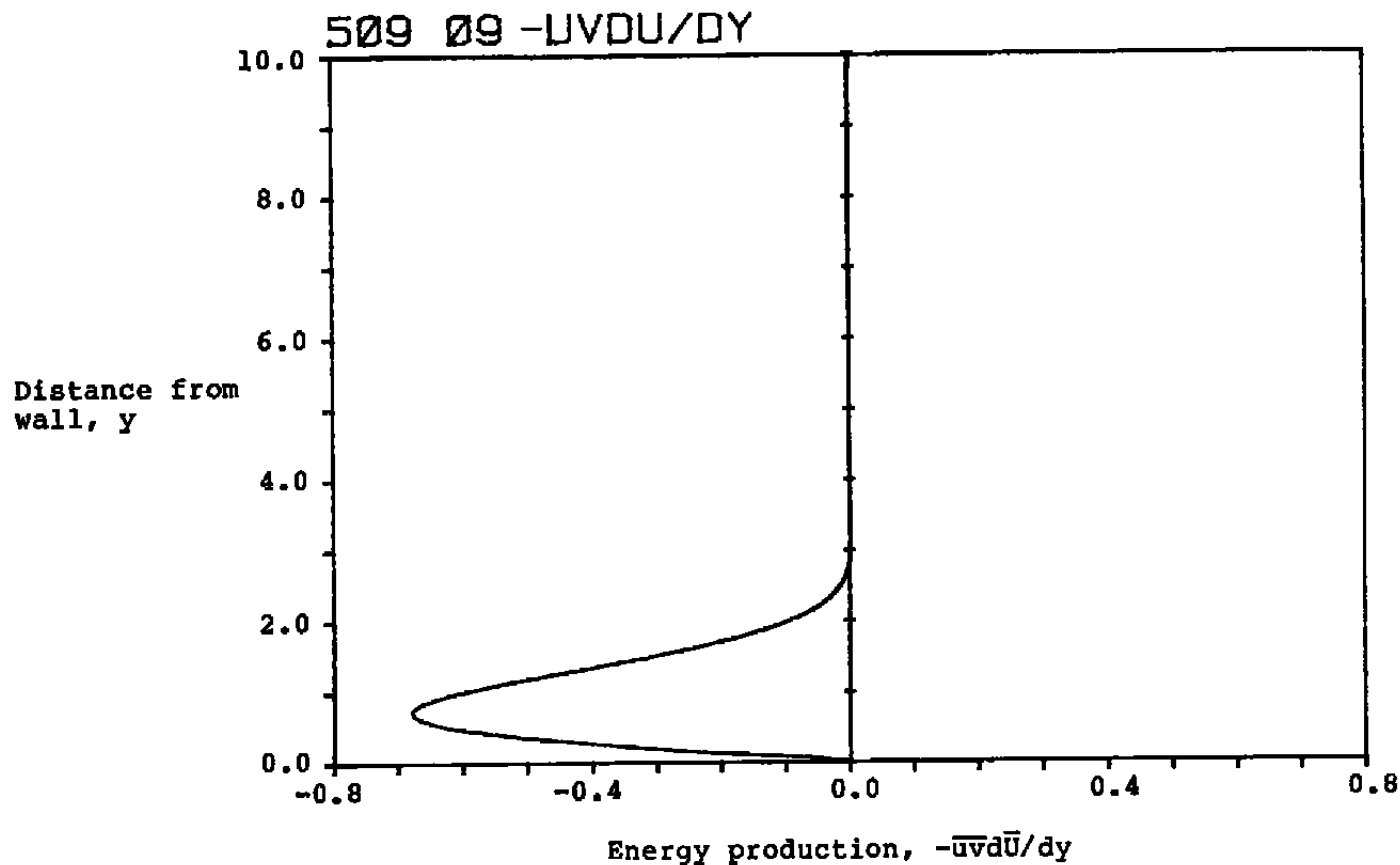
Figure 3.33 The variation of the energy production with distance from the wall for a decaying wave, exp(-βx), for $\beta = \omega = 0.5$ and $R_\delta = 1000$ for an unfavorable pressure gradient boundary layer with a Falkner-Skan parameter -0.05

541 Ø4 VRMS

Figure 3.34 Effects of frequency on the rms normal velocity
fluctuation, with the other parameters held constant.

542 Ø5 URMS

$\beta = 0.5$
$R_\delta = 1000$
Decaying wave
Blasius layer

$0.5 = \omega$
0.4
0.3
0.2
0.1

Distance from wall, y

rms longitudinal velocity fluctuation, $(\overline{u^2})^{1/2}$
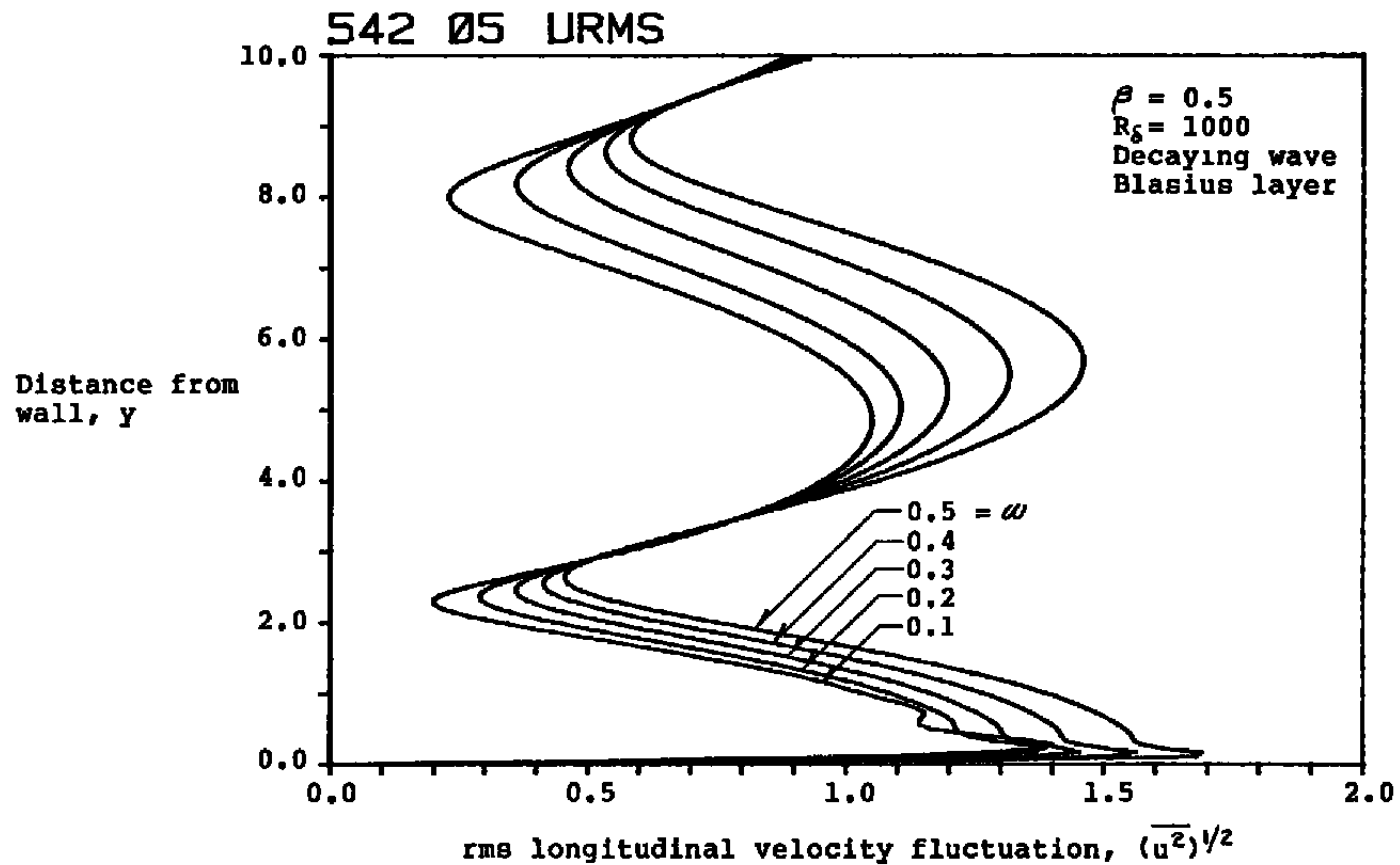
Figure 3.35   Effects of frequency on the rms longitudinal velocity
fluctuation, with the other parameters held constant.

argument seems unable to provide any guidance on the influence of Reynolds number, as discussed later.

The solution for the velocity fluctuation in the viscous sublayer, derived in Appendix B, shows that the ratio

$$\text{sublayer thickness/boundary layer thickness} = 1/(\omega R_\delta)^{1/2}$$

Hence, as the frequency is increased, the shorter times available for viscous diffusion to take place during one oscillation cycle leads to thinner sublayers. Calculations of the rms velocity for five frequencies differing by a factor of 5 are shown in Figure 3.36. These calculations show the thinning of the sublayer as frequency increases.

3.2.4 Effects of Reynolds Number

Calculations of the rms velocities with Reynolds numbers varying by a factor of 10 (from R_δ = 100 to 1000) are shown in Figures 3.37 and 3.38. Clearly, the velocities are rather insensitive to the Reynolds number, except in the sublayer.

From our discussion of the previous section, one would expect that one effect of increasing the Reynolds number would be to thin the sublayer, $\delta_s/\delta = (\omega R_\delta)^{-1/2}$. Evidence that this is true is shown in Figure 3.39 where the rms longitudinal velocity is plotted in the sublayer region for nine Reynolds numbers differing by a factor of 20.

In Figure 3.39, also note the apparent coalescence of the curves above the sublayer, which further supports our conclusion that the velocities are rather insensitive to R_δ except in the sublayer.

3.2.5 Effects of Reynolds Number and Frequency When ωR_δ is Held Constant.

Since the ratio of sublayer thickness to boundary layer thickness is $(\omega R_\delta)^{-1/2}$, then if the frequency and Reynolds number are changed but their product is held constant, then one would expect the sublayer to be relatively unchanged. To test this hypothesis, we calculated the following cases

ω = 2.0	R_δ = 250	ωR_δ = 500
ω = 1.0	R_δ = 500	ωR_δ = 500
ω = 0.5	R_δ = 1000	ωR_δ = 500
ω = 0.25	R_δ = 2000	ωR_δ = 500
ω = 0.125	R_δ = 4000	ωR_δ = 500

The rms longitudinal velocity in the sublayer is plotted in Figure 3.40 for these five cases. The sublayer thickness appears to be unchanged although the frequency and Reynolds number separately have been changed

543 Ø5 URMS

$\beta = 0.5$
$R_\delta = 1000$
Decaying wave
Blasius layer

$\omega = 0.1$
0.2
0.3
0.4
0.5

Distance from wall, y

rms longitudinal velocity fluctuation, $(\overline{u^2})^{1/2}$
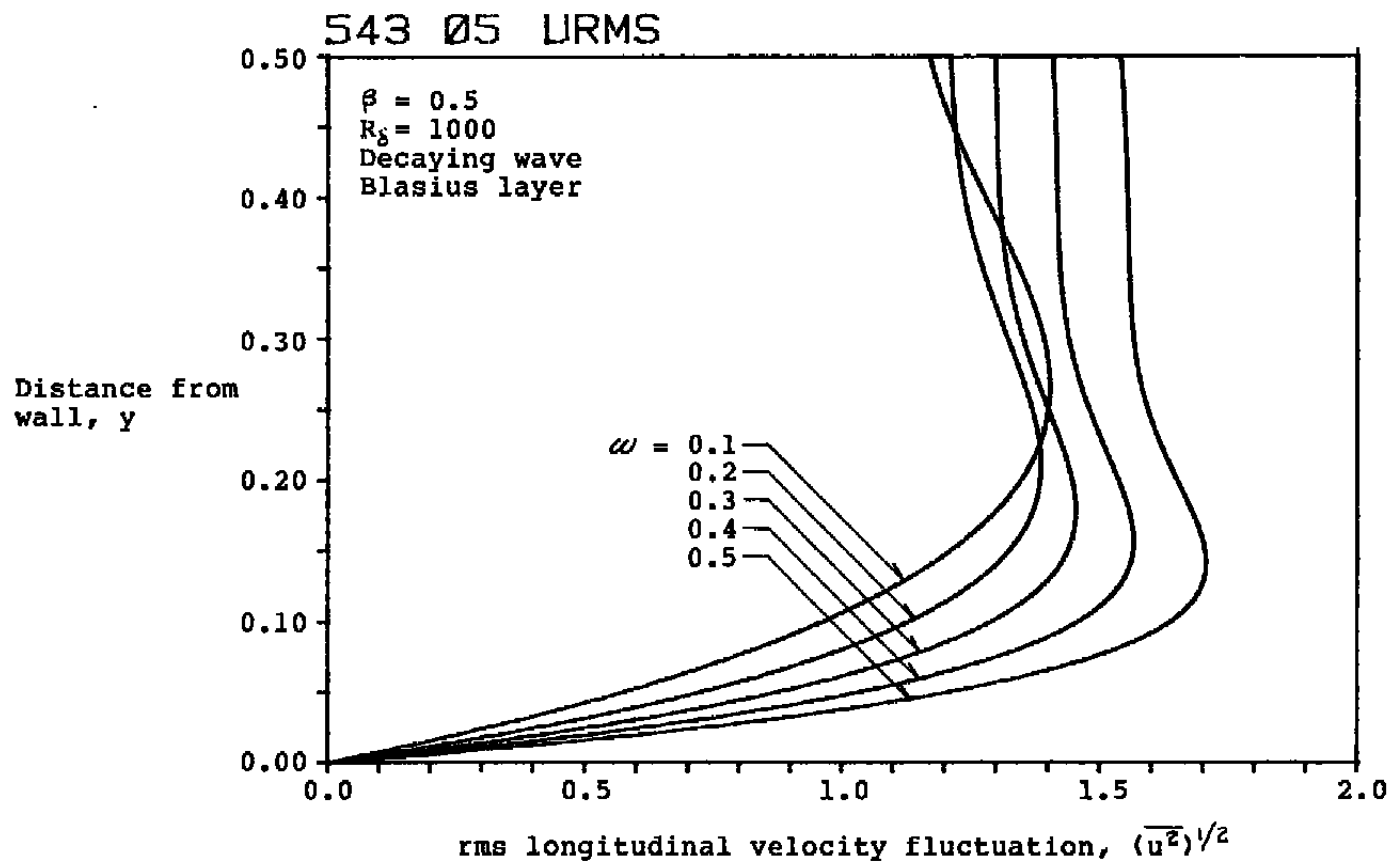
Figure 3.36   Effect of frequency on the rms longitudinal velocity fluctuation in the sublayer, with the other parameters held constant.

544 04 VRMS

$\beta = \omega = 0.5$
Decaying wave
Blasius layer

5 curves for $R_\delta = 100$ to 1000

Distance from
wall, y

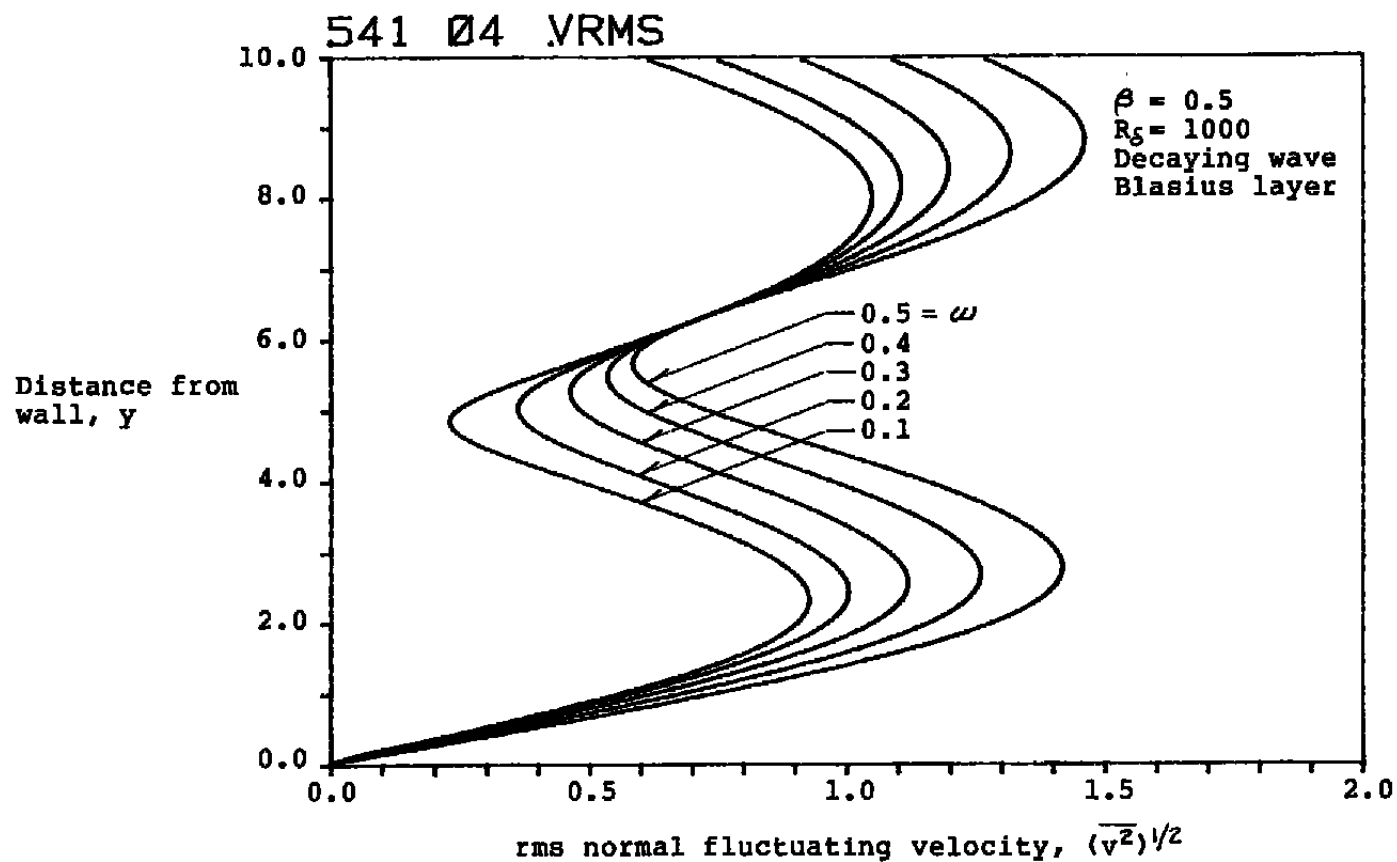rms normal fluctuating velocity, $(\overline{v^2})^{1/2}$
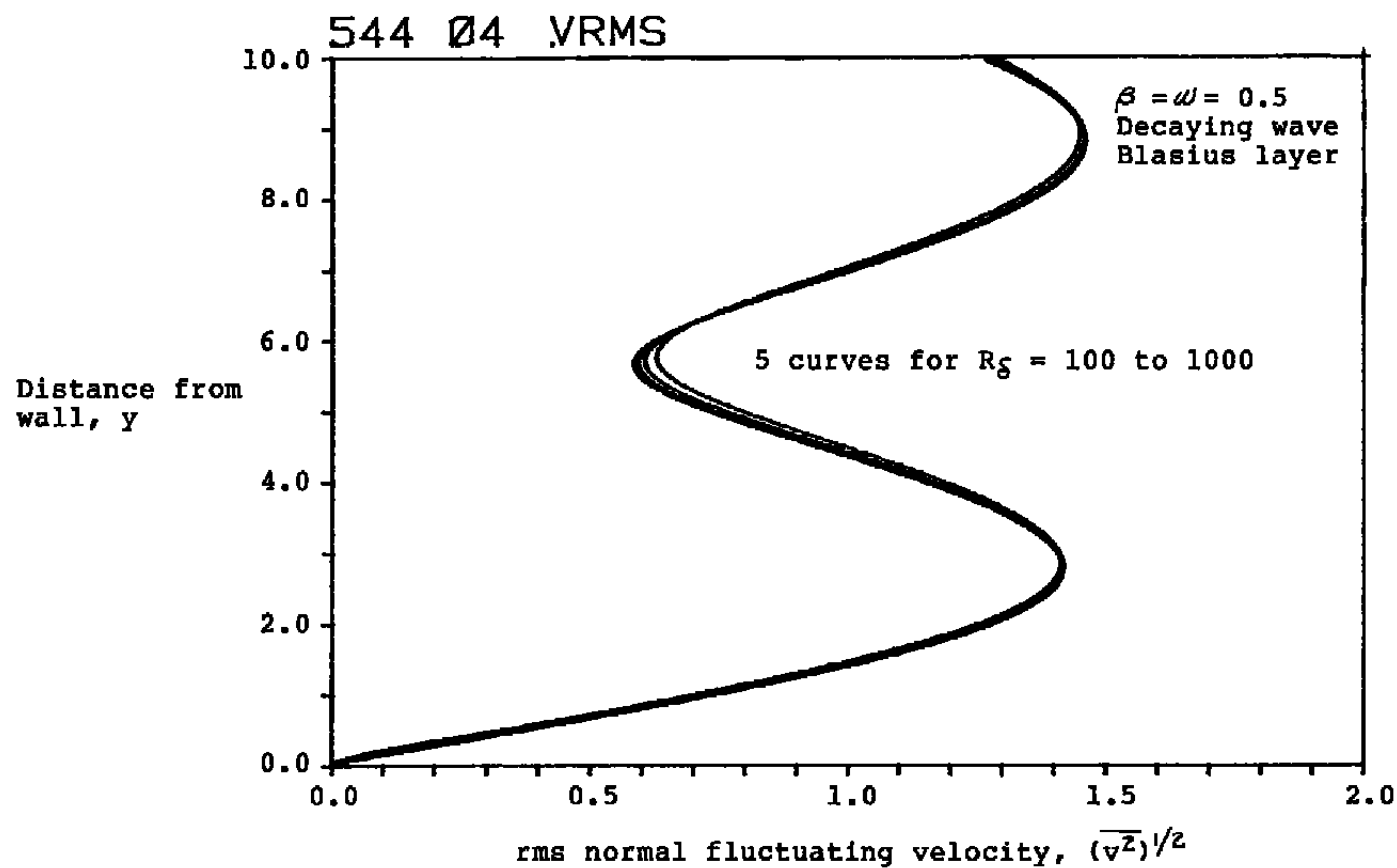
Figure 3.37   Effects of Reynolds number on the rms normal velocity
fluctuation, with the other parameters held constant.
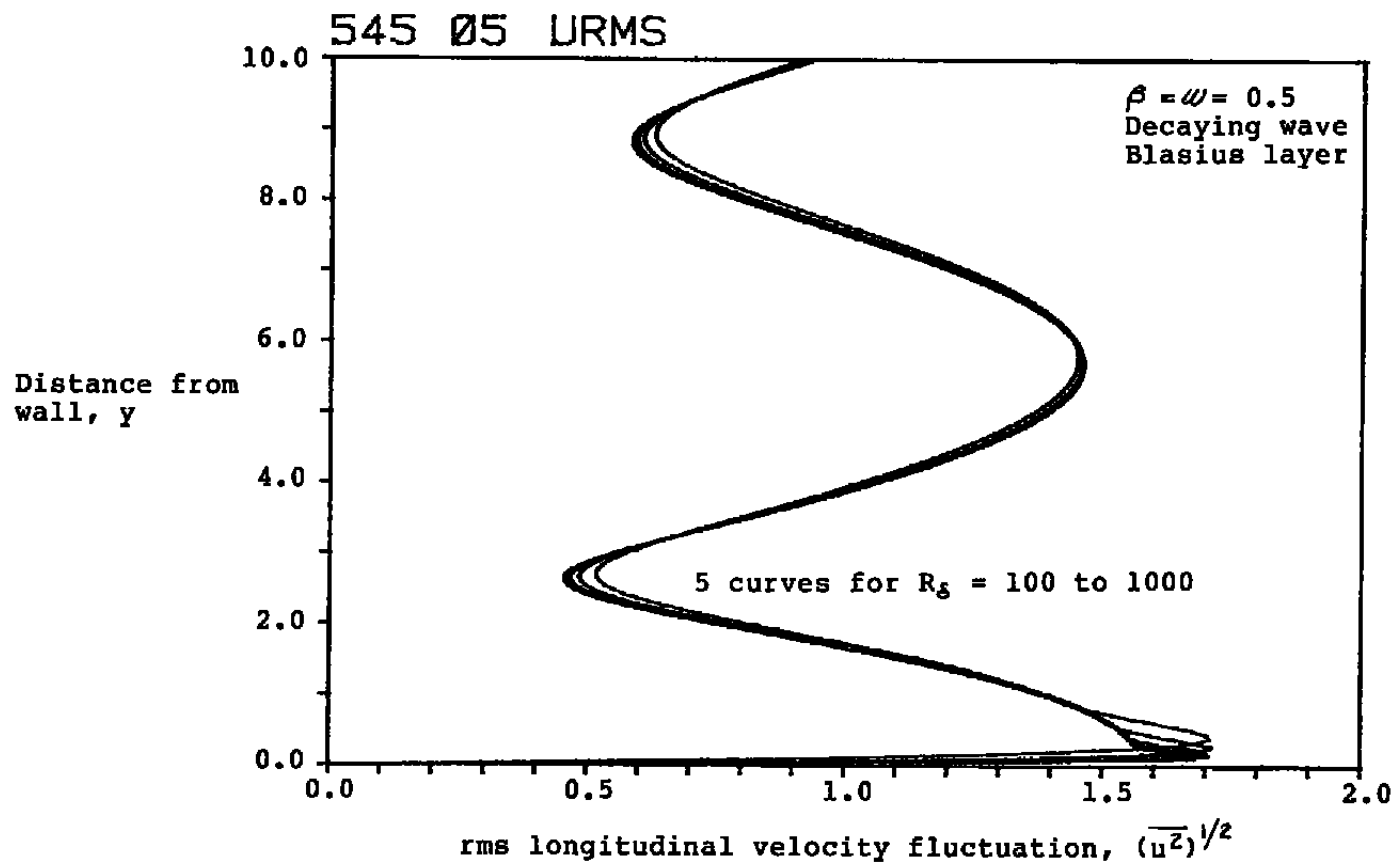
Figure 3.38 Effects of Reynolds number on tne rms longitudinal velocity fluctuation, witn tne other parameters held constant.

Figure 3.39   Effect of Reynolds number on the rms longitudinal velocity fluctuation in the sublayer. Note tne coalesence of the curves into the (nearly) Reynolds number independent curve outside of the sublayer.
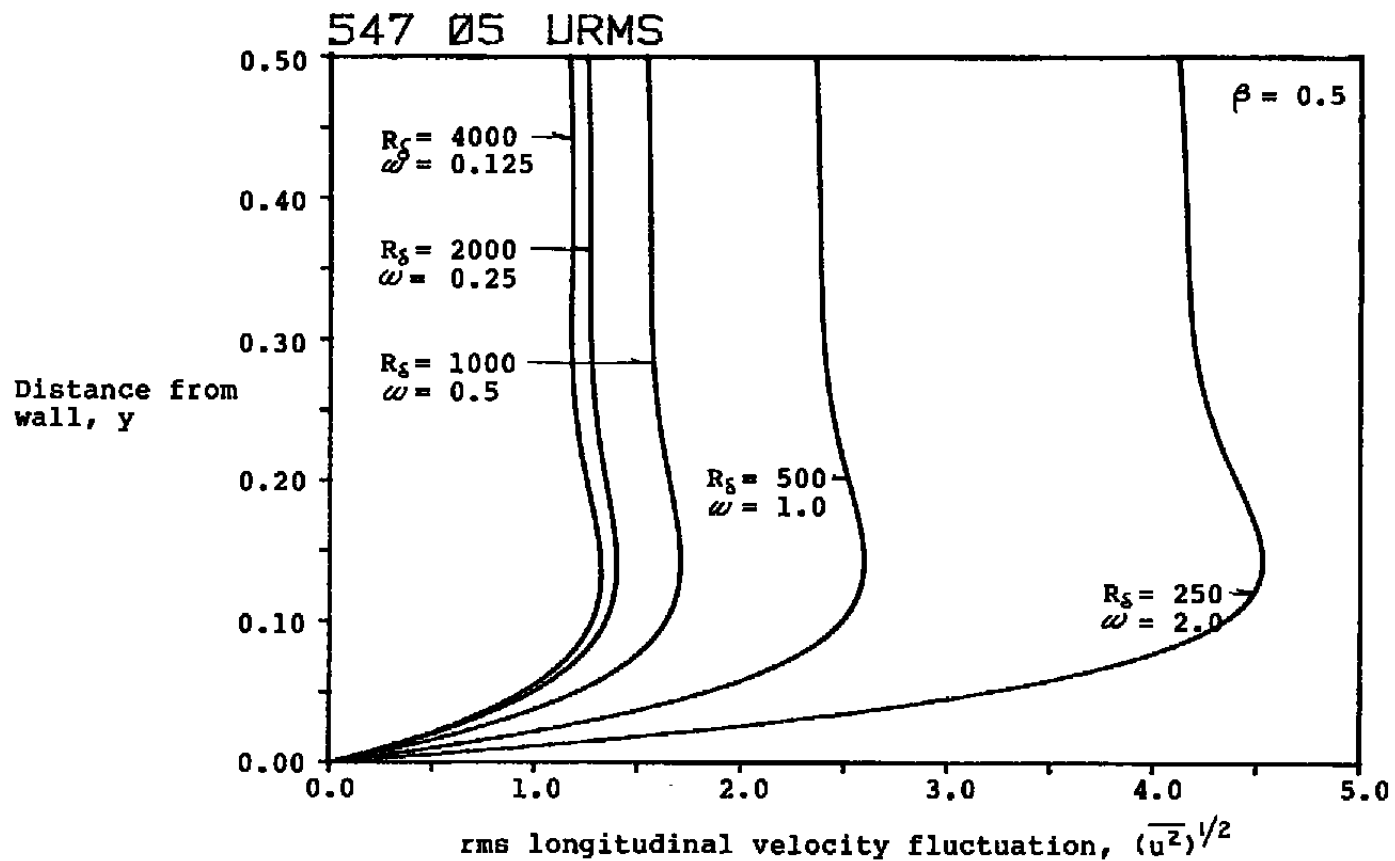
Figure 3.40 Effects of changing both the frequency and the Reynolds
number, but holding their product constant, $\omega R_\delta = 500$.

by a factor of 16.

3.2.6 Effects of y-wavenumber or Decay Rate

To obtain evidence of the influence of the y-wavenumber (or decay rate in the streamwise direction), we calculated the rms velocity for β=0.10, 0.25, 0.50, and 0.75 with the other parameters fixed. These results are plotted in Figure 3.41. The higher frequency oscillations associated with increasing the y-wavenumber are apparent. Also, the maximum amplitude increases as β decreases. Based upon the guidelines of Appendix A, the coefficient of $\sin\beta y$ is

$$\frac{m}{\beta} = \left(-\frac{R_s}{\beta} - 1 - i\,\frac{\omega R}{\beta^2}\right)^{1/2}$$

Hence, as β decreases, this coefficient increases, in agreement with our calculations for a Blasius layer.

3.3 NUMERICAL RESULTS FOR GROWING STANDING WAVES

3.3.1 Inviscid Relationship Between the Solutions for Decaying and Growing Waves

The Orr-Sommerfeld equation (eqn. 2.6b) can be separated into the following two real equations:

(1) Equation originating from the real part:

$$\left\{\bar{U}(D^2+\beta^2) - \bar{U}_{yy} - \frac{1}{r\beta R_s}(D^2+\beta^2)\right\}\phi_r + \frac{r\omega}{\beta}(D^2+\beta^2)\phi_i = 0 \tag{3.13}$$

(2) Equation originating from the imaginary part:

$$\left\{\bar{U}(D^2+\beta^2) - \bar{U}_{yy} - \frac{1}{r\beta R_s}(D^2+\beta^2)\right\}\phi_i - \frac{r\omega}{\beta}(D^2+\beta^2)\phi_r = 0 \tag{3.14}$$

where r=+1 or -1 for growing or decaying waves, respectively.

If $\phi(y) = \phi_r(y) + i\phi_i(y)$ is a solution for a decaying wave (r=-1), then we ask: Is the complex conjugate solution $\phi = \phi_r - i\phi_i$ a solution for the growing wave case (r=+1)? If one substitutes r=-1 with $\phi = \phi_r + i\phi_i$, and if one substitutes r=+1 with $\phi = \phi_r - i\phi_i$, one finds the two systems are identical only if the flows are inviscid. The viscous term does not transform in that manner.

As we shall see from numerical calculations for growing and decaying waves, this inviscid rule, well known from inviscid stability theory, is a practical guideline for the high Reynolds number viscous case as well.

548 04 VRMS

$\omega = 0.5$
$R_\delta = 1000$
Decaying wave
Blasius layer

$\beta = 0.75$

$\beta = 0.5$

$\beta = 0.25$

$\beta = 0.1$

Distance from wall, y

rms normal fluctuating velocity, $(\overline{v^2})^{1/2}$
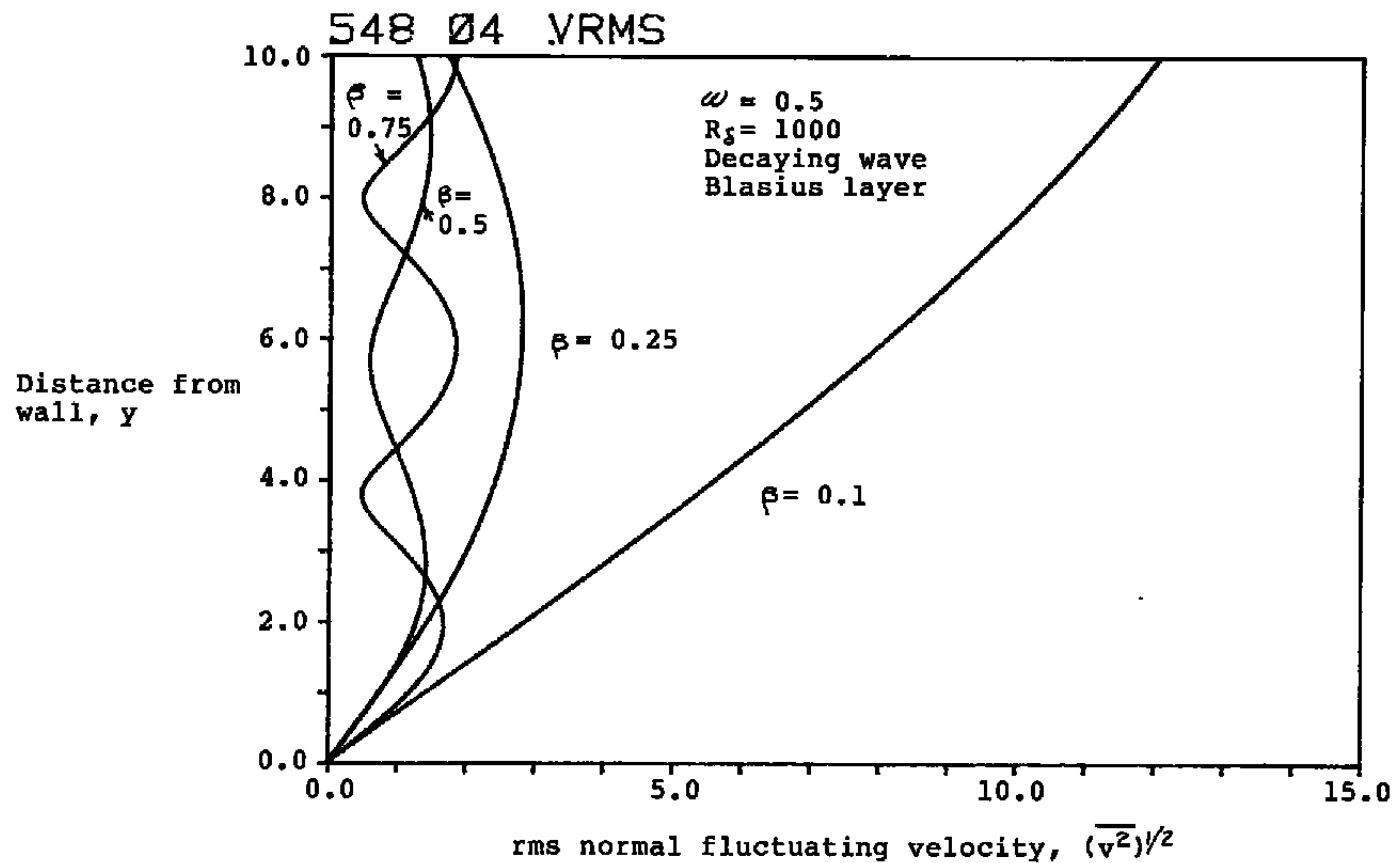
Figure 3.41   Effect of the y-wavenumber or decay rate on the rms
             normal velocity fluctuation, with tne other parameters
             held constant.

3.3.2 Blasius case with growing waves

Figures 3.42–3.47 present numerical results for a wave growing exponentially in the streamwise direction as $\exp(+\beta x)$. These figures can be compared with the results for the decaying wave as indicated below.

	$\exp(-\beta x)$ wave	$\exp(+\beta x)$ wave
φ	Figure 3.2	3.42
f	3.3	3.43
z	3.6	3.44
π	3.11	3.45
$-\overline{uv}$	3.17	3.46
$-\overline{uv}d\overline{U}/dy$	3.18	3.47

While φ for the $\exp(+\beta x)$ wave is not exactly the complex conjugate of φ for the $\exp(-\beta x)$ wave, the inviscid theorem appears to be a reasonable guideline for the large Reynolds number cases. The longitudinal amplitude, $f = f_r + if_i$, for the decaying wave is approximately $-f_r + if_i$ for the growing wave outside of the sublayer. The overshoot of f_r at the sublayer edge for a decaying wave appears to be similar to the overshoot of f_i for the growing wave. A significant discrepancy from the inviscid guideline arises for the pressure.

The Reynolds stress in Figure 3.46 has a reversal of sign compared with that stress in Figure 3.17. This sign change leads to a sign change in the energy production, Figure 3.47 as compared with 3.18. A positive energy production indicates that energy is being transferred from the mean flow to the disturbance flow.

3.4 NUMERICAL RESULTS WHEN THE NO-SLIP CONDITION AT THE WALL IS REPLACED BY A NO-SHEAR CONDITION.

To give some indication of the role of the viscous sublayer, in Figures 3.48–3.51 we replaced the no-slip condition, $u = 0$ or $\varphi_y = 0$, with a no-shear condition at the wall

$$u_y = 0 \quad or \quad \varphi_{yy} = 0 \quad at \quad y = 0 \tag{3.15}$$

These figures with a no-shear condition may be compared with the corresponding ones with a no-slip condition as tabulated below:

	no-slip	no-shear
φ	Figure 3.2	3.48
f	3.3	3.49
z	3.6	3.50
π	3.11	3.51

Figure 3.42 The variation of the normal velocity fluctuation with distance from the wall for a growing wave, exp($+\beta x$), for $\beta = \omega = 0.5$ and $R_\delta = 1000$ with a Blasius boundary layer.

489 02 F

Distance from wall, y

Complex amplitude of the longitudinal velocity fluctuation, f(y)

Figure 3.43 The variation of the longitudinal velocity fluctuation with distance from the wall for a growing wave, $\exp(+\beta x)$, with $\beta = \omega = 0.5$ and $R_\delta = 1000$ with a Blasius boundary layer.

489 Ø3 Z

Figure 3.44 The variation of the vorticity fluctuation with distance from the wall for a growing wave, exp(+βx), for $\beta = \omega = 0.5$ and $R_\delta = 1000$ with a Blasius bounaary layer.

.489 10 PI
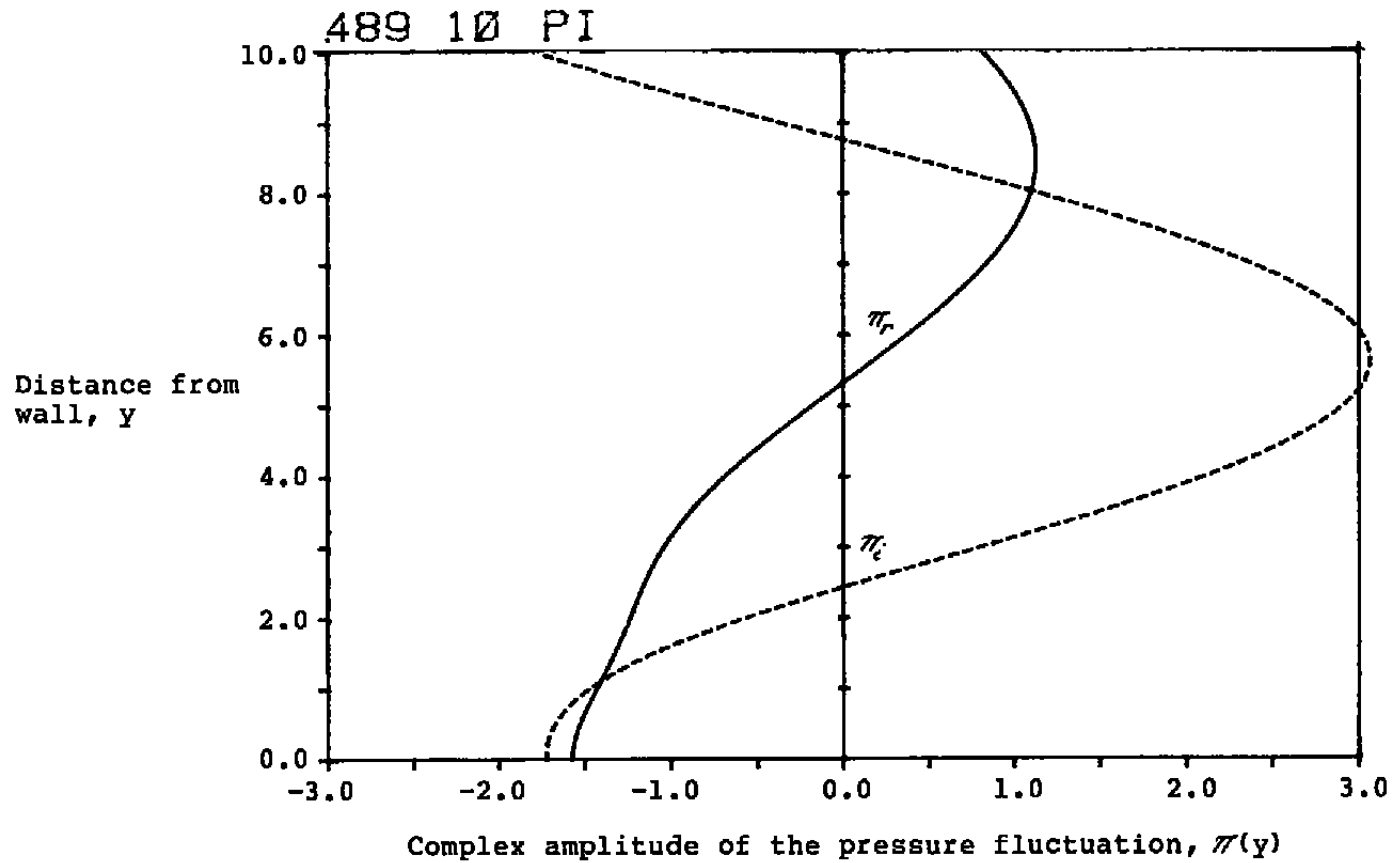
Figure 3.45   The variation of the pressure fluctuation with distance
from   the   wall for a growing wave, exp(+βx),   for
$\beta = \omega = 0.5$ and $R_\delta = 1000$ with a Blasius bounaary layer.
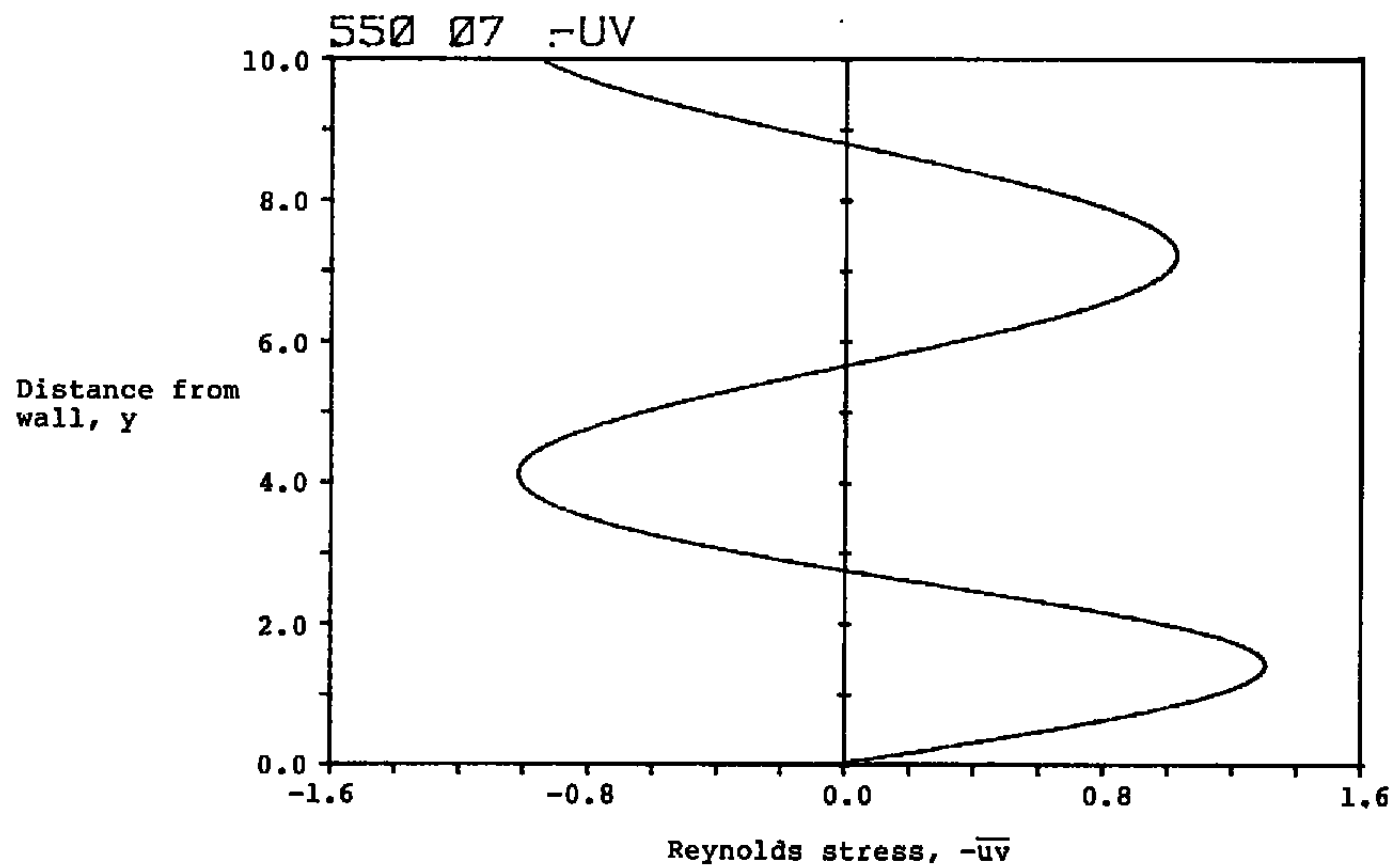
Figure 3.46 The variation of the Reynolds stress with distance from the wall for a growing wave, exp(+βx), for $\beta = \omega = 0.5$ and $R_\delta = 1000$ with a Blasius boundary layer.

489 09 -UVDU/DY
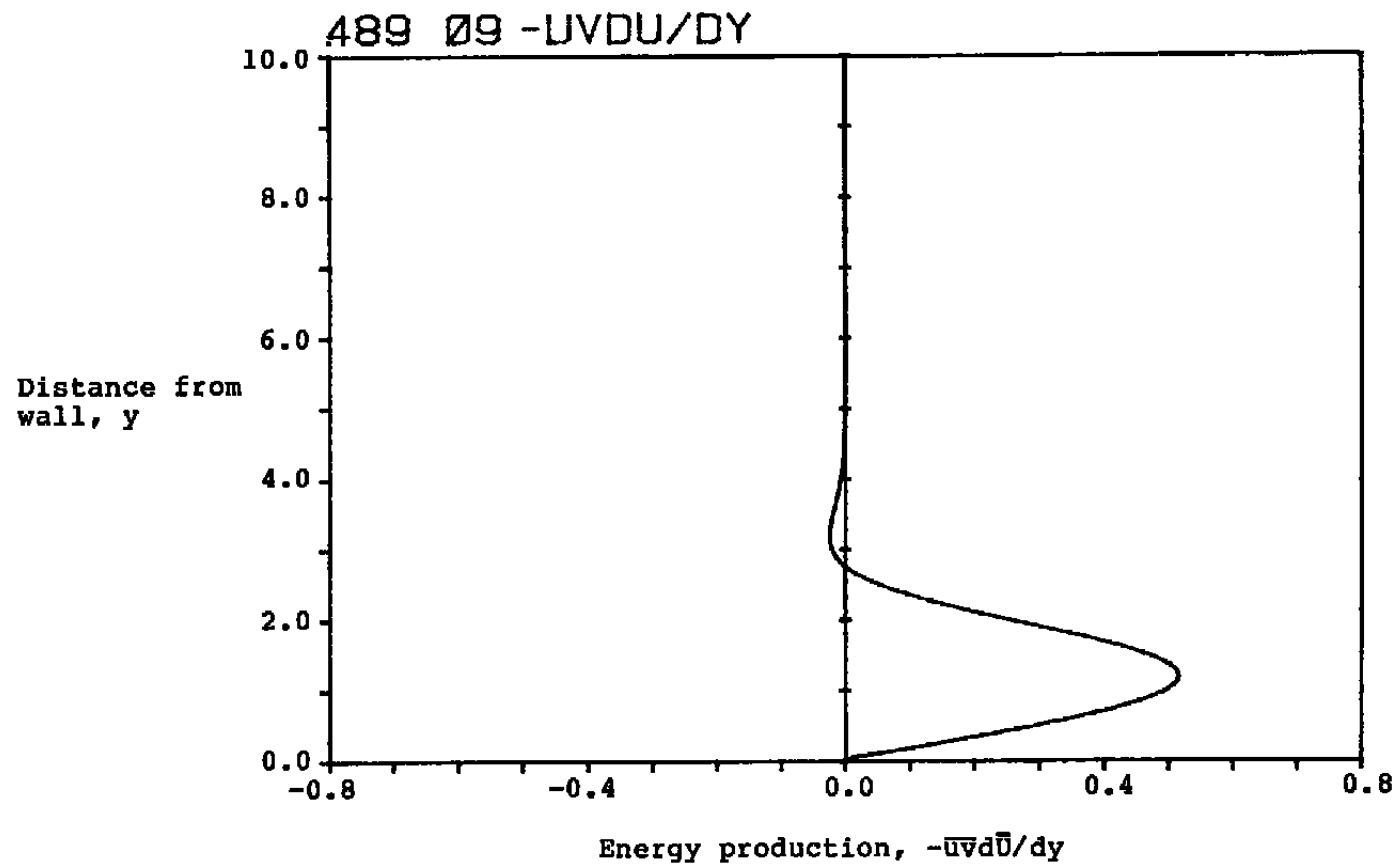
Figure 3.47   The variation of the energy production with distance from the wall for a growing wave, exp(+βx), for β =ω= 0.5 and R_δ=1000 with a Blasius boundary layer.

Figure 3.48 The variation of the normal velocity fluctuation with distance from the wall for a decaying wave, exp(-βx), for β =ω= 0.5 and R$_\delta$=1000 for a Blasius layer, and where the no-slip condition on the fluctuating flow has been replaced by a no-shear condition.

The impermeability condition at the wall was imposed for both sets of figures.

As expected and shown clearly in Figure 3.49 for the longitudinal velocity, no sublayer forms when the no-slip condition is replaced by a no-shear condition. For the variables plotted, the values above the sublayer region in Figures 3.2, 3.3, 3.6, and 3.11 are nearly the same as the values in Figures 3.48-3.51.

We conclude that the sublayer is relatively passive, i.e., it is driven by the external flow above the sublayer, and that external flow is not influenced very greatly by the sublayer. Except in the sublayer region itself of thickness $O(1/(\omega R_\delta)^{1/2})$, the results indicate that if the Reynolds number and frequency are large, $(\omega R_\delta)^{1/2} \gg 1$, then the replacement of the no-slip condition by a no-shear condition has a relatively small influence on the solutions. This result differs sharply from the active role which the sublayer takes for the Tollmien-Schlichting wave.
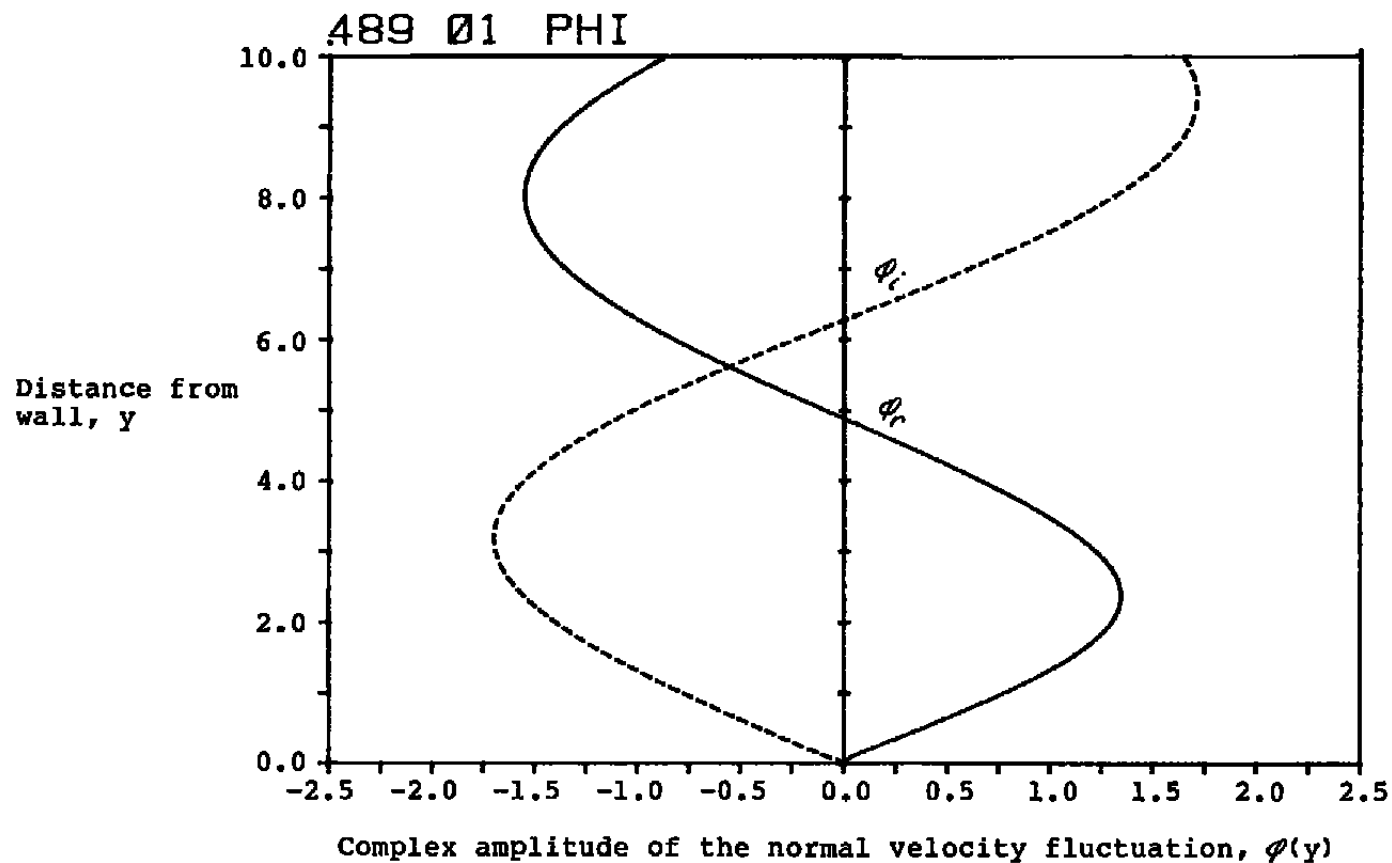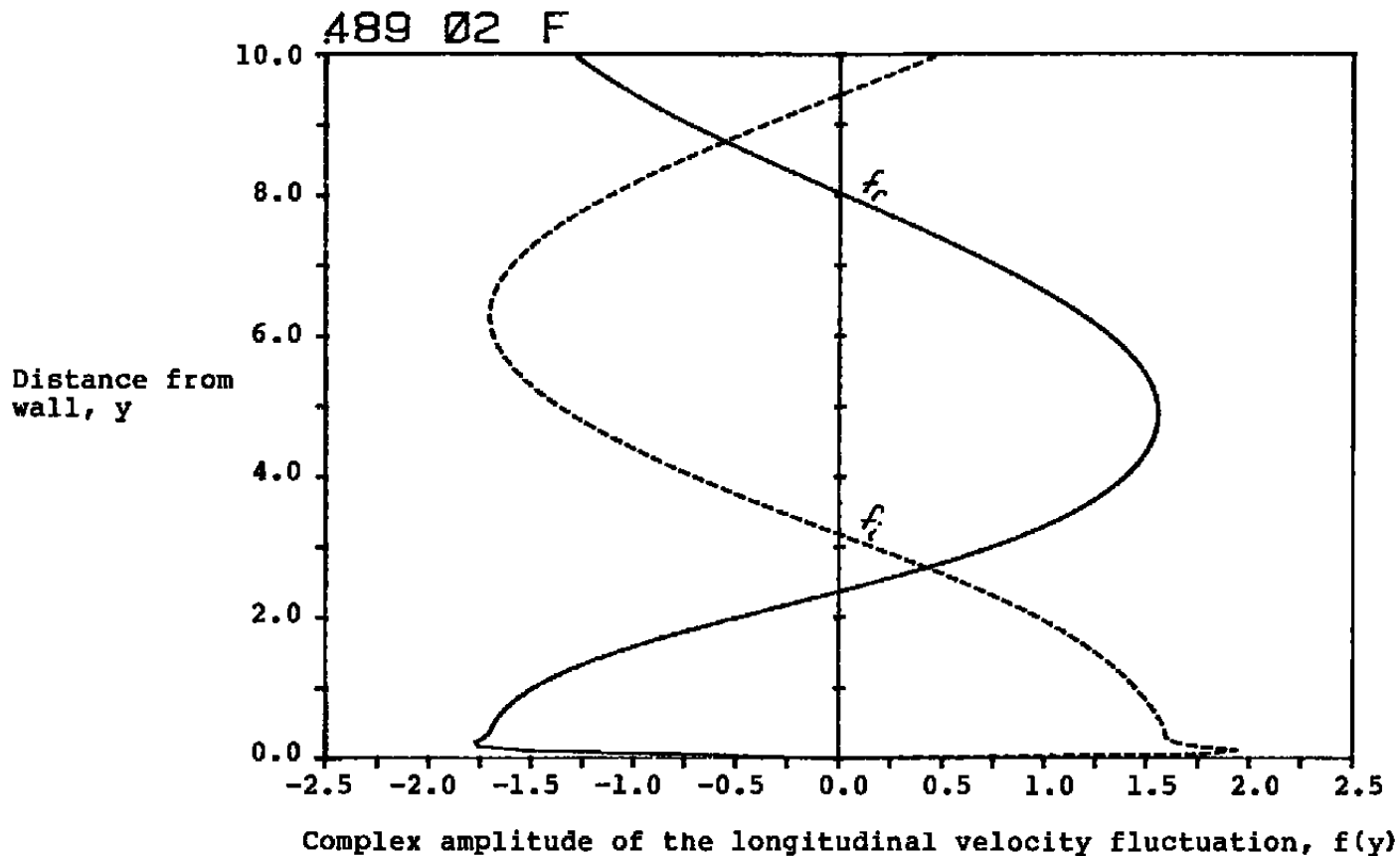
Figure 3.49   The variation of the longitudinal velocity fluctuation
with distance from the wall for a decaying wave,
$\exp(-\beta x)$, for $\beta = \omega = 0.5$ and $R_\delta = 1000$ for a Blasius layer,
and where the no-slip condition on the fluctuating flow
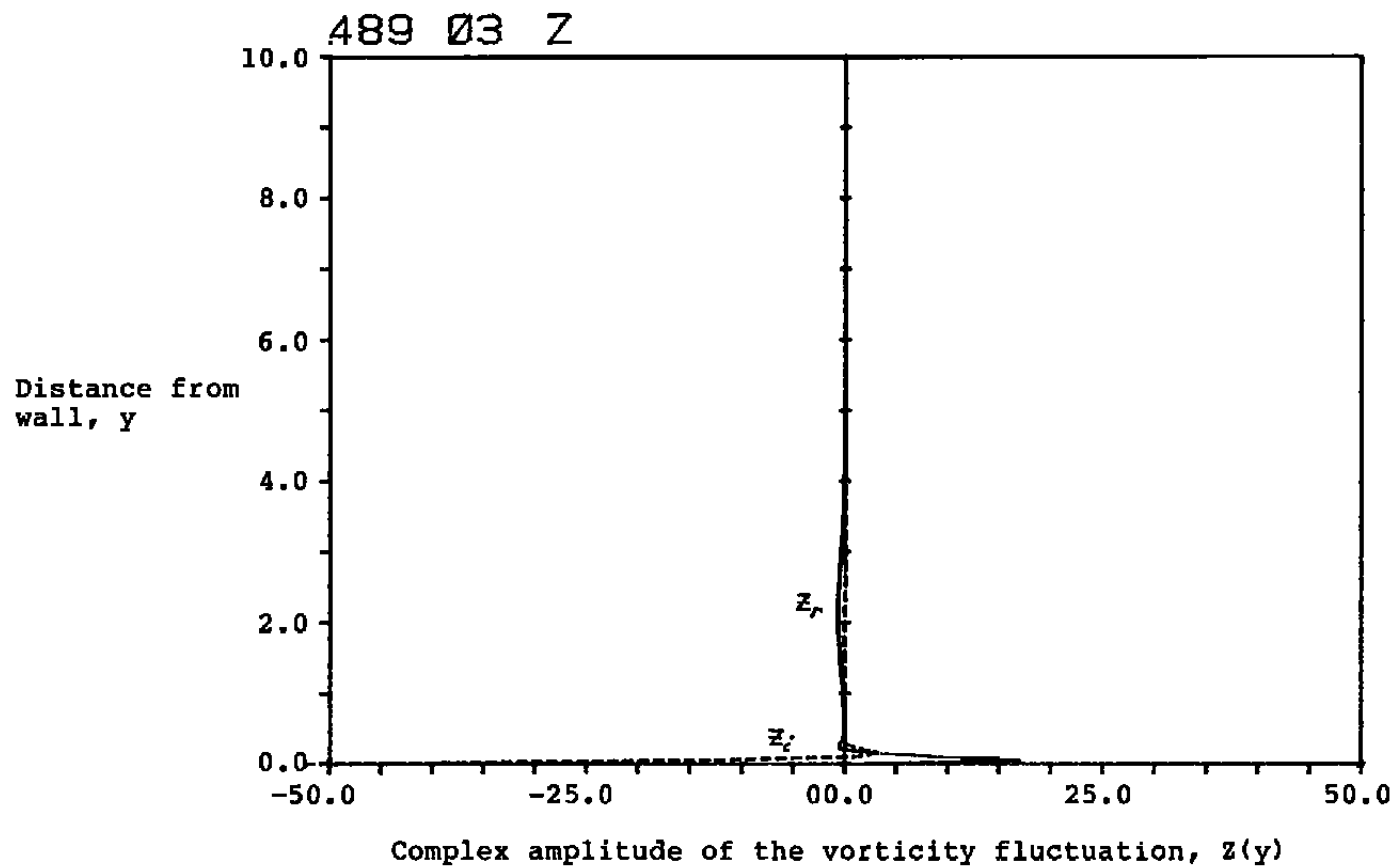has been replaced by a no-shear condition.
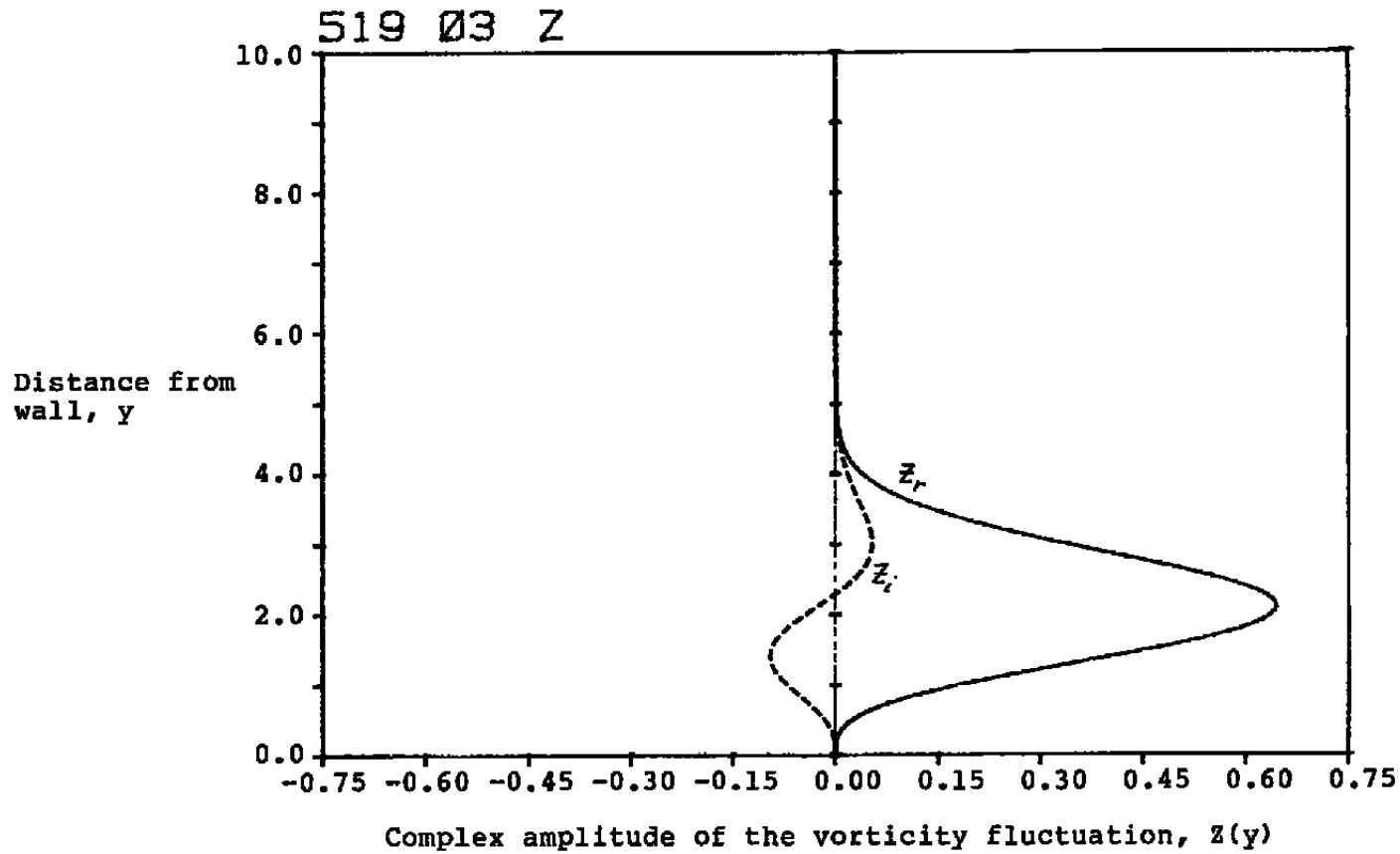
Figure 3.50   The variation of the vorticity fluctuation with distance from the wall for a decaying wave, $\exp(-\beta x)$, for $\beta = \omega = 0.5$ and $R_\delta = 1000$ for a Blasius layer, and where the no-slip condition on the fluctuating flow has been replaced by a no-shear condition.

519 10 PI
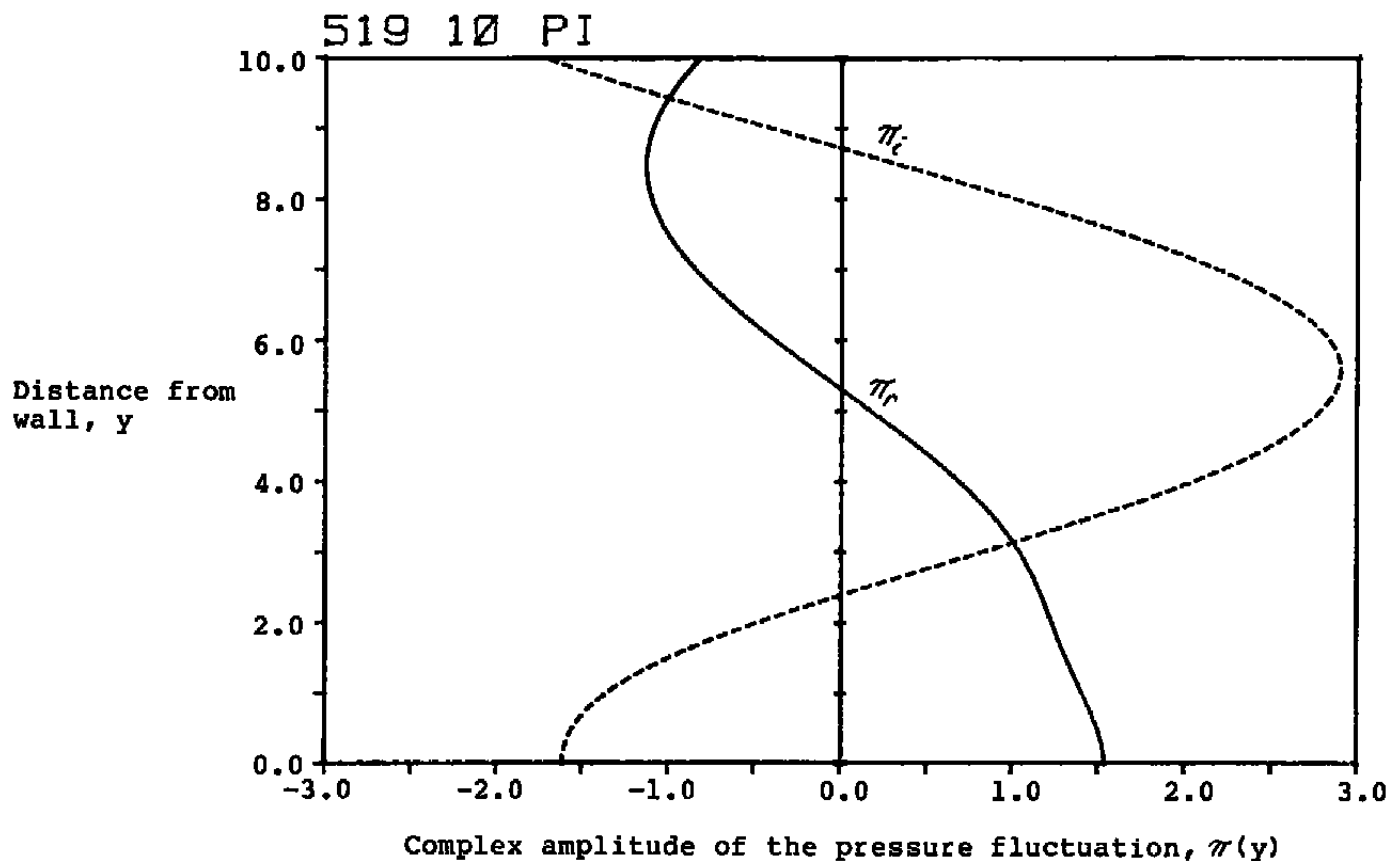
Figure 3.51 The variation of the pressure fluctuation with distance from the wall for a decaying wave, exp($-\beta$x), for $\beta 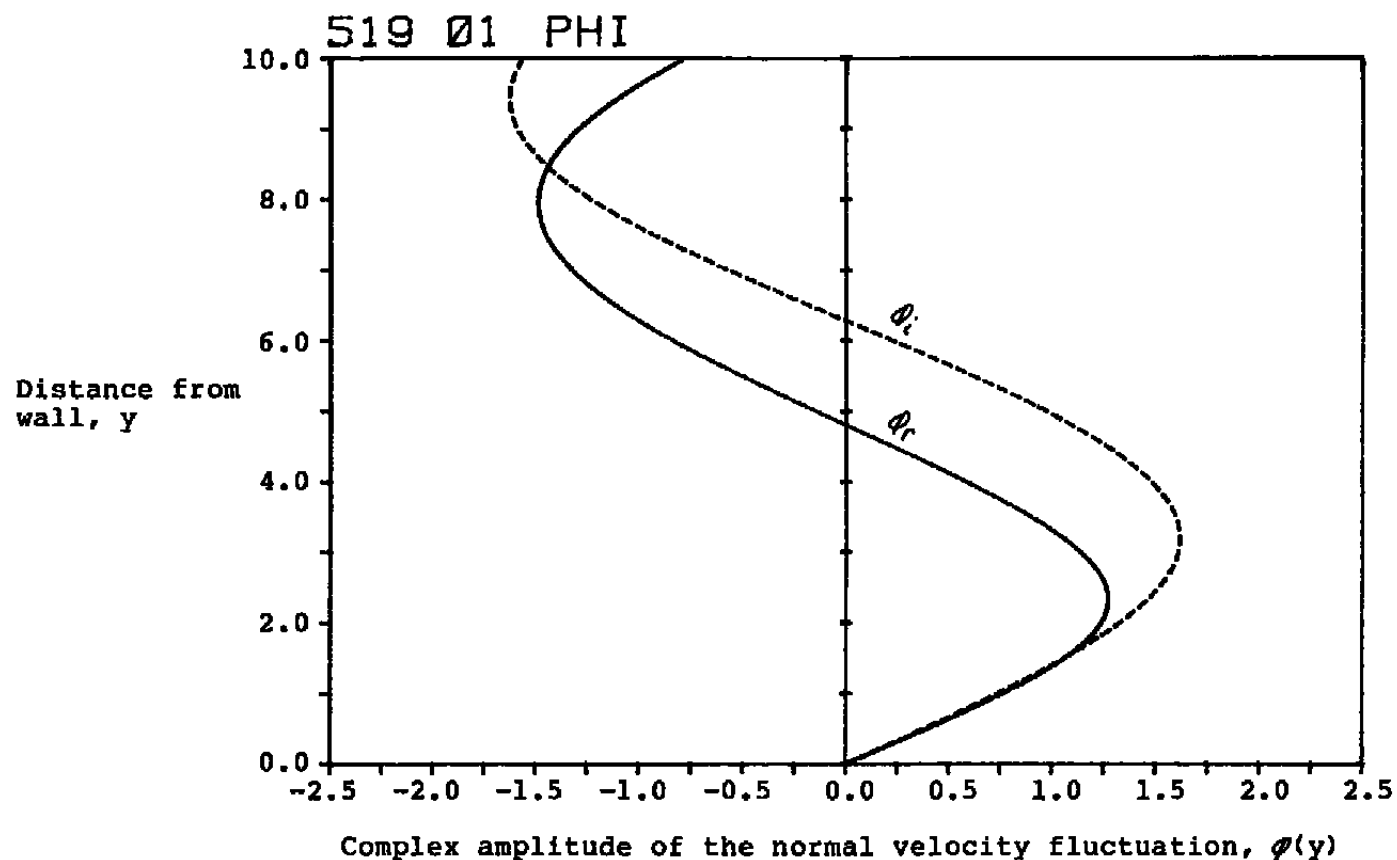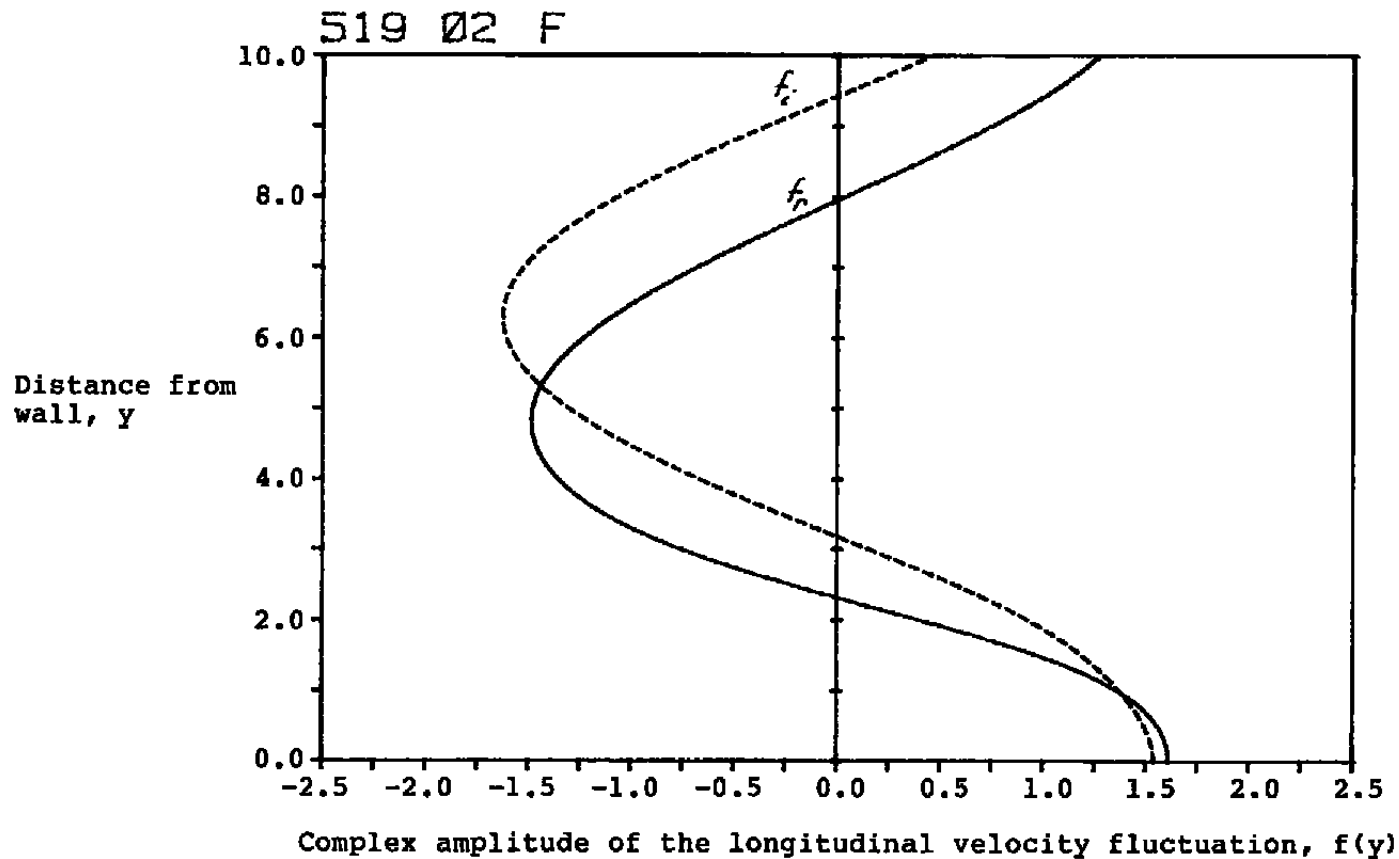= \mathscr{W} = 0.5$ and R_δ=1000 for a Blasius layer, and where the no-slip condition on the fluctuating flow has been replaced by a no-shear condition.

4.0 SUMMARY, DISCUSSION AND CONCLUSIONS

4.1 INTRODUCTORY COMMENTS

This report documents the analytical and numerical evidence of the existence of a pair of standing waves in a boundary layer. These waves oscillate sinusoidally in time, but because of the purely imaginary x-wavenumber and phase speed, the waves do not travel. The amplitudes vary exponentially in the streamwise direction without any spatial oscillation. Both growing and decaying solutions are possible. Far above the boundary layer, these irrotational fluctuations oscillate neutrally in the y-direction.

Some evidence of the existence of these waves is based on several numerical solutions of the Orr-Sommerfeld equation, analytical solutions of simplified forms of the Orr-Sommerfeld equation, and an asymptotic solution of the Orr-Sommerfeld equation. The asymptotic solution by Shunichi Tsuge as applied to the stability problem is summarized in Ref.26. The use of that asymptotic solution in the spatial initial-value problem will be summarized in another report.

The Orr-Sommerfeld equation describes the evolution of small-amplitude fluctuations in a boundary layer growing sufficiently slowly such that it is meaningful to represent it as a layer of uniform thickness. The characteristics of the boundary layer enter into the equation as two coefficients. The Falkner-Skan family of boundary layers was used so that evidence could be obtained for fluctuations in boundary layers with favorable, zero, and unfavorable mean pressure gradients. Also, since roughness can influence the mean profile, these profiles provide some indication of how roughness can influence the standing waves. Other profiles will be used later.

To illustrate how standing waves originate, the interaction between freestream vortical fluctuations and leading and trailing edges of a flat plate are summarized in Chapter 1. Those studies, while including the features of leading and trailing edges, do not include all of the features of the Orr-Sommerfeld equation. However, the problems share three essential features of the fluctuations in the freestream: (1) they oscillate in time, (2) decay or grow in the streamwise direction, and (3) are irrotational. This report documents the evidence that the Orr-Sommerfeld admits solutions with those characteristics, and that other features arise because of the shearing mean flow and viscosity. The problem of predicting the origin of the various waves is a topic of continuing research.

4.2 SUMMARY OF THE FORMULATION AND NUMERICAL TECHNIQUE

For small-amplitude disturbances in shear layers which develop sufficiently slowly such that the parallel-flow representation is

adequate, the objective is to obtain solutions of the equation

$$\left\{ \frac{\partial}{\partial t} + \bar{U}(y)\frac{\partial}{\partial x} - \epsilon \nabla^2 \right\} \nabla^2 v - \bar{U}_{yy}(y)\frac{\partial v}{\partial x} = 0 \qquad (4.1)$$

which are of the Fourier-Laplace form

$$v(x,y,t) = \varphi(y)\, e^{r\beta x - i\omega t} \qquad (4.2)$$

where β and ω are pure real. These standing-wave solutions are exponentially growing or decaying in the streamwise direction, and oscillate sinusoidally in time. The motivations for seeking solutions of this form are that such waves appear in several analytical solutions where the mean flow is uniform. Furthermore, in an asymptotic analysis of an initial-value problem with a boundary layer, two mathematical poles indicate that waves of this form would exist in boundary layers. For solutions of this form, the x-wavenumber is

$$\alpha = -i r \beta \qquad (4.3)$$
$$r = +1 \text{ for a growing wave}$$
$$r = -1 \text{ for a decaying wave}$$

The complex phase speed, which is pure imaginary, is $\quad c = i r \omega / \beta \qquad$ (4.4)

Letting $\alpha = -ir\beta$, the Orr-Sommerfeld equation is

$$\left\{ \left(\bar{U}(y) - \frac{ir\omega}{\beta} \right)(D^2 + \beta^2) - \bar{U}_{yy}(y) - \frac{1}{r\beta R_\delta}(D^2 + \beta^2)^2 \right\} \varphi(y) = 0 \qquad (4.5a)$$

The impermeability and no-slip boundary conditions at the wall, and the boundedness condition of the solution far-away, are

$$\varphi = D\varphi = 0 \quad \text{at } y = 0 \; ; \quad \varphi \text{ is bounded as } y \to \infty \qquad (4.5b,c,d)$$

When $\bar{U} = 1$ and $U_{yy} = 0$, the Orr-Sommerfeld equation has the solutions

$$\varphi(y) = A e^{-my} + B e^{my} + C \cos\beta y + D \sin\beta y \qquad (4.6)$$

or equivalently

$$\varphi(y) = A e^{-my} + B e^{my} + C_2 e^{-i\beta y} + D_2 e^{i\beta y} \qquad (4.7)$$

where the exponent is $m = \left(r\beta R_\delta - \beta^2 - i R_\delta \omega \right)^{1/2} \qquad$ (4.8)

For the boundary layer case, B = 0. For most cases, we normalize by setting C=1 in eqn.(4.6). In retrospect, the analytical results of Appendix A and the calculations suggest that setting the coefficient

D=1 would be a better choice, and might lead to amplitudes of the freestream disturbances to be less sensitive to the parameters. However, for any normal modes analysis, the amplitude $\phi(y)$ can be multiplied by a complex constant and rescaled. The essential requirement in carrying out calculations for the initial-value problem is consistency between the normalizations of the normal modes calculations and the initial-value theory.

Far-away from the boundary layer edge where the term Aexp(-my) is negligible, the flowfield varies sinusoidally

$$ v(x,y,t) = \left(\cos \beta y + D \sin \beta y \right) e^{\pm \beta x - i \omega t} \tag{4.9} $$

This freestream disturbance is irrotational. The constant D is obtained numerically.

In general, the constant D and the solution $\phi(y)$ of the Orr-Sommerfeld equation depend on the frequency, y-wavenumber, Reynolds number, mean velocity profile, and the choice of whether the wave is growing or decaying. The effects of the mean pressure gradient and one of the effects of surface roughness can be introduced through the mean velocity profile, $\bar{U}(y)$.

Numerical solutions of the Orr-Sommerfeld equation are obtained by an expansion in a series of (typically 48) Chebyshev polynomials. The coefficients of those polynomials are obtained as solutions of a set of linear, algebraic equations. The matrix of coefficients is reduced by Gauss-Jordan elimination.

Calculations are carried out on a Digital Equipment Corporation PDP-11/23 computer using 64K bytes of memory and another 64K bytes of extended memory for virtual arrays. The disk-overlayed FORTRAN IV program executes in about 145 seconds when using the KEF11-AA floating point chip, beginning with data for the mean velocity profile, and ending with the coefficients of the polynomials and the amplitude $\phi(y)$. The program executes in about 80 seconds when using the FPF-11 floating point processor.

4.3 SUMMARY OF RESULTS, DISCUSSION AND CONCLUSIONS

The calculations for the standing waves indicate that the longitudinal velocity fluctuation can be about as large inside the boundary layer as the fluctuation in the freestream. This conclusion differs significantly from the solutions with decaying vortices in the freestream, as can be seen for the rms longitudinal velocity in Figure 4.1 from Ref. 15. This plot has the same frequency, y-wavenumber, Reynolds number and mean velocity as for Figure 3.14, but the velocities deep inside the boundary layer are small in Figure 4.1. The corresponding plot for rms vorticity from Ref.15 is shown in Figure

600 05 URMS

Distance from wall, y

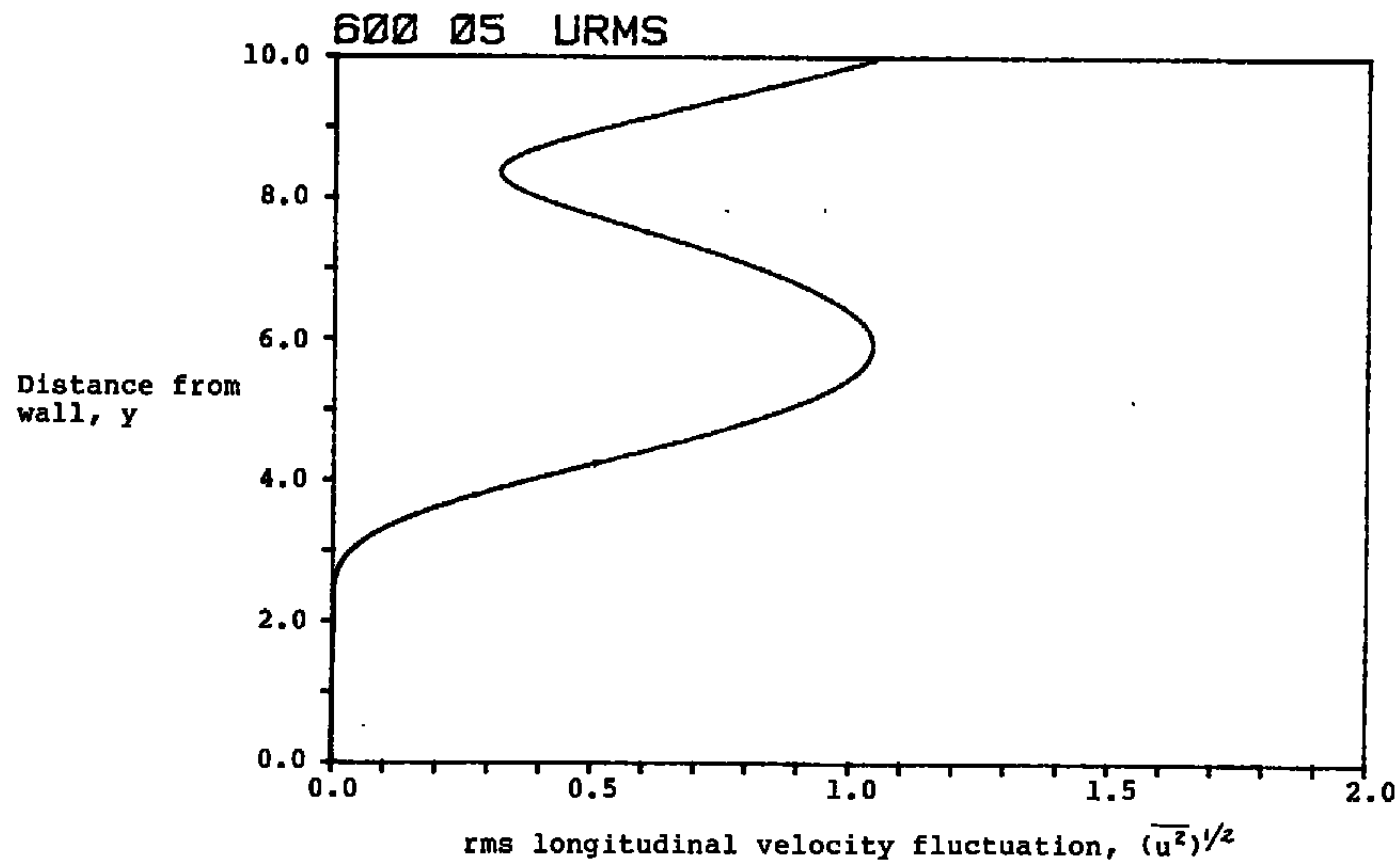rms longitudinal velocity fluctuation, $(\overline{u^2})^{1/2}$

Figure 4.1 The rms longitudinal velocity for the case of spatially-decaying vortical fluctuations for $R_\delta = 1000$, $\beta = \omega = 0.5$, and a Blasius boundary layer. Compare this figure for a travelling wave with Figure 3.14 for a standing wave.

4.2. This plot shows that a layer of vorticity exists near the boundary layer edge. The phase of this vorticity is such that the flow induced by this layer of vorticity tends to cancel the flow induced by the freestream vortical fluctuations. This cancellation process does not appear to take place with the standing waves. Inviscid, analytical solutions of the Rayleigh equation with broken-line mean velocity profiles would help clarify this process. However, the author has learned from several studies that the 2-D response in boundary layers is sensitive to the phase speed of freestream disturbances.

The rms longitudinal velocity for a Tollmien-Schlichting wave is plotted in Figure 4.3 for comparison with the other waves.

Although the "freestream disturbance" for the standing wave is irrotational, the fluctuating flow inside the boundary layer is rotational. That vorticity originates primarily from two sources: the production of fluctuating vorticity inside the boundary layer by the term $-v\bar{U}_{yy}$, and by diffusion in the y-direction, $\epsilon \zeta_{yy}$, to and from the wall in the unsteady viscous sublayer.

The main features of a thin viscous sublayer can be described by the unsteady, forced diffusion equation (B.1). The forcing arises from the pressure gradient impressed on the sublayer by the flow above the sublayer.

If the no-slip condition, u = 0 or $\psi_y = 0$, is replaced by a no-shear condition at the wall, $u_y = 0$ or $\psi_{yy} = 0$, calculations show that the disturbance is not significantly affected (except for the sublayer itself). The sublayer does not form when the no-shear condition is imposed. The result that the solution outside the sublayer region is relatively unchanged can be interpreted as the sublayer being relatively passive under the high Reynolds number, high frequency condition.

A remarkable balance takes place for these standing waves. The fluctuating vorticity decays (or grows) exponentially in the streamwise direction and oscillates in time in exactly the same fashion as the irrotational fluctuations in the freestream disturbance. The vorticity induces a flowfield which generates additional vorticity through the production term, and that flowfield also affects the diffusion processes in the sublayer. Also, the impermeability condition essentially sets up an image system. The "history" of the flowfield, including the oscillations and phasing, is important since the vorticity convecting downstream in the shear flow must arrive at each station and be altered by the production and diffusion in a such a manner that the vorticity field is also a standing wave. With these varied processes taking place simultaneously, it is amazing that a particular arrangement is possible such that the flowfield varies exponentially in space and oscillates in time.

Not all irrotational fluctuations, which decay or grow exponentially in the freestream and oscillate in time, are solutions of the Orr-Sommerfeld equation, although they may be solutions of the
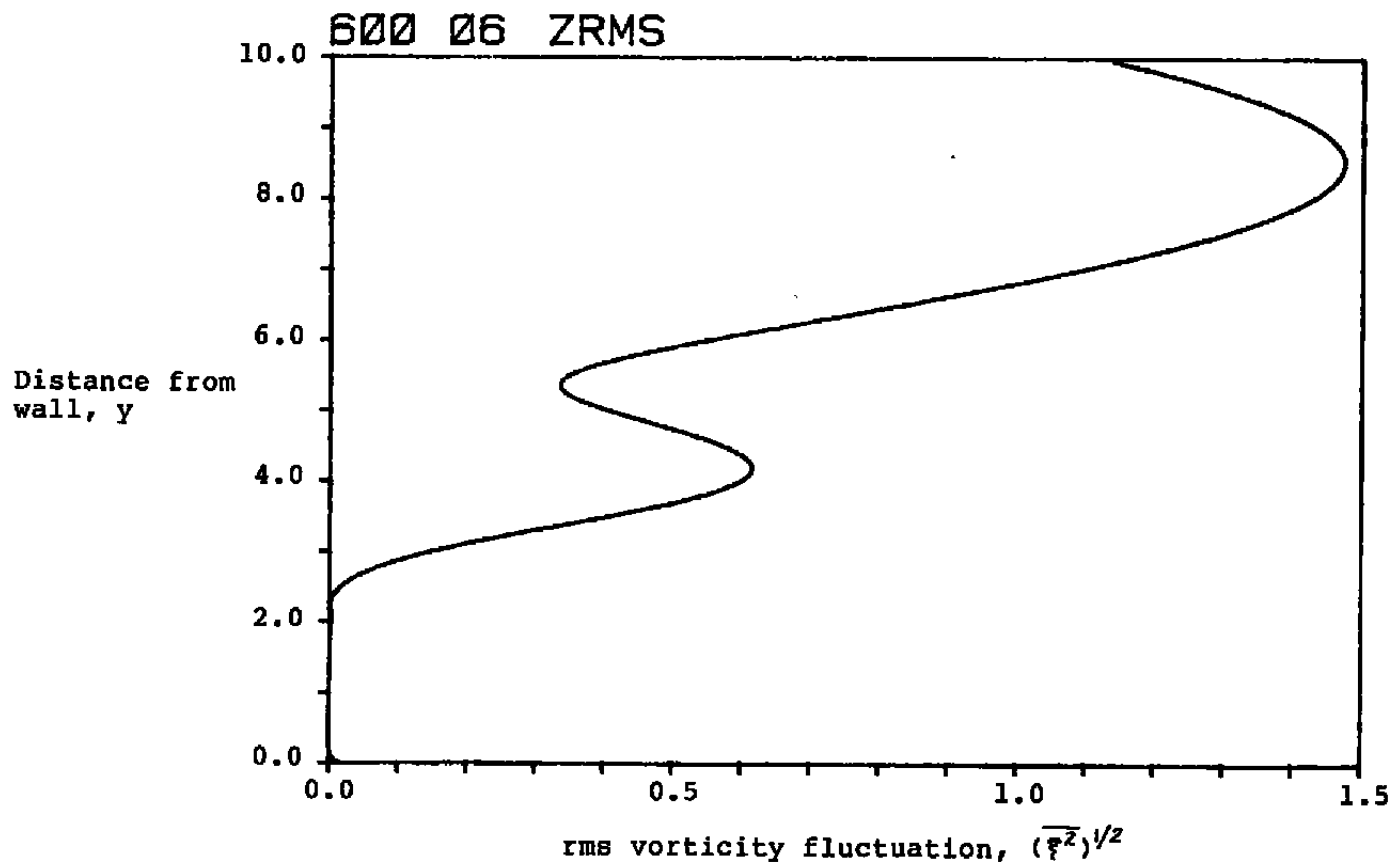
Figure 4.2   The rms fluctuating vorticity for the case of spatially-decaying vortical fluctuations for R_δ = 1000, $\beta = \omega = 0.5$, and a Blasius boundary layer. Note the bulge in vorticity near the boundary layer edge. The bulge further out is representative of the vortical fluctuations in the freestream.
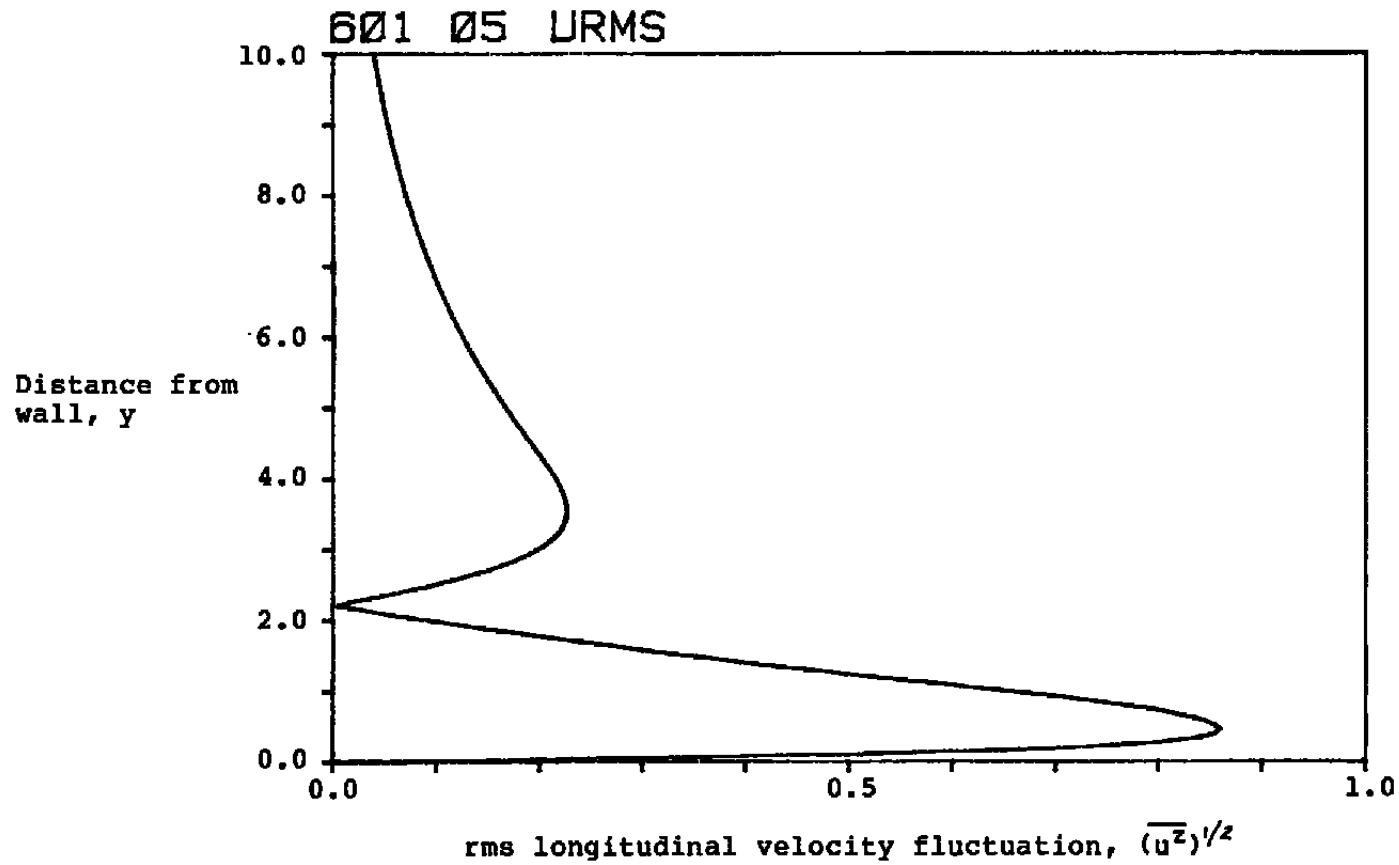
Figure 4.3   The rms   longitudinal   velocity for a Tollmien-Schlichting
             wave for R_δ = 821.835, α = (0.2888, 0.0), and ω = 0.1074
             with a Blasius boundary layer.

partial-differential equation (2.1). In the boundary layer, the flow may be much more complicated then the assumed solution form (2.3,2.4).

An important idea from the initial-value theories, however, is that the more complicated solutions can be constructed by superposition of the basic Fourier-Laplace solutions. In some cases, tne superposition is a summation of waves of finite amplitude. In other cases, the superposition is an integral over waves of infinitesimal strengths.

The other Fourier-Laplace solutions, including the stability waves and the two spatial-solutions with vortical fluctuations in tne freestream, also have remarkable balances which lead to solutions with simple functional dependences on x and t.

From the theory of inviscid stability waves, it is known that if φ is the solution for the wavenumber α, then φ^* is tne solution for the complex conjugate wavenumber, α^*. Calculations based on the viscous Orr-Sommerfeld equation, however, indicate that tne inviscid relationship is a reasonable guideline for relating the solutions for the viscous decaying and growing standing waves. The success is probably related to the passive character of the sublayer when the sublayer is thin, and the general insensitivity of the standing wave solutions to the Reynolds number (except in the sublayer). The details of the flow in the sublayer do not transform according to inviscid guidelines. The wavenumber for the growing-wave case, $\alpha = -i\beta$ is the complex conjugate of that wavenumber for the decaying case, $\alpha' = +i\beta$.

The functional dependence of the standing waves indicates that the waves do not travel in the streamwise direction. However, a movie shows that wave motion takes place in the y-direction. In the boundary layer, that motion is not a simple sinusoidal wave, and it does not travel in the y-direction with a constant speed. Far above the boundary layer where the only remaining influence of the boundary layer is through the value of the constant D, eqn.(4.9) can be rearranged as

$$V = \left\{ e^{i\beta \left(y - \frac{\omega}{\beta} t\right)} + E\, e^{-i\beta \left(y + \frac{\omega}{\beta} t\right)} \right\} e^{-\beta x} \tag{4.10}$$

This expression indicates that the irrotational freestream disturbance is a superposition of outgoing and incoming waves. The amplitudes of these waves are different since, in general, $E \neq 1$.

All of the available information is consistent with the conclusion that the two unsteady, exponentially-varying standing waves are basic, independent, Fourier-Laplace solutions of the viscous, parallel-flow Orr-Sommerfeld equation describing small-amplitude fluctuations in a boundary layer. This evidence is based on several analytical solutions, a formulation of the spatial initial-value problem using an asymptotic solution of the Orr-Sommerfeld equation, and the numerical calculations with adverse, zero, and favorable pressure gradient boundary layers. For mathematical completeness, these two solutions

join the list consisting of the discrete set of stability waves and the pair of solutions accounting for the propagation of vortical fluctuations in the freestream. While this report has focused on the standing waves in boundary layers, the author believes that equivalent waves arise in free-shear layers, jets, and wakes.

4.4 DESCRIPTION OF PROBLEMS WITH IRROTATIONAL DISTURBANCES IN THE FREESTREAM

An objective of this report is to document the evidence that a pair of standing wave solutions exists which have the characteristics of irrotational fluctuations "far-away" from the boundary layer. In all results, the vorticity and velocities satisfy parallel-flow equations. Those solutions summarized in Chapter 1 and in Appendix A all have a uniform mean flow. Consequently, there can be no Rayleigh, Tollmien-Schlichting, or other instability waves in those problems. Yet, both rotational and irrotational disturbances are present. The irrotational solutions fall into two classes:

(1) Travelling waves which arise through the impermeability condition of the plate. In more sophisticated, viscous solutions with shearing flows, these travelling waves are a part of the response of a boundary layer to vortical fluctuations in the freestream. This irrotational portion does not survive far-away from the boundary layer.

(2) Standing waves, which can also be set up by the impermeability condition, but which do not travel. Unlike the vortical fluctuations which have no pressure fluctuations in the freestream, these standing waves have (sometimes strong) pressure fluctuations which can be estimated from linear equations. This flowfield is not describable by stability waves, and is not describable by the solutions (1) above.

An initial-value problem formally illustrates that the two standing waves are entities distinct from the poles of the stability waves and from the branch lines of the vortical fluctuations. The standing waves in this report are described by the viscous Orr-Sommerfeld equation with a boundary layer, rather than the uniform flows as used in Chapter 1 and Appendix A. The formal linking of (a) the standing waves set up by the interactions of vortical fluctuations with the leading edge, as analyzed in Refs.6 and 7, and (b) the standing waves described by the Orr-Sommerfeld equation is a topic of continuing research which is not likely to be resolved rigorously in the near future. The information presently available is based on a sequence of problems: (a) solutions of the Orr-Sommerfeld equation, (b) uniform-flow, viscous solutions, (c) uniform-flow inviscid solutions, and (d) uniform-flow inviscid solutions with a leading edge. In each of the problems (a,b,c), the standing waves reappear in ever-simplier forms. The two problems (c,d) have identical

equations and boundary conditions downstream of the leading edge, and both problems have standing waves. In the future, the solution from problem (d) will be Fourier-analyzed to show how the solutions from problem (c) formally enter into problem (d). The author has little doubt that such a link is possible and will serve as a guideline to analyzing the more complicated viscous cases.

The presence of irrotational fluctuations around airfoils and in turbomachinery is no surprise to unsteady aerodynamicists. Potential fluctuations appear in the unsteady aerodynamics theories of airfoils encountering gusts, airfoils oscillating in angle of attack, airfoils oscillating in the direction perpendicular to the freestream, and unsteady flap motions. Experimental data confirms the presence of such fluctuations. Potential fluctuations arise when rotor blades pass by stator blades in compressors and turbines. While some of these irrotational fluctuations are travelling-waves, the unsteady circulation about an airfoil is a standing wave for that airfoil. The flows induced by the vortex sheet shed from the trailing edge are irrotational (except at the sheet itself). These flows also have standing and travelling wave components, where the standing wave arises because of the interaction between the vortex sheet and the airfoil itself. Far-downstream of the airfoil, the principal contribution is the travelling wave induced by the vortex sheet itself.

The model of an airfoil oscillating in a direction perpendicular to the flow suggests that some of the _linear features of model vibration at low frequencies_ would appear as standing waves. The oscillating dipole character of an oscillating cylinder beside a boundary layer is a unsteady standing wave. Oscillating airfoils, oscillating source-sinks, and airfoils with oscillating flaps which are positioned in the vicinity of a plate with a boundary layer will also produce standing waves. Travelling waves of various forms will also arise in these cases.

The standing waves appear to be one of the downstream influences of the leading edge, and one of the upstream influences of a trailing edge of a body interacting with freestream vorticity fluctuations. The diffusive wave which travels _upstream_, as described in Refs. 17 and 27, is another mechanism for upstream influence in this elliptic problem. Rockwell (Ref. 25) comprehensively reviews the complex and interesting unsteady flows arising when vortical fluctuations interact with leading edges.

Refs. 28-35 are examples of numerical solutions which have been obtained for unsteady boundary layer problems with finite difference, vortex filament, and spectral techniques. These investigators have been faced with the difficulty of properly posing the boundary conditions on the downstream, outer, and upstream boundaries of their calculational regions. This problem with boundary conditions will become more severe as the disturbances adopt the characteristics of freestream turbulence and its interaction with the leading edge, as the amplitudes increase, and as 3-D and other significant features are included.

The standing waves could be an important factor in obtaining numerical solutions in a rectangular domain, since those waves are a mechanism by which the upstream and downstream boundary conditions can influence the flow elliptically. Improperly formulated boundary conditions could excite extraneous fluctuations in the calculational domain. The magnitude of these unwanted disturbances would depend on the amplitudes at the boundaries, as well as the y-wavenumber which dictates the growth/decay rate in the domain, and the length of the domain itself. The reader is reminded that y-wavenumber = 0 for non-decaying waves is a possible limiting case of these standing waves. Standing waves with small y-wavenumbers would influence the entire calculational domain. The "purification" of a solution, by identification and elimination of unwanted waves in the calculation, could be a useful numerical procedure.

In other cases as suggested by the paragraphs above, the proper boundary conditions should incorporate standing waves which naturally enter into and leave the calculational region.

Possible topics for future research include the investigations of (1) 3-D standing waves, (2) the compressible counterparts to the present incompressible waves, (3) standing waves in parallel-flow jets, wakes, and free-shear layers, (4) standing waves in nonparallel shearing layers, and (5) standing waves in boundary layers as described by the unsteady Prandtl boundary layer equation. More detailed studies are needed to (6) determine the influence of surface roughness on these waves. Further development of (7) the initial-value problem would permit an initial disturbance to be decomposed into the various standing and travelling waves. (8) The processes which create irrotational fluctuations in the freestream deserve detailed study. These processes include the interaction of vortical freestream disturbances with leading and trailing edges, the unsteady motions of airfoils and vibrations of models, and the combined irrotational/rotational disturbances set up in turbomachinery.

In closing, many additional examples can be cited where potential fluctuations arise in practical engineering problems. This research is intended to show that they also appear as solutions of the Orr-Sommerfeld equation if the proper parameters and exterior boundary conditions are selected.

REFERENCES

1. Rogler, Harold L. and Reshotko, Eli., "Disturbances in a boundary layer introduced by vortex array representations of free stream turbulence", Workshop on Low Speed Boundary Layer Transition, Rand Corporation, Santa Monica, California (16-17 July 1974); Abstract appears in R-1752-ARPA/ONR by William S. King (June 1975).

2. --- "Spatially decaying array of vortices", The Physics of Fluids, vol. 19, no. 12 (December 1976).

3. ---"Disturbances in a boundary layer introduced by a low intensity array of vortices", Proceedings of the International Symposium on Modern Developments in Fluid Dynamics, Haifa, Israel (16-23 December 1973), J. Rom (Editor), published by SIAM (1977); also SIAM J. Appl. Math., vol. 28, no. 2 (March 1975).

4. Telionis, Demetri P., "Calculations of time-dependent boundary layers", Unsteady Aerodynamics, Vol.I, Proceedings of a symposium held at the Univ. of Arizona, edited by R.B. Kinney (July 1975).

5. Loehrke, R.I., Morkovin, M.V., and Fejer, A.A., "Review – Transition in nonreversing oscillating boundary layers", vol. 97, no. 4, Journal of Fluids Engineering (December 1975).

6. Rogler, Harold L., "Freestream vorticity disturbances adjusting to the presence of a plate – – a quarter-plane problem", Journal of Applied Mechanics, vol. 44, no. 4 (December 1977).

7. ---"The interaction between vortex-array representations of freestream turbulence and impermeable bodies", Paper 75-116, 13th AIAA Aerospace Sciences Meeting (January 1975).

8. ---"The interaction between vortex-array representations of freestream turbulence and semi-infinite flat plates", Journal of Fluid Mechanics, vol. 87, part 3 (1978).

9. ---"Rotational and irrotational freestream disturbances interacting with a semi-infinite plate", Eighth U.S. National Congress of Applied Mechanics, Univ. of Cal. at Los Angeles (26-30 June 1978).

10. Rogler, Harold L. and Reshotko, Eli, "Freestream fluctuations interacting inviscidly with semi-infinite plates"
(to be published).

11. Tollmien, W., "Uber die Entstehung der Turbulenz", Gesellschaft der Wissenschaften. Gottingen. Mathematisch-Naturwissenschaftliche Klasse. Nachrichten (1929).

12. Mack, Leslie M., "A numerical study of the temporal eigenvalue spectrum of the Blasius layer", *J. Fluid Mech.*, vol.73 (1976).

13. Corner, D.,Houston, D.J.R.,and Ross, M.A.S., "Higher eigenstates in boundary-layer stability theory", *J. Fluid Mech.*, vol.77, part 1 (1976).

14. Grosch, C.E. and Salwen, H., "The continuous spectrum of the Orr-Sommerfeld equation. Part 1. The spectrum and the eigenfunctions", *J. Fluid Mech.*, vol. 87 (1978).

15. Rogler, Harold L., "Vorticity fluctuations propagating downstream and interacting with Falkner-Skan boundary layers" (to be published).

16. Rogler, H. and Tsuge, S., "Standing waves which decay or grow exponentially in the streamwise direction", *Bulletin of the American Physical Society*, vol.25, no.9 (1980).

17. ---"Initial-value problem and solutions for three-dimensional disturbances in boundary layers and free-shear layers", *Bulletin of the American Physical Society*, vol.26, no.9 (1981).

18. Rogler, H., "The production of higher and lower modes and the decay of an array of vortices near a boundary", *Bulletin of the American Physical Society*, vol.20, no.9 (1975).

19. Hultgren, Lennart S. and Gustavsson, L. Hakan, "Algebraic growth of disturbances in a laminar boundary layer", *Physics of Fluids*, vol.24, no.6 (June 1981).

20. Bechert, D. and Michel, U., "The control of a thin free shear layer with and without a semi-infinite plate by a pulsating flow field", *Acustica*, vol.33, no.5 (1975).

21. Dovgal', A.V., Kozlov, V.V., and Levchenko, V. Ya., "Experimental investigation into the reaction of a boundary layer to external periodic disturbances", *Fluid Mechanics (Russian)*, vol.15, no.4 (July-August 1980); Translated from Izvestiya Akademii Nauk SSSR, Mekhanika Zhidkosti i Gaza, no.4 (July-August 1980).

22. Reshotko, Eli, "Remark on Engineering Aspects of Transition", *Transition and Turbulence*, edited by Richard E. Meyer, Academic Press (1981).

23. Nachtsheim, Phillip R. and Swigert, Paul, "Satisfaction of asymptotic boundary conditions in numerical solution of systems of nonlinear equations of boundary layer type", NASA E-2959 (1965).

24. Prandtl, L., "Bemerkungen uber die Entstehung der turbulenz", Z. angew. Math. Mech., 1, pp.431-436 (1921).

25. Rockwell, D., "Oscillations of impinging shear layers", AIAA 20th Aerospace Sciences Meeting, AIAA Preprint 82-0047 (11-13 January 1982).

26. Tsuge, S., "Methods of separation of variables in turbulence theory", NASA CR-3054 (1978).

27. Rogler, Harold L., "Waves which travel upstream in boundary layers", AEDC-TR-83-4 (to be published).

28. Ludloff, H.F., De Santo, D.F., and Parthasarathy, R., "Attempts at derivation of transition from laminar into turbulent flow along a flat plate", AFOSR TN 60-105, New York University (January 1960).

29. Wray, Alan and Hussaini, M.Y., "Numerical Experiments in boundary layer stability", AIAA 18th Aerospace Sciences Meeting (14-16 January 1980).

30. Leonard, A., "Numerical simulation of interacting, three-dimensional vortex filaments", Lecture Notes in Physics, vol. 35, Springer-Verlag, Berlin (1975).

31. Grosch, Chester E., "Numerical simulation of instability and transition", Low-Speed Boundary Layer Transition Workshop (16-17 July 1974); Abstract appears in R-1752-ARPA/ONR by William S. King (June 1975).

32. Fasel, H., "Investigation of the stability of boundary layers by a finite difference model of the Navier Stokes equations", J. Fluid Mech., vol. 78, part 2 (1976).

33. Miller, G. and A. Callegari, A., "The effects of acoustical disturbances on boundary layer transition", NYU/DAS 78/01, New York University/Dept. of Applied Science, 26-36 Stuyvesant Street (Barney Bldg), New York, New York 10003 (January 1978).

34. Orszag, S.A., "Turbulence and Transition: A Progress Report", Proceedings of the Fifth International Conference on Numerical Methods in Fluid Dynamics Springer-Verlag, Berlin (1976).

35. Murdock, John W., "Tollmien-Schlichting waves generated by unsteady flow over parabolic cylinders", Paper-AIAA-81-0199, AIAA 19th Aerospace Sciences Meeting (12-15 January 1981).

36. Jordinson, R., "Spectrum of eigenvalues of the Orr-Sommerfeld equation for Blasius flow", Physics of Fluids, vol.14 (1971).

37. Antar, Basil N. and Benek, John A., "Temporal eigenvalue spectrum of the Orr-Sommerfeld equation for the Blasius boundary layer", Physics of Fluids, vol. 21, no. 2 (February 1978).

38. Rogler, Harold L., "Fluctuations in a boundary layer introduced by traveling-wave irrotational freestream disturbances", Low-speed Boundary-Layer Transition Workshop: II, RAND Corporation (13-15 September 1976).

39. ---- "The coupling between freestream disturbances, driver oscillations, forced oscillations, and stability waves in a spatial analysis of a boundary layer", Conference Proceedings of the Fluid Dynamics Panel Symposium on Laminar-Turbulent Transition, Advisory Group for Aerospace R and D Conference Proceedings No. 224 (2-4 May 1977).

40. Murdock, John W. and Stewartson, Keith, "Spectra of the Orr-Sommerfeld equation", Physics of Fluids, vol. 20, no. 9 (September 1977).

41. Salwen, H. and Grosch, C. E., "The spatial continuum eigenfunctions of the Orr-Sommerfeld equation", Bull. Am. Physical Soc., 22, no. 10 (1977).

42. Ellinwood, J. W., "Forced response of a Blasius flat-plate boundary layer to an external vortex street", SAMSO-TR-79-65 (5 July 1979).

Appendix A. ANALYTICAL SOLUTIONS FOR STANDING WAVES
IN A UNIFORM MEAN FLOW NEAR A WALL

A.1 INVISCID SOLUTION

For an inviscid flow with $\bar{U} = 1$, eqn.(2.1) reduces to

$$\left\{ \frac{\partial}{\partial t} + \frac{\partial}{\partial x} \right\} \nabla^2 v = 0$$

(A.1)

and the Orr-Sommerfeld equation, eqn.(2.6b), reduces to

$$\left(1 - \frac{ir\omega}{\beta} \right)\left(\varphi_{yy} + \beta^2 \varphi \right) = 0$$

(A.2)

where $r = +1$ for a growing wave and -1 for a decaying wave. For the cases of interest with β and ω both real and nonzero, the leading coefficient cannot vanish. The solution of the equation is generally

$$\varphi = A e^{i\beta y} + B e^{-i\beta y}$$

(A.3)

where A and B are complex constants. To satisfy the impermeability condition, then $A = -B$ and the solution is

$$\varphi = 2 A i \sin \beta y$$

(A.4)

Hence for the inviscid case with a uniform mean flow, only a sine wave arises, and the complex amplitude φ is the same for both growing and decaying waves. This flow is irrotational.

A.2 VISCOUS SOLUTIONS

Eqn.(2.1) reduces to the following equation for a uniform mean flow

$$\left\{ \frac{\partial}{\partial t} + \frac{\partial}{\partial x} - \epsilon \nabla^2 \right\} \nabla^2 v = 0$$

(A.5)

The Orr-Sommerfeld equation reduces to

$$\left[\left(1 - \frac{ir\omega}{\beta} \right) - \frac{1}{r\beta R_\delta} \left(D^2 + \beta^2 \right) \right] \left(D^2 + \beta^2 \right) \varphi = 0$$

(A.6)

The characteristic length δ in the nondimensionalizations is a dummy parameter for this uniform flow case. While that length could be defined as the characteristic viscous length, the same nondimensionalizations will be used here as defined in Chapter 2 so that our analytical results can be compared with the numerical solutions. For solutions of exponential form, the four independent solutions are

$$\varphi(y) = A e^{-my} + \underset{O}{B} e^{my} + \underset{1}{C} \cos\beta y + D \sin\beta y \qquad (A.7)$$

where the exponent is

$$m = \left(r\beta R_\delta - \beta^2 - i\omega R_\delta \right)^{1/2} = R_\delta^{1/2} \left(r\beta - \frac{\beta^2}{R_\delta} - i\omega \right)^{1/2} \qquad (A.8)$$

Introducing the impermeability and no-slip conditions, then

$$\varphi(y) = - e^{-my} + \cos\beta y - \frac{m}{\beta} \sin\beta y \qquad (A.9)$$

The choice of growing or decaying waves influences the solution through the exponent m.

Rather than normalizing the solution by setting the constant $C = 1$, the choice $D = 1$ is also valid. With this normalization, the solution is

$$\varphi(y) = \frac{\beta}{m} e^{-my} - \frac{\beta}{m} \cos\beta y + \sin\beta y$$

As $R_\delta \to \infty$, $m \to \infty$, and the inviscid solution is recovered except for the arbitrary constant. This normalization is not used below.

From the continuity equation, the longitudinal velocity is

$$u = f(y) e^{r\beta x - i\omega t} \text{ where } f(y) = r\left(-\frac{m}{\beta} e^{-my} + \sin\beta y + \frac{m}{\beta} \cos\beta y \right) \quad (A.10)$$

From the definition of vorticity,

$$\zeta \equiv v_x - u_y = Z(y) e^{r\beta x - i\omega t} \qquad (A.11)$$

the vorticity amplitude is

$$Z(y) = R_\delta \left(-1 + \frac{ir\omega}{\beta} \right) e^{-my} \qquad (A.12)$$

Since $m \to \infty$ as $R_\delta \to \infty$, the rotational region is reduced to a layer of vanishing thickness with infinite vorticity. Hence a vortex sheet is positioned at the wall. For finite Reynolds numbers, note that the value of vorticity at the wall is proportional to the Reynolds number.

If the no-slip condition, $\varphi_y(0) = 0$, is replaced by a no-shear condition, $\varphi_{yy}(0) = 0$, then the solution is $A = B = C = 0$, or $\varphi(y) = D\sin y$. Hence, the viscous solution reduces to the inviscid form for all Reynolds numbers with the no-shear form of the wall boundary condition. No sublayer or rotational region forms.

Appendix B. SUBLAYER SOLUTION FOR STANDING WAVES

When Prandtl (Ref.13) analyzed the viscous sublayer and first demonstrated how viscosity could be destablizing in a boundary layer, he made three assumptions:

(1) The fluctuating pressure is impressed upon the thin sublayer.

(2) The mean velocity is sufficiently small in the sublayer such that it can be neglected.

(3) The fluctuating velocity perpendicular to the plate can be neglected in the x-momentum equation.

These assumptions will now be applied to the sublayer of the standing wave. The objective is to obtain a closed-form solution which illustrates the essential features of the sublayer. Introducing these assumptions and using the same nondimensionalizations as defined in Chapter 2, then the x-momentum equation reduces to the unsteady, forced diffusion equation

$$u_t = -p_x + \epsilon u_{yy} \qquad \text{where} \quad u = f(y)\, e^{r\beta x - i\omega t} \qquad (B.1)$$

Outside of the sublayer but not too far from the wall, the diffusion term is neglected, and a balance exists between the pressure gradient and the unsteady term

$$u_t = -p_x \qquad (B.2)$$

where the pressure varies as

$$p = \pi_\infty\, e^{r\beta x - i\omega t} \qquad (B.3)$$

where r=+1 or -1 for growing or decaying waves. Hence the complex amplitudes of the pressure and velocity are related by

$$i\omega f_\infty = r\beta \pi_\infty \qquad (B.4)$$

and this pressure is assumed to be constant across the sublayer. The momentum equation then reduces to

$$-i\omega f = -r\beta \pi_\infty + \epsilon f_{yy} \qquad (B.5)$$

with boundary conditions

$$f = 0 \;\; at\; y = 0 \;\; and\; f \to f_\infty \;\; as\; y \to \infty \qquad (B.6a,b)$$

Seeking solutions of form exp(my), then the homogeneous solution is

$$m = \pm\left(-i\omega R_\delta\right)^{1/2} \qquad (B.7)$$

while the particular integral is a constant with the value

$$r \, \pi_\infty = f_\infty \tag{B.8}$$

Hence the solution for the amplitude of the longitudinal velocity is

$$f(y) = f_\infty \left\{ 1 - exp\left[-(1-i)(\omega R_\delta/2)^{1/2} y\right] \right\} \tag{B.9}$$

This amplitude is plotted in Figure 3.4.

NOMENCLATURE

English

$a_m, a_m^{(q)}$ — coefficient of the mth Chebyshev polynomial in the expansion of the qth derivative of φ

$$d^q\varphi/d\hat\eta^q = \sum_{m=0}^{N-1} a_m^{(q)} T_m(\hat\eta) \qquad \text{where } a_m^{(o)} \equiv a_m$$

A,B,C,D — constants in the uniform-flow solution of the Orr-Sommerfeld equation

$c = c_r + ic_i$ — complex phase speed

ci,si — cosine and sine integrals

C_2, D_2 — complex constants used in eqn.(4.7)

D=d/dy — ordinary derivative in the y-direction

$D^n = d^n/dy^n$ — nth ordinary derivative $(D^o\varphi = \varphi)$

$E = (\overline{u^2} + \overline{v^2})/2$ — averaged disturbance kinetic energy per unit mass

E — complex constant used in eqn.(4.10)

$f(y) = f_r + if_i$ — complex amplitude of the longitudinal velocity

f_∞' — value of f at the sublayer edge; value in the freestream

$i = (-1)^{1/2}$

m — exponent; index on Chebyshev polynomial

m_{FS} — Falkner-Skan parameter

N — number of terms in the series $\varphi = \sum_{m=0}^{N-1} a_m T_m$

p — disturbance pressure

r — integer with value +1 for a growing wave and -1 for a decaying wave

R_δ — Reynolds number based on characteristic thickness of the boundary layer

Real[ ], $\mathscr{R}$[ ] — real part of the argument [ ]

t — time

T_m — mth Chebyshev polynomial

u,v	disturbance velocities in the x and y directions
$\bar{U},\bar{V}$	mean velocities in the x and y directions
U_∞	mean x-velocity in the freestream. For Falkner-Skan boundary layers, the notation $U_\infty(x)$ emphasizes that this is the mean velocity at the boundary layer edge at the position x downstream of the vertex of the wedge
x	coordinate parallel to plate and in streamwise direction
X(x,t;ϵ)	function appearing in eqn.(1.16) and defined in (1.17b)
y	cordinate normal to the plate
y_I	phase shift used in Section 1.3
y_e	y-value of the boundary layer "edge"
z=x+iy	complex coordinate
Z(y)	complex amplitude of the fluctuating vorticity

Greek and Script

α	x-wavenumber
β	y-wavenumber
β_{FS}	$\pi\beta_{FS}$ is the vertex angle of the wedge along which the Falkner-Skan boundary layer develops
$\nabla = i\frac{\partial}{\partial x} + j\frac{\partial}{\partial y}$	gradient operator
$\nabla^2 = \frac{\partial^2}{\partial x^2} + \frac{\partial^2}{\partial y^2}$	Laplacian operator
δ	characteristic thickness of the boundary layer. For a Falkner-Skan boundary layer, this length is defined as $$\delta \equiv \left(\frac{2}{m_{FS}+1}\frac{\nu X}{U_\infty(x)}\right)^{1/2}$$
δ_s	characteristic thickness of the viscous sublayer
$\epsilon=1/R$	inverse of Reynolds number
μ	viscosity
ν	kinematic viscosity
$\vec{\zeta}$	vorticity vector

$\zeta(x,y,t)$ disturbance vorticity in the z-direction

$\pi(y) = \pi_r + i\pi_i$ amplitude of pressure disturbance

ρ mass density

$\phi(y) = \phi_r + i\phi_i$ complex amplitude of the normal velocity disturbance

ψ streamfunction

ω frequency

Superscripts, Subscripts, and Miscellaneous Notation

$\overline{(\;\;)}$ (a) ensemble average or suitable time average
                (b) for periodic disturbances, the time average over one time period

$$\overline{u^2} = \frac{\omega}{2\pi}\int_0^{2\pi/\omega} u^2\,dt$$

*   complex conjugate

e   boundary layer edge

r,i   real and imaginary parts of a complex number or variable

s   sublayer

$()_x$ partial derivative with respect to x